NASA CR-132528

APPLICATION OF THE SCALAR AND VECTOR POTENTIALS TO THE AERODYNAMICS OF JETS

by

H. L. Russell and J. G. Skifstad

August 1973

Thermal Science and Propulsion Center
School of Mechanical Engineering
Purdue University
Lafayette, Indiana

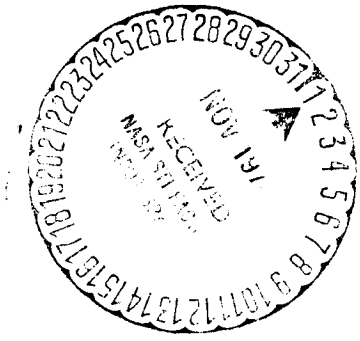

NASA Grant No. NGL 15-005-094
Purdue Research Foundation PRF-5551

ACKNOWLEDGMENTS

This investigation comprises part of a research program on the aerodynamics of jets, sponsored under NASA Grant No. NGL-15-005-094. The authors gratefully acknowledge the support and especially the encouragement and cooperation of the project monitor, Mr. Richard J. Margason of the NASA Langley Research Center. Discussions with Dr. R. E. Lynch, Div. of Mathematical Sciences, Purdue University, regarding numerical methods were most helpful. The work was completed in 1971; publication of this report has been delayed largely because of other commitments of the senior author (J.G.S.).

TABLE OF CONTENTS

LIST OF TABLES

LIST OF FIGURES

LIST OF NOMENCLATURE

A	exact value of an integral
$\vec{A}$	vector potential
A_1	surface area
$\vec{A}_1$	a vector normal to and equal in magnitude to the surface area A_1
C	a constant in the expression for velocity potential, Equation (79)
C_p	pressure coefficient
e	virtual origin of the jet
$E(k)$	complete elliptic integral of the second kind
E_m	mass entrainment rate
$\vec{E}_p$	irrotational-solenoidal contribution to the vector $\vec{U}$ from the surface integrals Equation (13)
G	Green's function of the second kind
H	a harmonic function
I	a numerical approximation for an integral
I_m	integral moment of vorticity
k	modulus for complete elliptic integral functions
K_1	a constant in the expression for the mass flow rate, Equation (35)
$K(k)$	complete elliptic integral of the first kind
M	momentum flux
m	exponent in the empirical expression for the velocity distribution in the jet
$\vec{m}$	dipole strength
$\vec{n}$	the unit outward normal vector of a surface element
p	pressure

$\vec{P}_1$ position vector for an image of a source point

p_∞ ambient pressure of the atmosphere

$\vec{Q}$ a vector field such that $\vec{Q} = \vec{U} - \vec{T}$

$\vec{R}$ distance from a source point to a field point

R magnitude of the distance between a source point and a field point

r radial coordinate in a cylindrical coordinate system

r_I inner boundary of the mixing layer of the jet

r_o outer boundary of the jet

$r_{1/2}$ radius at which the velocity is half that at the axis of the jet

S a surface bounding a region in space

dS a differential surface element

$d\vec{S}$ the product of the unit outward normal vector and the differential surface element

$\vec{T}$ a vector field such that $\nabla \times \vec{T} = \nabla \times \vec{U}$, $\nabla \cdot \vec{T} = \nabla \cdot \vec{U}$, and $\vec{T} \cdot d\vec{S} = \vec{U} \cdot d\vec{S}$

$\vec{U}$ a vector field

U_m maximum axial velocity

$\vec{W}$ a vector field such that $\nabla^2 \vec{W} = -\vec{U}$

$\vec{X}$ a position vector

X, Y, Z rectangular coordinates

x, y, z transformed coordinates

z axial coordinate in a cylindrical coordinate system

Greek Symbols

Γ circulation

δ the delta function

ε the error of a numerical approximation

η a transformation variable

θ a cylindrical coordinate

θ, ρ, ϕ spherical coordinates

λ a transformation variable

μ a transformation variable

ξ $(18.5\ r_1)/z_1$ for the axisymmetric jet

ρ mass density

τ a region in space

ϕ scalar potential

ψ gradient of a scalar

$\vec{\omega}$ vorticity vector field

Subscripts

C pertaining to the centerline of the jet

I irrotational field

j pertaining to the jet

m maximum value

p peripheral component

r radial component (cylindrical coordinates)

S solenoidal field

x transformed radial component

y transformed axial component

z axial component (cylindrical coordinates)

θ peripheral component (cylindrical coordinates)

θ azimuthal component (spherical coordinates)

ρ radial component (spherical coordinates)

τ	a region in space
ϕ	colatitude component (spherical coordinates)
1	pertaining to a source point

Superscripts

C	core region of the jet
D	developed region of the jet
' (Prime)	per unit length

ABSTRACT

An analytical investigation was conducted to examine the applicability of a method based on the Stokes potentials (vector and scalar potentials) to computations associated with the aerodynamics of jets. The principal merits of the method were found to be that the aerodynamic field near the nozzle could be well represented and that the influence of a nonuniform velocity profile at the nozzle exit plane could be explicitly determined. Other aspects of the computations indicated accuracy comparable with other methods but at the expense of more complexity in the computations. An additional benefit of the theory was that it provided the rationale for developing useful approximate analytical models for computations of the type considered.

Computations were made for an axisymmetric jet exhausting into a quiescent atmosphere for the purposes of exploring the computational aspects of the method and for comparison with the available experimental data and other theories. It was found that the velocity profile at the exit of the nozzle and the integral moment of vorticity in the jet flow were the most significant factors in the computations. The latter is shown to be in agreement with the asymptotic form of the theory. Those factors suggest that knowledge of the velocity at the

axis of the jet, together with the location of the half-velocity points along the jet are sufficient to yield reasonably accurate aerodynamic field computations for the particular flowfield considered. Computations support that conclusion.

One of the approximate analytical models considered in the study essentially replaced the jet flowfield by a conical vortex sheet. That model was the simplest considered and yielded accurate results. It is, accordingly, recommended for computational purposes.

The comparison with experimental data showed agreement within the scatter of the available data. The theory indicated clearly the inconsistency among the different theoretical characterizations of jet flowfields, and suggests the need for more accurate relations.

I. INTRODUCTION

A number of problems in fluid mechanics involve the interaction between viscous and inviscid flows. For most purposes, as in boundary layer theory, the inviscid flow is determined without consideration of the viscous flow region whereas the effects of the inviscid flow on the flow in the viscous layer are considered. More recent interest in the aerodynamics of jets, the "strong interaction" problems, separating and reattaching flows, etc., have placed more emphasis on the mutual interactions of the two regions. Analytical models for such flows are in various stages of development. One analytical method, applicable to incompressible flows or for aerodynamic purposes, based on the Stokes potentials (scalar and vector potentials), has not yet received much attention.

It is the purpose of this investigation to examine the latter method in the context of problems associated with the aerodynamics of jets. Such flows are of considerable significance in the aerodynamics of V/STOL aircraft, the dispersion of pollutants, etc. Analytical methods for handling them are not yet well developed. The emphasis in this connection is on the influence of a turbulent jet in inducing an aerodynamic flow. The flow in the turbulent jet is presumed known either from experimental data or from other theoretical considerations.

As part of the investigation, the properties of the turbulent flow most influential in computing the aerodynamic field were evaluated.

Asymptotic relations were developed to yield greater insight into the method. In the interest of simplifying such computations, several approximate models were examined. Numerical computations were made for the case of an axisymmetric jet exhausting through a plane baffle plate, serving to further classify the advantages and disadvantages of the method.

The use of the scalar and vector potentials arises naturally from the fundamental theorem of vector field theory. Most applications have been associated with electromagnetic field theory; applications in fluid mechanics have been rare. Since the concept is not familiar to those with prime interests in fluid mechanics, a brief review of the relevant aspects of vector field theory have been included in the text.

The results of the investigation show that the method offers unique advantages in the computation of the induced aerodynamic field, particularly close to the origin of the jet. At more distant positions, the method yields results comparable to those obtained by other less complicated methods. An additional benefit provided in the application of the method is that it offers an independent means for comparing the consistency of different representations of the turbulent jet flow. The examination of approximate models for the jet flow showed that quite reasonable approximations for the induced aerodynamic field could be obtained from knowledge of only the centerline velocity and the positions of points in the jet at which the velocity is half that on the axis.

II. ANALYSIS

Since the basis for the analytical methods to be considered lies in vector field theory, an introductory description of the relevant elements of that theory is presented in the first part of this section. The remaining parts of this section present discussions of solenoidal fields, time dependent fields, axisymmetric fields, and Green's function, respectively.

A. Vector Field Theory

1. Fundamental Theorem

Consider a vector field $\vec{U}(\vec{X})$ which depends upon the position $\vec{X}$ in space. The field $\vec{U}$ may be uniquely defined in a simply connected region τ by specifying the divergence and curl of $\vec{U}$ throughout τ and the normal component of $\vec{U}$ on the surface S bounding the region τ. A proof of uniqueness, following Lass[1], is as follows: Let $\vec{T}$ be another vector field with divergence and curl equal to those of $\vec{U}$, and with $\vec{T} \cdot d\vec{S} = \vec{U} \cdot d\vec{S}$ on S.* Select a vector $\vec{Q}$ which is the vector difference between $\vec{U}$ and $\vec{T}$, $\vec{Q} \equiv \vec{U} - \vec{T}$. This vector is irrotational, solenoidal, and its scalar product with $d\vec{S}$ is zero.

---

*$d\vec{S} = \vec{n}\, dS$, where $\vec{n}$ is the unit outward normal vector of the surface element, and dS is the differential surface element.

$$\nabla \cdot (\vec{U} - \vec{T}) = \nabla \times (\vec{U} - \vec{T}) = (\vec{U} - \vec{T}) \cdot dS = 0$$

The vector $\vec{Q}$, since it is irrotational, may be represented in terms of a scalar function ϕ such that

$$\vec{Q} = - \nabla \phi$$

The solenoidal condition then yields

$$\nabla \cdot \vec{Q} = - \nabla^2 \phi = 0$$

Applying Green's theorem in the first form yields

$$\int_\tau [\phi \nabla^2 \phi + (\nabla \phi)^2] \, d\tau = \int_S \phi \, \nabla \phi \cdot d\vec{S} = \int_S \phi \, \vec{Q} \cdot d\vec{S} = 0$$

and therefore the volume integral of $(\nabla \phi)^2$ is zero. Hence, $\nabla \phi = 0$ inside τ, and $\vec{Q} = -\nabla \phi = 0$, so that $\vec{U} = \vec{T}$ inside τ. For an infinite domain, the condition that $\vec{U} \to 0$ as $1/R^{1+\epsilon}$ as $R \to \infty$ with $\epsilon > 0$ is required.[2]

2. The Scalar and Vector Potentials

Explicit representation of the vector field in terms of the volume distribution of its divergence and curl, and its normal component on the surface may be obtained by introducing the Stokes potentials[3], normally called the scalar and vector potential of the field. Following Morse and Feshbach[4(a)], let

$$\vec{W}(\vec{X}) = \frac{1}{4\pi} \int_\tau \frac{\vec{U}_1(\vec{X}_1)}{R(\vec{X}, \vec{X}_1)} \, d\tau_1 \qquad (1)$$

where $R = |\vec{X} - \vec{X}_1|$

$\vec{X}$ = the field point position vector

$\vec{X}_1$ = the source point position vector

$d\tau_1$ = the volume element with respect to integration over the source field

Refer to Fig. 1 for the geometry associated with this representation. Equation (1) represents a solution of the vector Poisson equation $\nabla^2 \vec{W} = -\vec{U}$. Thus,

$$\vec{U} = -\nabla^2 \vec{W} = -\nabla(\nabla \cdot \vec{W}) + \nabla \times (\nabla \times \vec{W}) \tag{2}$$

Equation (2) yields a representation of the vector field $\vec{U}$ in terms of the negative gradient of a scalar and the curl of a vector. Let

$$\phi \equiv \nabla \cdot \vec{W}, \tag{3}$$

and

$$\vec{A} \equiv \nabla \times \vec{W} \tag{4}$$

The scalar ϕ and the vector $\vec{A}$ are the scalar and vector potentials of the vector field $\vec{U}$, respectively. The general representation of a vector field as the sum of an irrotational field and a solenoidal field has been attributed to Helmholtz.[4(a)] Denoting the irrotational field by $\vec{U}_I$ and the solenoidal field by $\vec{U}_S$, then,

$$\vec{U} = \vec{U}_I + \vec{U}_S$$

where $\vec{U}_I = -\nabla \phi$

$\vec{U}_S = \nabla \times \vec{A}$

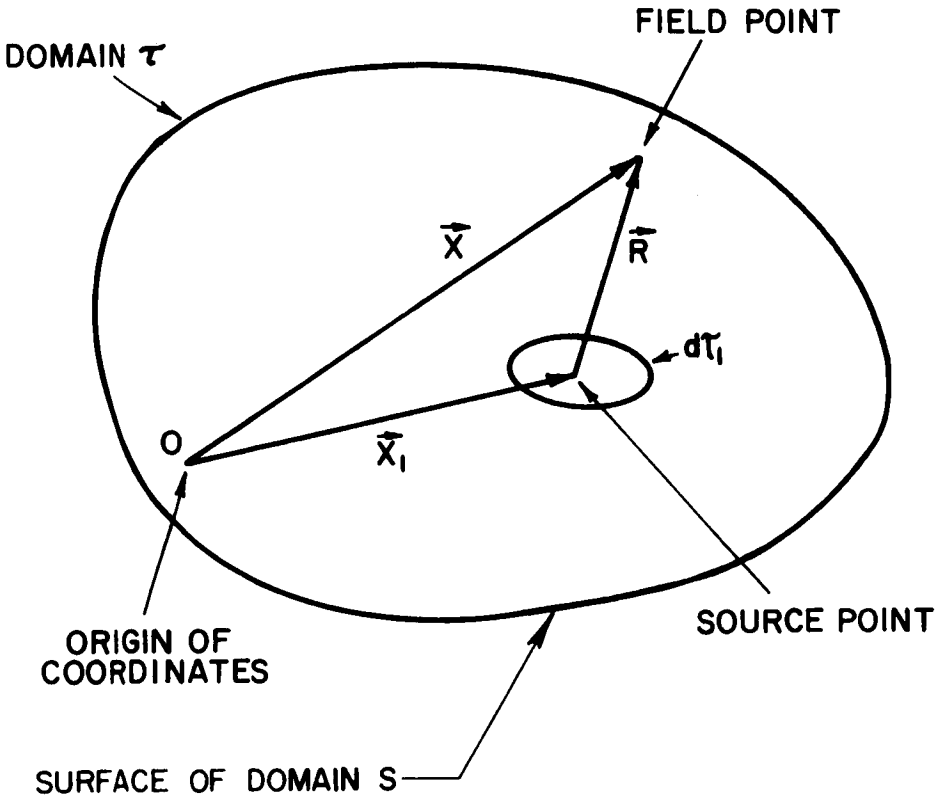

FIGURE I. GEOMETRY ASSOCIATED WITH THE VECTOR NOTATION

Taking the divergence of Equation (1) with respect to the field point coordinates $\vec{X}$ yields*

$$\phi = \frac{1}{4\pi}\int_{\tau} \vec{U}_1 \cdot \nabla \frac{1}{R}\, d\tau_1$$

where the operator ∇ is with respect to the field point $\vec{X}$. Because of the symmetry of R with respect to $\vec{X}$ and $\vec{X}_1$, however, one has

$$\nabla \left(\frac{1}{R}\right) = - \nabla_1 \left(\frac{1}{R}\right) \tag{5}$$

where the operator ∇_1 is with respect to the source point X_1. Thus,

$$\phi = - \frac{1}{4\pi} \int_{\tau} \vec{U}_1 \cdot \nabla_1 \left(\frac{1}{R}\right) d\tau_1$$

Noting the $\vec{U}_1 \cdot \nabla_1 \left(\frac{1}{R}\right) = \nabla_1 \cdot \left(\frac{1}{R} \vec{U}_1\right) - \frac{1}{R} \nabla_1 \cdot \vec{U}_1$ and making use of the Gauss divergence theorem, the scalar potential may be finally written

$$\phi = \frac{1}{4\pi} \int_{\tau} \frac{\nabla_1 \cdot \vec{U}_1}{R}\, d\tau_1 - \frac{1}{4\pi} \int_{S} \frac{\vec{U}_1 \cdot d\vec{S}_1}{R} \tag{6}$$

Equation (6) relates ϕ to the divergence of $\vec{U}$ in τ and to the normal component of $\vec{U}$ on S.

---

*Variables with a subscript 1 denote evaluation at the source point $\vec{X}_1$.

Taking the curl of Equation (1) yields

$$\vec{A} = -\frac{1}{4\pi}\int_{\tau} \vec{U}_1 \times \nabla \frac{1}{R}\, d\tau_1$$

Using the identity, Equation (5), results in the expression

$$\vec{A} = \frac{1}{4\pi}\int_{\tau} \vec{U}_1 \times \nabla_1 \left(\frac{1}{R}\right) d\tau_1$$

By employing the vector identity

$$\vec{U}_1 \times \nabla_1 \left(\frac{1}{R}\right) = \frac{1}{R}\nabla_1 \times \vec{U}_1 - \nabla_1 \times \left(\frac{\vec{U}_1}{R}\right),$$

the integrand may be expressed in the form

$$\vec{A} = -\frac{1}{4\pi}\int_{\tau} \left[\nabla_1 \times \left(\frac{\vec{U}_1}{R}\right) - \frac{\nabla_1 \times \vec{U}_1}{R}\right] d\tau_1$$

Making use of the appropriate vector integral theorem related to the Gauss theorem, one has

$$\int_{\tau} \nabla_1 \times \left(\frac{\vec{U}_1}{R}\right) d\tau_1 = -\int_{S} \frac{\vec{U}_1 \times d\vec{S}_1}{R}$$

which yields, finally

$$\vec{A} = \frac{1}{4\pi}\int_{\tau} \frac{\nabla_1 \times \vec{U}_1}{R}\, d\tau_1 + \frac{1}{4\pi}\int_{S} \frac{\vec{U}_1 \times d\vec{S}_1}{R} \qquad (7)$$

Equation (7) relates the vector potential to the curl of $\vec{U}$ throughout τ and to the tangential components of $\vec{U}$ on S.

Taking the negative gradient of Equation (6) with respect to the field point $\vec{X}$, and using the identity

$$\nabla \frac{1}{R} = - \frac{\vec{R}}{|\vec{R}|^3}$$

one obtains

$$- \nabla \phi = + \frac{1}{4\pi} \int_\tau (\nabla_1 \cdot \vec{U}_1) \frac{\vec{R}}{|\vec{R}|^3} d\tau_1 - \frac{1}{4\pi} \int_S (\vec{U}_1 \cdot \vec{n}_1) \frac{\vec{R}}{|\vec{R}|^3} dS_1 \qquad (8)$$

Equation (8) shows the irrotational field is related to the divergence of $\vec{U}$ throughout τ and to the normal components of $\vec{U}$ on S.

Taking the curl of Equation (7) yields

$$\nabla \times \vec{A} = \frac{1}{4\pi} \int_\tau (\nabla_1 \times \vec{U}_1) \times \frac{\vec{R}}{|\vec{R}|^3} d\tau_1 + \frac{1}{4\pi} \int_S (\vec{U}_1 \times \vec{n}_1) \times \frac{\vec{R}}{|\vec{R}|^3} dS_1 \qquad (9)$$

Equation (9) shows the solenoidal field is related to the curl of $\vec{U}$ throughout τ and to the tangential components of $\vec{U}$ on S.

Equations (6) and (7), and (8) and (9), respectively express the potentials and the field values in terms of the volume distribution of the divergence and curl of $\vec{U}$ and the components of $\vec{U}$ on the boundary of the domain.

3. Field Components on the Boundary

The representation given by Equations (8) and (9) does not correspond with the statements made in Sec. II A 1. in the sense that the surface integral in Equation (9) involves the tangential components of $\vec{U}$ on $\vec{S}$ rather than the normal components alone. It may be shown, however, that the combination of the surface integrals in Equations (8) and (9) give rise to a field that is irrotational and solenoidal, so that specification of the divergence and curl of the field throughout the region, together with only the normal component of $\vec{U}$ on the surface of a simply connected region is sufficient to define the field to within a constant vector.

To demonstrate the latter, consider the vector field to be represented by the sum of three velocity fields in the region τ and on its surface.

$$\vec{U} = \vec{U}_{I\tau} + \vec{U}_{S\tau} + \vec{E}_p \tag{10}$$

where

$$\vec{U}_{I\tau} = \frac{1}{4\pi} \int_\tau (\nabla_1 \cdot \vec{U}_1) \frac{\vec{R}}{|\vec{R}|^3} \, d\tau_1 \tag{11}$$

$$\vec{U}_{S\tau} = \frac{1}{4\pi} \int_\tau (\nabla_1 \times \vec{U}_1) \times \frac{\vec{R}}{|\vec{R}|^3} \, d\tau_1 \tag{12}$$

and

$$\vec{E}_p = -\frac{1}{4\pi} \int_S (\vec{U}_1 \cdot \vec{n}_1) \frac{\vec{R}}{|\vec{R}|^3} \, dS_1 + \frac{1}{4\pi} \int_S (\vec{U}_1 \times \vec{n}_1) \times \frac{\vec{R}}{|\vec{R}|^3} \, dS_1 \tag{13}$$

Let the region exterior to τ and extending to infinity contain no sources for the field, that is, $\nabla \cdot U = \nabla \times \vec{U} = 0$ outside τ. Since the field

$\vec{U}$ in τ due to a given distribution of sources in space does not depend on the particular choice of τ, let a new domain τ' be defined to include τ and part of the region exterior to τ. For any point in τ, then, the volume integrals yielding $\vec{U}_{I\tau}$ and $\vec{U}_{S\tau}$ do not depend on the choice for τ'. Thus, the remaining field $\vec{E}_p$ and therefore the surface integrals which determine $\vec{E}_p$ must be independent of the choice of τ'. Taking τ' sufficiently large, the surface integrals vanish subject to the condition that $\vec{U} \to 0$ sufficiently fast[2] as $R \to \infty$, and so they vanish identically. Thus, $\vec{E}_p = 0$ for this case. For the general situation, then, the surface integrals may be seen to represent the contribution to $\vec{U}$ of all sources ($\nabla \cdot \vec{U}$, $\nabla \times \vec{U}$) outside τ. Inverting the domains in the foregoing example, let $\nabla \cdot \vec{U} = \nabla \times \vec{U} = 0$ within τ, and non-zero in some bounded region exterior to τ. Thus, $\vec{E}_p$ is then solenoidal and irrotational within τ and may be represented by a harmonic function given in terms of its normal components over S,

$$\vec{E}_p = -\frac{1}{4\pi} \int_S \nabla G\,(\vec{X}, \vec{X}_1)\, \vec{U}_1 \cdot d\vec{S}_1 \qquad (14)$$

where $G\,(\vec{X}, \vec{X}_1)$ is Green's function of the second kind[5] for τ. This problem of finding a potential function, harmonic in a region τ, bounded by a surface S, and having normal derivatives given on the boundary is known as Neumann's problem. The general representation of the field as given by Equation (10) is also described by Batchelor[6(a)].

B. Solenoidal Fields

Most of the discussion in the following section is concerned with incompressible flow, for which the divergence of the velocity field is

zero. Thus, the volume integral involving the divergence of the source field (equation (11)) for this case will be zero. The velocity field may then be expressed as

$$\vec{U} = \vec{U}_{S_\tau} + \vec{E}_p \tag{15}$$

Thus, the determination of a solenoidal field is completely determined by evaluating a volume integral of the curl of the vector field and then solving the appropriate problem in potential theory. It is this problem that is of principal concern in the following sections.

C. Time Dependent Fields

In many situations in fluid mechanics, time-varying phenomena must be considered. Frequently, this phenomena is in the form of turbulence. As long as one is not concerned with relativistic theory and relativistic effects, time may be regarded merely as a parameter of the vector field. For that case, all of the above relations are valid for a time varying field $\vec{U}(\vec{X}, t)$. Because of the linear character of the vector equations, the time averaged field is simply that computed from the time averaged divergence, curl, and surface normal components of the field. Stating this another way, the time averaged field is that field computed from the divergence and curl of the time averaged field and the surface normal components. Thus, time averaged equations have the same form as the steady state equations.

D. Axisymmetric Fields

For axisymmetric fields with no tangential component

$$\vec{U} = U_r \vec{i}_r + U_z \vec{i}_z \qquad \text{(cylindrical coordinates)}$$

or

$$\vec{U} = U_\rho \vec{i}_\rho + U_\phi \vec{i}_\phi \qquad \text{(spherical coordinates)}$$

then

$$\nabla \times \vec{U} = \left(\frac{\partial U_r}{\partial z} - \frac{\partial U_z}{\partial r} \right) \vec{i}_\theta \qquad \text{(cylindrical coordinates)}$$

or

$$\nabla \times U = \frac{1}{\rho} \left(\frac{\partial \rho \, U_\phi}{\partial \rho} - \frac{\partial U_\rho}{\partial \phi} \right) \vec{i}_\theta \qquad \text{(spherical coordinates)}$$

and

$$\vec{R} = [X_r \vec{i}_r + X_\theta \vec{i}_\theta + X_z \vec{i}_z] - [X_{r1} \vec{i}_{r1} + X_{\theta 1} \vec{i}_{\theta 1} + X_{z1} \vec{i}_{z1}]$$

(cylindrical coordinates)

$$R = [X_\rho \vec{i}_\rho + X_\phi \vec{i}_\phi + X_\theta \vec{i}_\theta] - [X_{\rho 1} \vec{i}_{\rho 1} + X_{\phi 1} \vec{i}_{\phi 1} + X_{\theta 1} \vec{i}_{\theta 1}]$$

(spherical coordinates)

The geometry of the fields are shown in Figs. 2 and 3. The coordinates with subscript 1 correspond to a source point and the nonsubscripted coordinates correspond to a field point.

E. Green's Function for a Semi-Infinite Domain

Assuming the divergence, the curl, and the normal component of a vector field $\vec{U}$ are specified within a given domain, it can be useful to employ Green's function of the second kind to determine the component of the vector field denoted by $\vec{E}_p$ (Equation 14). Since

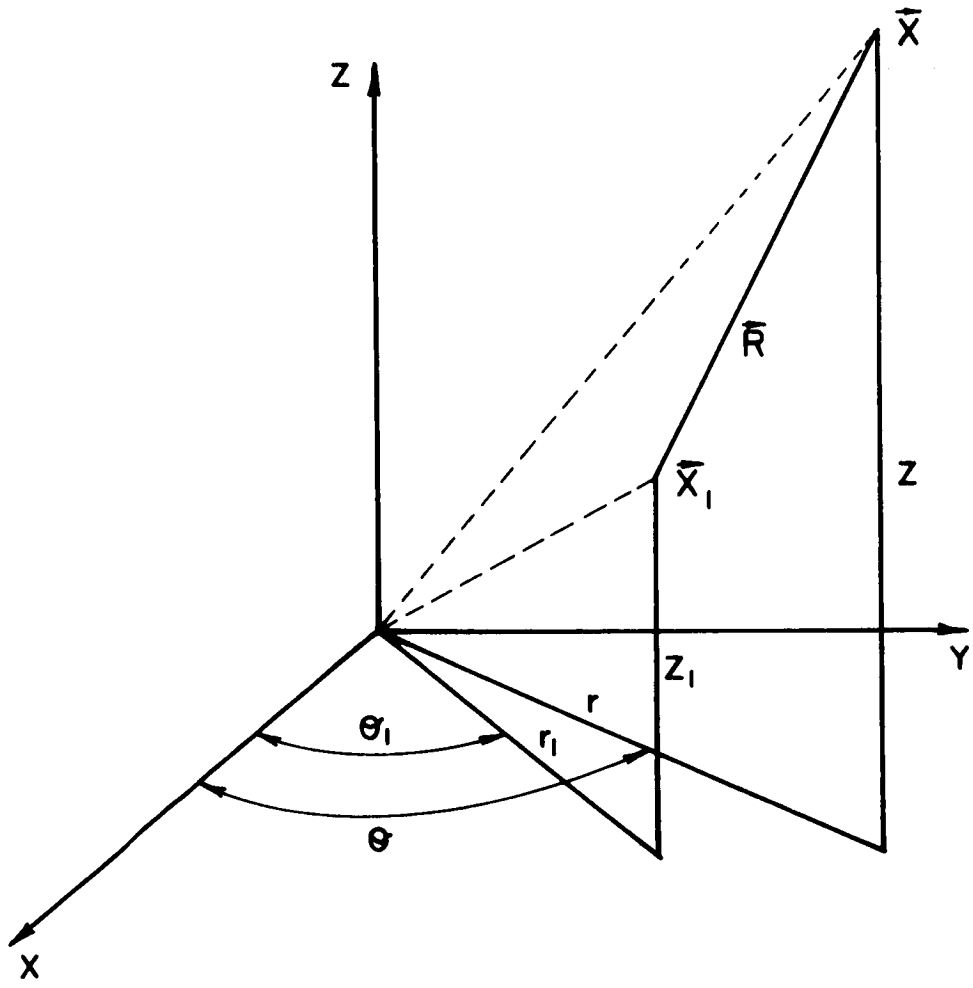

FIGURE 2. CYLINDRICAL COORDINATES

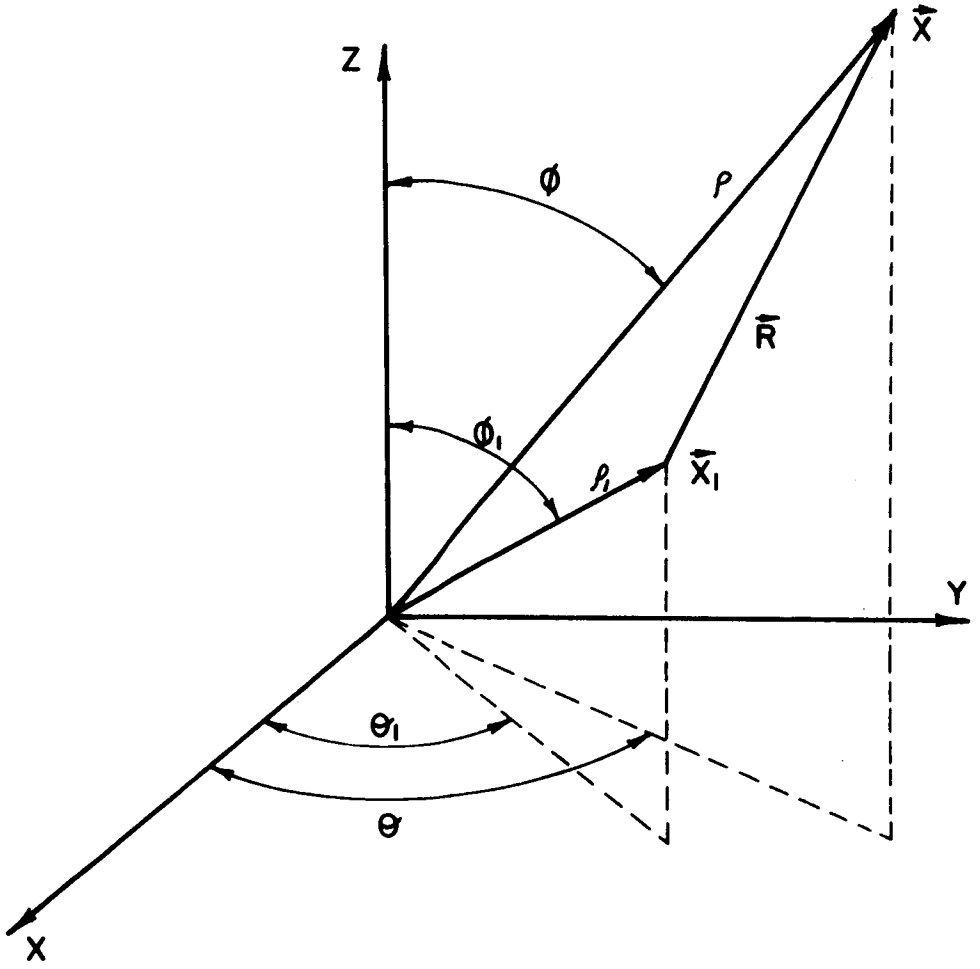

FIGURE 3. SPHERICAL COORDINATES

$\vec{E}_p$ is irrotational it may be represented by the gradient of a scalar ψ. Thus, it follows from Equation (14) that

$$\psi = \frac{1}{4\pi} \int_S G\,(\vec{X}, \vec{X}_1)\, \vec{U}_1 \cdot d\vec{S}_1$$

with $\nabla^2\ \psi = 0$ throughout the domain.

Consider a simply connected finite region τ. To obtain the Green's function for this region, the following vector function is used.

$$\psi_1\ \nabla \frac{1}{R} - \frac{1}{R} \nabla\ \psi_1$$

where ψ_1 is harmonic within the domain τ. Express Green's theorem in the second form

$$\int_\tau (\psi_1\ \nabla^2 \frac{1}{R} - \frac{1}{R}\ \nabla^2\ \psi_1)\ d\tau_1 = \int_S (\psi_1 \frac{\partial}{\partial n} (\frac{1}{R}) - \frac{1}{R} \frac{\partial \psi_1}{\partial n})\ dS_1. \qquad (16)$$

The volume integral involving $\nabla^2\ \psi_1$ is zero. Solving the left side of Equation (16) for field points within the region τ, it follows that

$$\psi = -\frac{1}{4\pi} \int_S (\psi_1 \frac{\partial}{\partial n} (\frac{1}{R}) - \frac{1}{R} \frac{\partial \psi_1}{\partial n})\ dS_1 \qquad (17)$$

since $\nabla^2\ 1/R = 0$ except at $R = 0$ where it takes on a value of -4π. Equation (17) appears to indicate, that to obtain a solution for ψ, both ψ_1 and $\partial\psi_1/\partial n$ must be known on the surface. This is contradictory to Equation (14) which requires only the normal derivative ($\vec{U}_1 \cdot d\vec{S}_1 = \frac{\partial \psi_1}{\partial n}\ dS_1$). It is possible to express the integrand of Equation (17) in terms of $\partial\psi_1/\partial n$ alone.

In accordance with the presentation by Kellogg[5], consider a function H which is harmonic in τ, and form the vector function $\psi_1 \nabla H - H \nabla \psi_1$ analogous to that shown above for $H = 1/R$. Thus, Green's theorem in the second form for this vector function yields

$$0 = -\frac{1}{4\pi} \int_S \left(\psi_1 \frac{\partial H}{\partial n} - H \frac{\partial \psi_1}{\partial n}\right) dS_1 \tag{18}$$

Addition of Equations (17) and (18) yields

$$\psi = -\frac{1}{4\pi} \int_S \left[\psi_1 \frac{\partial}{\partial n}\left(\frac{1}{R} + H\right) - \frac{\partial \psi_1}{\partial n}\left(\frac{1}{R} + H\right)\right] dS_1. \tag{19}$$

The combined scalar $\left(\frac{1}{R} + H\right)$ is called Green's function of the second kind. The scalar potential may be eliminated from the integrand by requiring that the normal derivative of Green's function on the surface be zero.

The function H must differ from $-1/R$, in general since H is harmonic at all points within τ whereas $1/R$ has a singularity within τ. It may be noted that the surface integral of $\frac{\partial}{\partial n}\frac{1}{R}$ is -4π and the surface integral of the normal derivative of the harmonic function H is zero. If $\partial H/\partial n$ differs from $-\frac{\partial}{\partial n}\frac{1}{R}$ by a constant at points on the surface, the surface integral involving ψ_1 yields a constant. With that choice for $\partial H/\partial n$, Equation (19) provides a relation for ψ in terms of $\partial \psi_1/\partial n$ on the surface to within a constant. The determination of Green's function $G(\vec{X}, \vec{X}_1)$ then reduces to solving the following problem.

$$G(\vec{X}, \vec{X}_1) = \frac{1}{R} + H(\vec{X}, \vec{X}_1) \tag{20}$$

where H is a harmonic function in τ satisfying the boundary conditions

$$\frac{\partial H}{\partial n} = - \frac{\partial \ 1/R \ (\vec{X}, \vec{X}_1)}{\partial n} + C \tag{21}$$

on the surface of the domain where C is a constant.

As an example, consider the semi-infinite domain shown in Fig. 4. The point $\vec{P}_1$ is the image with respect to the plane Z = 0 of the source point $\vec{r}_1$. If H is given the harmonic value $1/|\vec{r} - \vec{P}_1|$, and substituted into Equation (21), the results obtained are

$$\frac{\partial}{\partial n} \frac{1}{|\vec{r} - \vec{P}_1|} = - \frac{\partial}{\partial n} \frac{1}{|\vec{r} - \vec{r}_1|} \text{ on } S_1 \tag{22}$$

Thus

$$G = \frac{1}{|\vec{r} - \vec{r}_1|} + \frac{1}{|\vec{r} - \vec{P}_1|} \tag{23}$$

Note that the quantities $|\vec{r} - \vec{r}_1|$ and $|\vec{r} - \vec{P}_1|$ are equal whenever r_1 is on Z = 0. The required Green's function for the semi-infinite domain is then simply 2/R. For an infinite domain the appropriate Green's function degenerates to 1/R. Green's functions for various domains are discussed at length in Reference 4 (b).

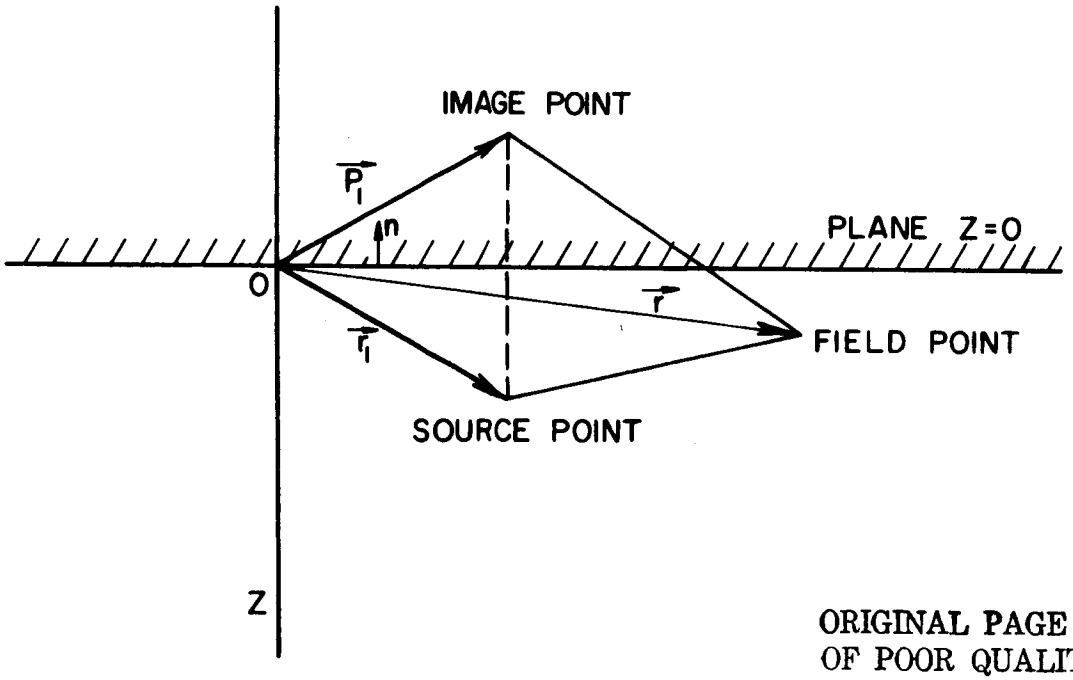

ORIGINAL PAGE IS
OF POOR QUALITY

FIGURE 4. SEMI-INFINITE DOMAIN

III. THE AERODYNAMIC FIELD OF A JET

Referring to Fig. 5, a jet exhausting into an airstream has the property that most of the turbulent flow remains confined within a relatively narrow, curved column. There generally will be a turbulent wake behind the jet, but for this discussion, it is convenient to consider the entire flow field to be comprised of two parts: the jet flow, and the flow outside the jet, or the aerodynamic field. The jet flow occupies that region containing any significant vorticity. The vorticity in the aerodynamic field, then, is presumed to be negligible. Experimental data for jet flows support such a separation of the flowfield based upon the absence or presence of vorticity[7]. The vorticity within the jet flow will consist of streamwise components as well as peripheral components, in general. The surface bounding the two regions is not a streamtube because the turbulent mixing action of the jet flow results in entrainment of air from the aerodynamic field.

Consider the simply connected region τ containing a jet. The velocity field $\vec{U}$ is uniquely defined by its divergence and curl throughout the region and the normal component of $\vec{U}$ on the surface bounding the region. For most purposes in aerodynamics, the field may be presumed to be solenoidal (incompressible)*. This solenoidal field $\vec{U}$, as previously shown (Equation (15)), may then be expressed

*The entire flowfield is here assumed to be incompressible, which would be a reasonable approximation for low-speed jets. For near sonic or supersonic jets, this would be clearly untenable.

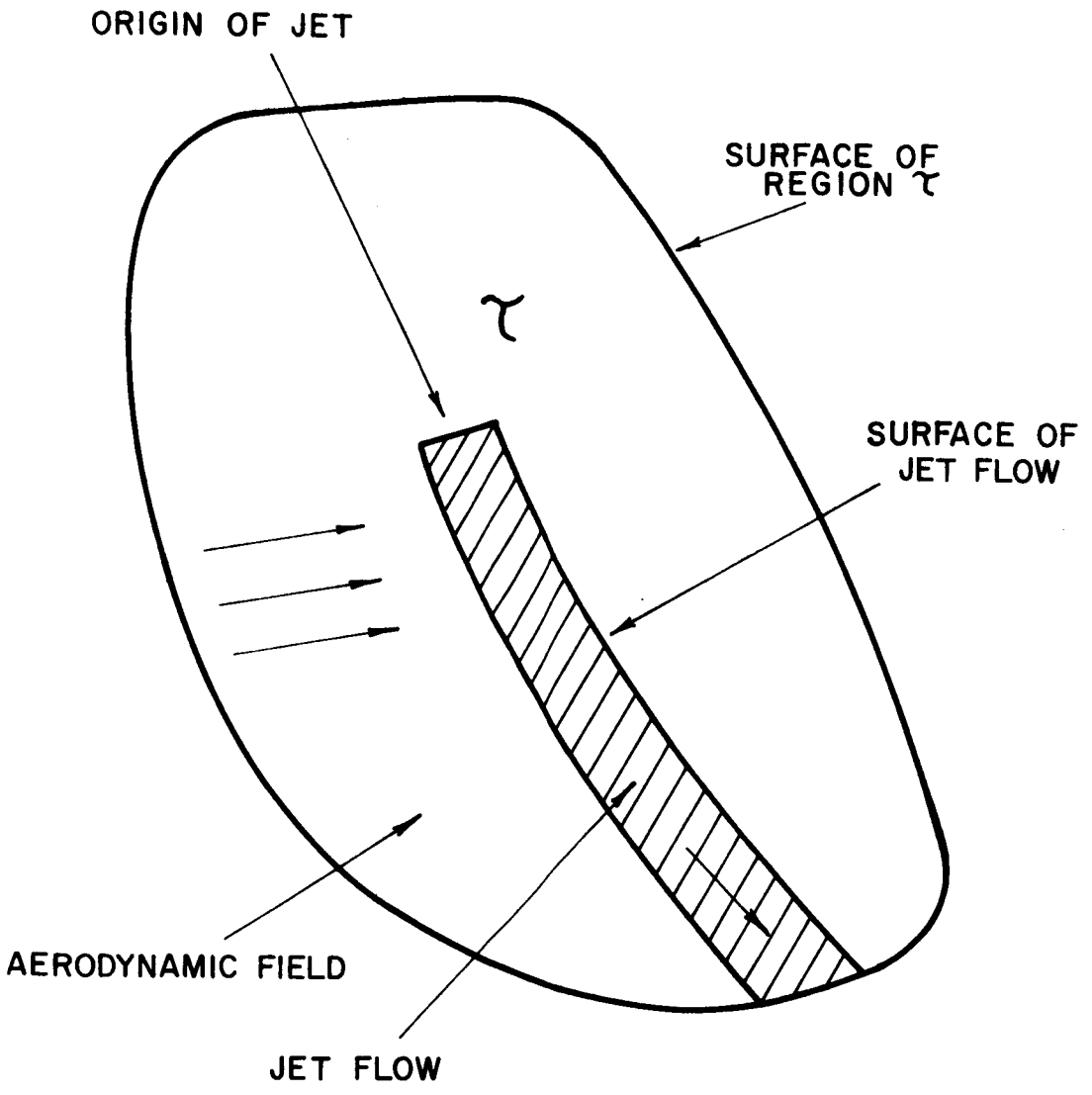

FIGURE 5. AERODYNAMIC FIELD AND JET FLOW

as the sum of the two component fields

$$\vec{U} = \vec{U}_{S\tau} + \vec{E}_p \tag{15}$$

The field $\vec{U}_{S\tau}$ depends on the distribution of vorticity throughout the region. However, the vorticity is confined to the jet flow. Thus, $\vec{U}_{S\tau}$ is solely dependent upon the sources within the jet flow. The remaining component field depends only on the distribution of the normal component of $\vec{U}$ on the surface of the region.

It is possible to determine the aerodynamic field in two ways. The first makes use of only the scalar potential, and the second utilizes both a scalar and a vector potential. In the following discussion, the symbol ϕ will be employed to denote the scalar potential of the aerodynamic flow field when the field is completely determined by only the scalar potential. The symbol ψ will denote the scalar potential for a flow field characterized by both a scalar and a vector potential. In the latter situation, the scalar potential ψ alone does not entirely characterize the flow field.

A. Method Based on the Scalar Potential

Consider a domain chosen in such a way as to exclude the jet flow. Refer to Fig. 6. The boundary (I) of the domain then contains the surface of the jet flow as one of its parts. Since the aerodynamic field within the domain is entirely irrotational and solenoidal, it may be completely represented by the potential field component $\vec{E}_p$ of Equation (10). Recalling Equation (14), the relation for $\vec{E}_p$ is

$$\vec{E}_p = -\frac{1}{4\pi} \int_S vG\,(\vec{X}, \vec{X}_1)\, \vec{U}_1 \cdot d\vec{S}_1 \tag{14}$$

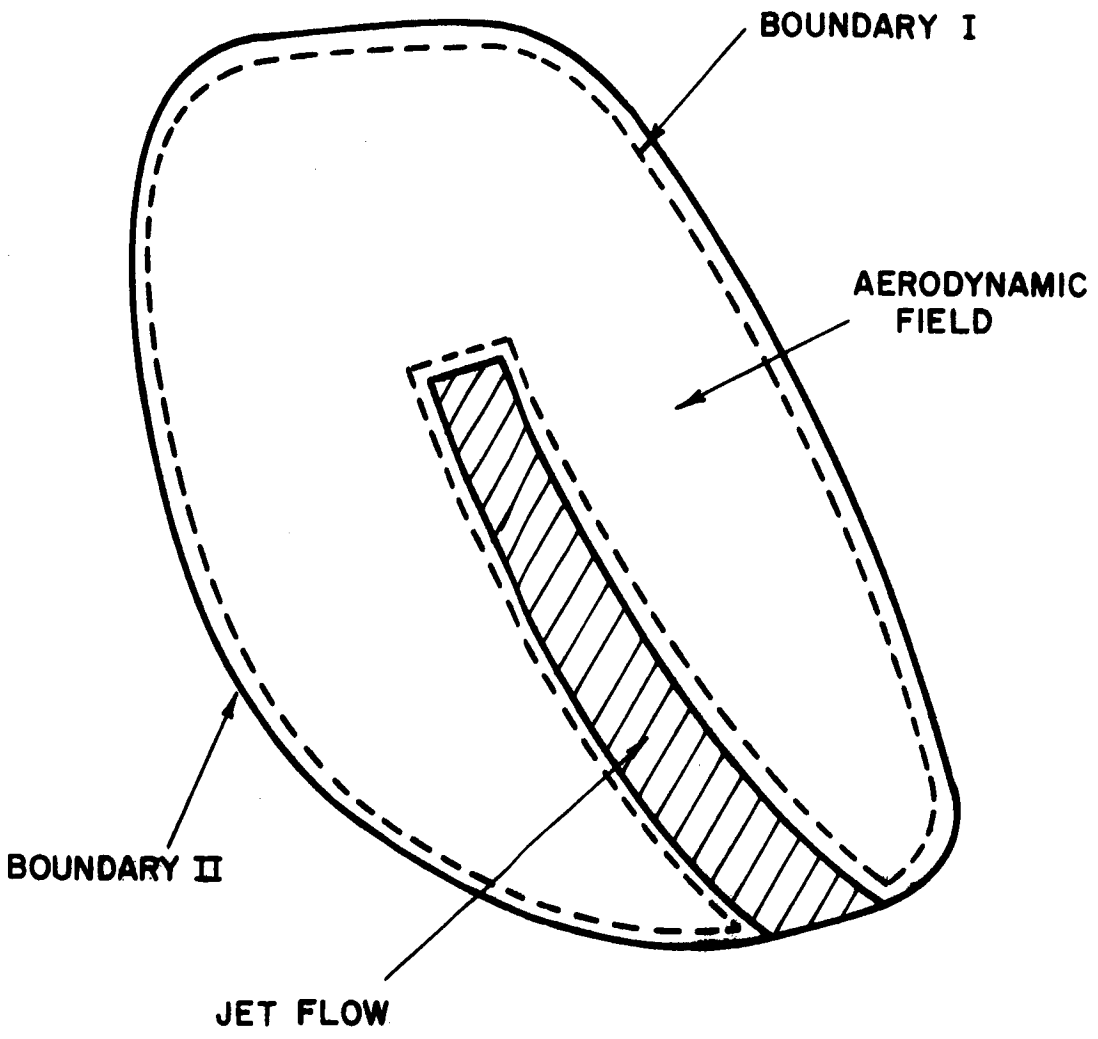

FIGURE 6. DOMAINS FOR AERODYNAMIC FIELD

Any solution for $\vec{E}_p$ in the subject domain requires specification of the normal component $\vec{U}_1 \cdot \vec{dS}_1$ on the surface of the domain. For most applications, such values may be obtained for the parts of the surface not bounding the jet flow. For those parts of the surface bounding the jet, values for $\vec{U}_1 \cdot \vec{dS}_1$ are available only with a rather high degree of uncertainty, even for simple jet configurations. That is true of data obtained either analytically or experimentally[8]. Furthermore, even if the boundary conditions on the surface of the jet could be obtained with acceptable accuracy, the solution of the potential problem (either by evaluating Green's function for the domain, or by alternate methods) remains complex except for problems with simple symmetry.

B. Method Based on the Stokes Potentials

Consider a boundary (II) taken around the region containing both the jet flow and the aerodynamic field (Fig. 6). This defines a domain for which the velocity field $\vec{U}$ is represented by $\vec{U}_{S\tau} + \vec{E}_p$ since the vorticity within the jet flow is not zero. This choice for the domain eliminates the requirement for knowing the normal component of $\vec{U}$ along the surface of the jet flow. In other words, the surface of the jet flow is no longer a boundary of the domain. The field in the region exterior to the jet flow is irrotational. Thus, the volume integral for the determination of $\vec{U}_{S\tau}$ in Equation (15) is taken only over the region occupied by the jet flow.

The formulation of this problem is somewhat more involved than the method of the scalar potential. Rewriting Equation (15), the

relationship for $\vec{U}$ is

$$\vec{U} = \frac{1}{4\pi}\int_{\tau} (\nabla_1 \times \vec{U}_1) \times \frac{\vec{R}}{|\vec{R}|^3}\, d\tau_1 - \frac{1}{4\pi}\int_{S} \nabla G\,(\vec{X}, \vec{X}_1)\, \vec{U}_1 \cdot dS_1 \qquad (24)$$

Now, the solution for $\vec{U}_{S\tau}$ involves the vorticity distribution within the jet region. Certainly the distribution is not known with precision for any turbulent jet. Nonetheless, the integral is the value required rather than the vorticity distribution proper, so that the uncertainty of the integrand may not be a serious problem in some circumstances. That is, if the integrand is only approximated, it may still be possible to obtain accurate values for the integral. This will be considered in Section IV. As far as the evaluation of the Green's function for the domain is concerned, there is more flexibility compared with the method in the preceding subsection. The choice of the domain can be made in any convenient way without requiring the boundary of the jet flow to be a part of the boundary of the domain.

C. Vorticity in the Jet Flow

The vorticity distribution in a turbulent jet is strictly a time-varying function. As noted in Sec. II, however, when only the time averaged vector field is to be determined, specification of the time averaged vorticity field and time averaged boundary conditions are sufficient to determine the solenoidal field (Equation (15)). This is due to the linearity of the vector field equations.

For most jets the principal time-averaged vorticity component is peripheral, or normal to the streamwise direction of the jet flow.

That is, the peripheral component of vortex lines form closed curves about the axis of the jet. For a jet in a cross-flow, there will be in addition, to this peripheral component, components of vorticity in the streamwise direction along the jet. The vorticity lines, resulting from the peripheral and streamwise components, will then be of a helical character. It is advantageous, for the purposes of discussion and for computations as well, to consider the vorticity field as separated into the sum of peripheral components and a streamwise component. Thus, for the vorticity field $\vec{\Omega}_1$,

$$\vec{\Omega}_1 = \vec{\Omega}_p + \vec{\Omega}_z \tag{25}$$

where $\vec{\Omega}_p$ is the peripheral component and lies in a surface normal to the streamwise direction, and $\vec{\Omega}_z$ is the streamwise component.

The magnitude of the peripheral component of vorticity in the jet flow has a distribution such as that illustrated in Fig. 7. The vorticity on the axis of the jet is zero, and the vorticity approaches zero asymptotically near the edge of the jet. Maximum values of vorticity are reached at positions between the axis and the edge of the jet flow.

Computations of the aerodynamic field induced by a jet by means of Equation (15) requires specification of the vorticity throughout the jet flow region. As mentioned before, precise data for the vorticity are not available, either from experimental data, or from analytical relations, even for jet flows of the simplest symmetry. However, there is not actually a need for precise vorticity data to obtain reasonably accurate data for the aerodynamic field, because only an

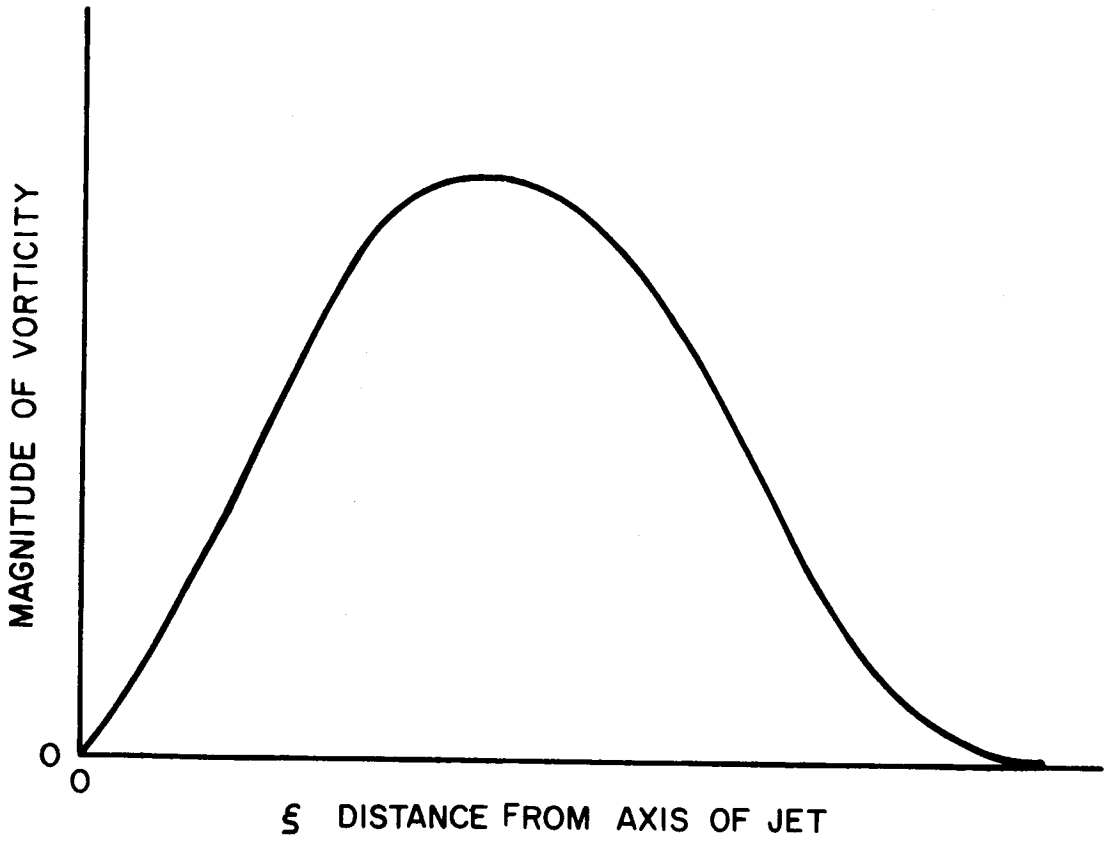

FIGURE 7. PERIPHERAL COMPONENT OF VORTICITY

integral of the vorticity is involved in the computations. It is then possible to obtain acceptable approximations for the computation of the aerodynamic field if only certain integral properties of the vorticity distribution are known, that is, providing the field points of interest are not close to the surface of the jet. At field points extremely close to the jet, of course, more accurate data become necessary.

When field points are sufficiently far from the jet flow region, the value of $|\vec{R}|$ in Equation (12) does not vary much over a cross section of the jet flow. The integral, then, can be reduced in an approximate way to a simpler relation involving only the integral of the vorticity and its moments over finite volume elements of the jet flow. This approximation leads to useful computational simplifications. For some problems, the integral of the vorticity for the region can be related to data for the jet flow that is known with considerable accuracy. Aerodynamic computations for such jet flows employing these methods might be expected to be of comparable or higher accuracy than computations previously made with other methods.

To illustrate the foregoing remarks, consider the contribution to the velocity at a field point $\vec{X}$ due to the vorticity within a small section of the jet flow. Refer to Fig. 8. The dimensions of the section of the jet flow under consideration are presumed to be small in comparison with the distance from the element to the field point. The section is a plane slice of the jet flow field of infinitesimal thickness. The extension to finite elements of the jet flow will be considered later.

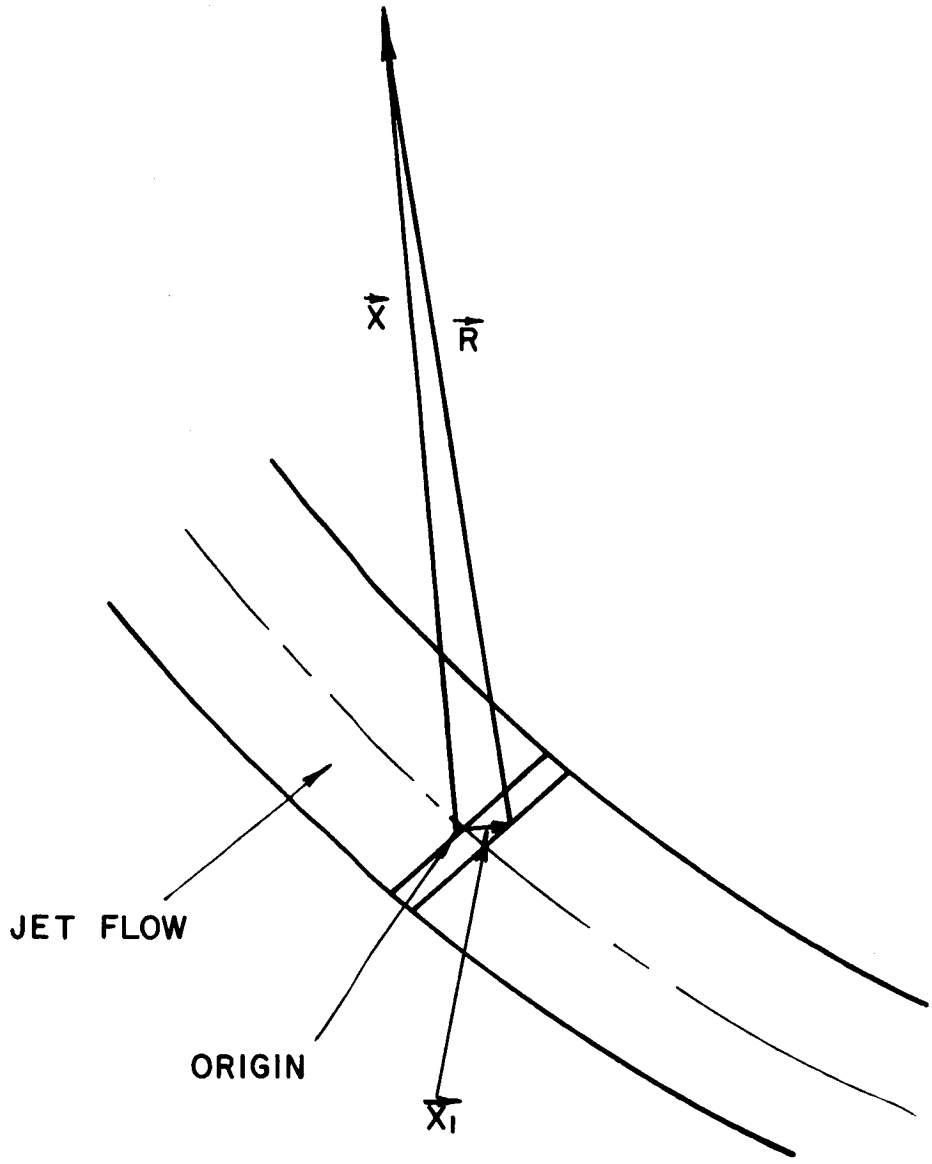

FIGURE 8. SMALL SECTION OF JET FLOW

Equation (12) may be expressed in the form

$$\vec{U}_{S\tau} = -\frac{1}{4\pi}\int_{\tau} \vec{\Omega}_1 \times \nabla \frac{1}{R}\, d\tau_1 \tag{26}$$

Expanding 1/R as a Taylor's series in $\vec{X}_1$, yields[6(b)]

$$\frac{1}{|\vec{X}-\vec{X}_1|} = \frac{1}{X} - X_{1i}\frac{\partial}{\partial X_i}\left(\frac{1}{X}\right) + \frac{1}{2}X_{1i}X_{1j}\frac{\partial^2}{\partial X_i\,\partial X_j}\left(\frac{1}{X}\right) \cdots$$

where $X = |\vec{X}|$

The subscripts denote components and the summation convention is implied. If only the first and second terms are retained, then in vector form

$$\frac{1}{|\vec{X}-\vec{X}_1|} = \frac{1}{X} - \vec{X}_1 \cdot \nabla\frac{1}{X}$$

Substituting for 1/R in Equation (26), yields the approximate equation

$$\vec{U}_{S\tau} \cong -\frac{1}{4\pi}\int_{\tau} \vec{\Omega}_1 \times \left[\nabla\frac{1}{X} - \vec{X}_1 \cdot \nabla\left(\nabla\frac{1}{X}\right)\right] d\tau_1$$

Since X is not a function of the source coordinates, $\vec{X}_1$, this equation can be expressed as

$$\vec{U}_{S\tau} \cong \frac{1}{4\pi}\nabla\frac{1}{X} \times \int_{\tau} \vec{\Omega}_1\, d\tau_1 + \frac{1}{4\pi}\int_{\tau} \vec{\Omega}_1 \times \left[\vec{X}_1 \cdot \nabla\left(\nabla\frac{1}{X}\right)\right] d\tau_1 \tag{27}$$

However, the integral of the first term can be expressed as

$$\int_{\tau} \vec{\Omega}_1\, d\tau_1 = \int_{\tau} \Omega_{1i}\, d\tau_1 = \int_{\tau} \nabla_1 \cdot (X_{1i}\,\vec{\Omega}_1)\, d\tau_1$$

From the divergence theorem, then

$$\int_{\tau} \nabla_1 \cdot (X_{1i} \vec{\Omega}_1)\, d\tau_1 = \int_S X_{1i} \vec{\Omega}_1 \cdot d\vec{S}_1 \tag{28}$$

Considering Equation (28) and the expression for the vorticity in Equation (25), yields for the integrand of Equation (28)

$$\int_S X_{1i} \vec{\Omega}_1 \cdot d\vec{S}_1 = \int_S X_{1i} (\vec{\Omega}_p + \vec{\Omega}_z) \cdot d\vec{S}_1 \tag{29}$$

It can be concluded that since $\vec{\Omega}_p$ is everywhere tangent to the surface S of the element then the contribution from the peripheral component of vorticity in Equation (29) is zero. If the streamwise component of vorticity, $\vec{\Omega}_z$, is non-zero, then the first term of Equation (27) yields

$$\frac{1}{4\pi} \nabla \frac{1}{X} \times \int_{\tau} \vec{\Omega}_1\, d\tau_1 = \frac{1}{4\pi} \nabla \frac{1}{X} \times \int_{\tau} \vec{\Omega}_z\, d\tau_1 \tag{30}$$

Since the first term yields no contribution of the peripheral component to $\vec{U}_{S_\tau}$, the second term of Equation (27) must be used to evaluate its contribution. Likewise, if the integral of the streamwise component in the first term is also zero, then the higher-order approximation must be obtained, using the second term of Equation (27).

Consider now the case where the vorticity is entirely peripheral, $\vec{\Omega}_z \equiv 0$. The first integral in Equation (27) is zero. The expression for $\vec{U}_{S_\tau}$ in Equation (27), using the vector identity

$$\nabla \times (\phi \vec{A}) = \phi \nabla \times \vec{A} + (\nabla \phi) \times \vec{A}$$

then becomes

$$\vec{U}_{S\tau} \cong -\frac{1}{4\pi} \nabla \times \int_{\tau} \vec{\Omega}_1 \vec{X}_1 \cdot \nabla \frac{1}{X} d\tau_1 \tag{31}$$

Rewriting the dyadic $\vec{\Omega}_1 \vec{X}_1$ in the integrand in terms of skew-symmetric and symmetric parts, yields for the integral in Equation (31)

$$\int_{\tau} \vec{\Omega}_1 \vec{X}_1 \cdot \nabla \frac{1}{X} d\tau_1 = \frac{1}{2} \int_{\tau} (\vec{\Omega}_1 \vec{X}_1 \cdot \nabla \frac{1}{X} - \vec{X}_1 \vec{\Omega}_1 \cdot \nabla \frac{1}{X}) d\tau_1 + \frac{1}{2} \int_{\tau} (\vec{\Omega}_1 \vec{X}_1 \cdot \nabla \frac{1}{X} + \vec{X}_1 \vec{\Omega}_1 \cdot \nabla \frac{1}{X}) d\tau_1$$

Noting that the second integral on the right can be rewritten as

$$\frac{1}{2} \left\{ \int_{\tau} (\vec{\Omega}_1 \vec{X}_1 + \vec{X}_1 \vec{\Omega}_1) d\tau_1 \right\} \cdot \nabla \frac{1}{X}$$

and since

$$\int_{\tau} (X_{1i} \Omega_{1j} + X_{1j} \Omega_{1i}) d\tau_1 = \int_{\tau} \nabla \cdot (X_{1i} X_{1j} \vec{\Omega}_1) d\tau_1 = 0$$

only the first integral (skew-symmetric part) contributes to $\vec{U}_{S\tau}$ in this case. Using the vector identity

$$\vec{B} (\vec{C} \cdot \vec{A}) - \vec{A} (\vec{C} \cdot \vec{B}) = -\vec{C} \times (\vec{A} \times \vec{B})$$

the skew-symmetric integral can be written as

$$-\frac{1}{2} (\nabla \frac{1}{X}) \times \int_{\tau} (\vec{X}_1 \times \vec{\Omega}_1) d\tau_1$$

Substituting this value for the integral in Equation (31) and using the vector identities

$$\nabla \times (\vec{A} \times \vec{B}) = \vec{B}\cdot\nabla\vec{A} - \vec{A}\cdot\nabla\vec{B} + \vec{A}\nabla\cdot\vec{B} - \vec{B}\nabla\cdot\vec{A}$$

$$\nabla (\vec{A}\cdot\vec{B}) = \vec{A}\cdot\nabla\vec{B} + \vec{B}\cdot\nabla\vec{A} + \vec{A}\times (\nabla\times \vec{B}) + \vec{B}\times (\nabla \times \vec{A})$$

finally yields,

$$\vec{U}_{S\tau} \cong \frac{1}{8\pi} \nabla \left[(\nabla \frac{1}{X}) \cdot \int_\tau \vec{X}_1 \times \vec{\Omega}_1 \, d\tau_1 \right] \tag{32}$$

Equation (32) shows that for the conditions considered, that of peripheral vorticity only, the significant term remaining involves only the integral of the moment $\vec{X}_1 \times \vec{\Omega}_1$, over the volume element of the jet. It is possible to relate the latter integral to the circulation about a vortex ring or an element of a vortex sheet, and then to the velocity in the jet flow. If one considers the more general case for $\nabla \left\{ \nabla \frac{1}{X} \cdot \int_\tau (\vec{X}_1 \times \vec{\Omega}_1) \, d\tau_1 \right\}$ it is possible to relate this term to either a combination of a source doublet and a vortex doublet.

For computational purposes, it is possible to replace the volume distribution of vorticity in the element of the jet by a discrete, closed line vortex of appropriate properties. The properties of the line vortex corresponding to the volume distribution of vorticity may be evaluated as follows.

For a plane closed curve C, the line integral

$$\vec{A}_1 = \frac{1}{2} \oint_C \vec{X}_1 \times d\vec{X}_1 \tag{33}$$

yields a vector normal to the surface of a magnitude equal to the area enclosed by the curve C (Fig. 9). The circulation, Γ, is defined as the line integral of $\vec{U}_1$ around a closed curve C bounding an arbitrary

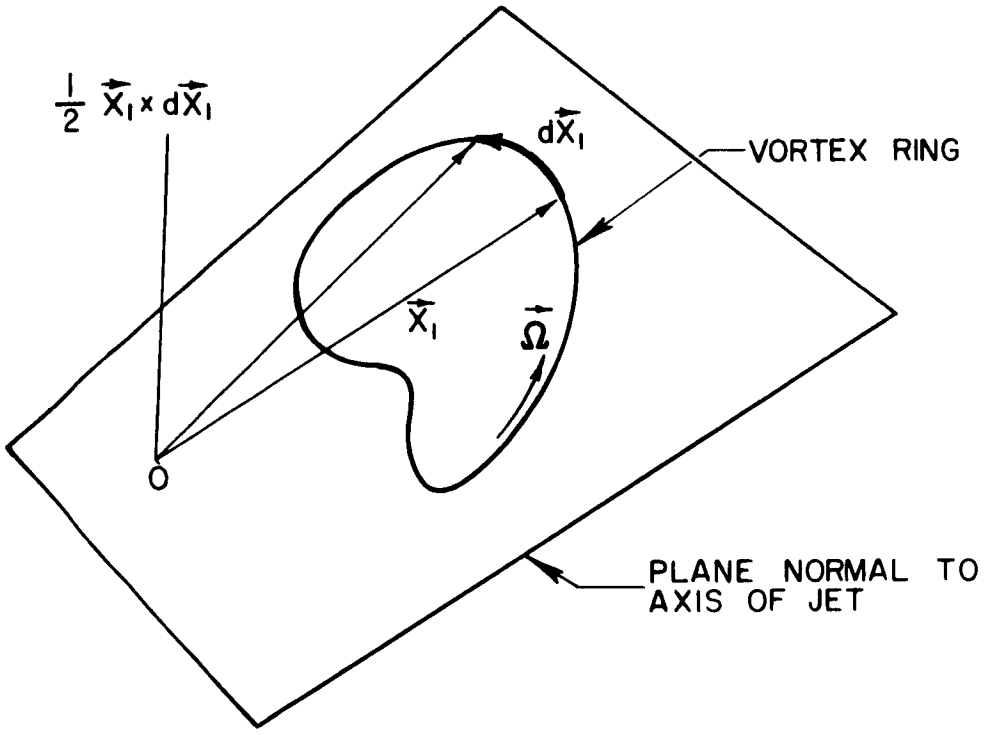

FIGURE 9. GEOMETRY FOR THE LINE INTEGRAL

surface in the flow. Thus

$$\Gamma = \oint_C \vec{U}_1 \cdot \vec{dL}_1$$

where $\vec{dL}_1$ is an element of the curve. By employing Stoke's theorem the relation between circulation and vorticity may be expressed as

$$\int_S \vec{\omega}_1 \cdot \vec{dS}_1 = \oint_C \vec{U}_1 \cdot \vec{dL}_1 = \Gamma \tag{34}$$

where the surface integral is over the surface bounded by the curve C.

Considering one-half times the integral of Equation (32) and using Equations (33) and (34), yields for a closed ring vortex in the plane normal to the axis of the jet.

$$\frac{1}{2} \int_\tau \vec{X}_1 \times \vec{\Omega}_1 \, d\tau_1 = \frac{1}{2} \int_\tau (\vec{X}_1 \times \vec{dX}_1) \, \Omega_p \, \vec{dS}_1$$

where the surface element dS_1 is that of the cross section of the vortex ring and $\vec{dX}_1$ denotes the differential line element along the vortex ring. The above expression may be written

$$\frac{1}{2} \int_C (\vec{X}_1 \times \vec{dX}_1) \int_S \vec{\Omega}_p \cdot \vec{n} \, dS_1 = \Gamma \vec{A}_1$$

where $\vec{\Omega}_p$ is the vorticity of the closed ring vortex in the direction $\vec{dX}_1$ and A_1 is the area enclosed by the ring. By considering a series of vortex rings along the axis of the jet, an element of a vortex sheet is obtained.

Considering finally $\nabla\left[\nabla \frac{1}{X} \cdot \int_\tau (\vec{X}_1 \times \vec{\Omega}_1) \, d\tau_1\right]$ and letting the integral term be represented by $\vec{m}$, yields

$$\nabla\left(\nabla\frac{1}{X}\cdot\vec{m}\right)=(\vec{m}\cdot\nabla)\frac{\vec{X}}{X^3}=\vec{X}\left[\vec{m}\cdot\left(\nabla\frac{1}{X^3}\right)\right]+\frac{1}{X^3}(\vec{m}\cdot\nabla)\vec{X}$$

and expanding the above, results in an expression for the field of a dipole singularity.

$$\nabla\left(\nabla\frac{1}{X}\cdot\vec{m}\right)=-\frac{3\vec{X}(\vec{X}\cdot\vec{m})}{X^5}+\frac{\vec{m}}{X^3}$$

Thus, Equation (32) can also be expressed as a velocity field induced by a dipole of strength $\vec{m}$ equal to the integral of the moment $\vec{X}_1 \times \vec{\Omega}_1$.

The streamwise component of vorticity $\vec{\Omega}_z$ is more difficult to treat analytically, but the following might be noted. Considering the first order approximation expressed by Equation (30), this yields for an equivalent line vortex

$$\frac{1}{4\pi}\nabla\frac{1}{X}\times\int_\tau\vec{\Omega}_z\,d\tau_1=\frac{\Gamma}{4\pi}\nabla\frac{1}{X}\times\int d\vec{X}_1$$

where $d\vec{X}_1$ is a vector element of the line vortex. When Γ is zero (no net rotation of the jet), the second term involving $\vec{\Omega}_z$ in Equation (27) must be considered. By analogy with the foregoing for $\vec{\Omega}_p$, it may be anticipated that the contribution will be equivalent to that of a vortex doublet.

All of the above approximations are for large R. As previously stated, more accurate approximations may be required for points of the aerodynamic field close to the jet flow. The foregoing approximations provide insight into the nature of the analysis, as will be shown in the following sections.

IV. THE AXISYMMETRIC JET IN A QUIESCENT ATMOSPHERE

As an application of the methods discussed in the foregoing sections, the most elementary situation with regard to jet flows is that of the axisymmetric jet exhausting into a quiescent environment. The vorticity in a jet of that type is entirely peripheral. No streamwise vorticity is present, except in the turbulent motion of the fluid. Since only the time averaged properties of the flow field are of significance in computations of the steady aerodynamic field, turbulent fluctuations do not enter the computations. Before examining the computational aspects of determining the induced aerodynamic field, the nature of an axisymmetric jet is briefly reviewed below. A synopsis of some of the literature pertinent to such jets is included in Appendix A.

A turbulent jet exhausting into a quiescent atmosphere is generally considered to comprise three regions (Fig. 10). Region I, the potential core region, is characterized by a central region of uniform "potential flow,"* separated from the aerodynamic field by a turbulent mixing layer. The mixing layer grows in thickness downstream from the lip of the nozzle. At the end of the potential core region the inner boundary of

---

*Such a characterization presumes the dominant flow from the nozzle is essentially uniform. There will always be boundary layers present adjacent to the wall. In some situations, the flow from the nozzle might have the appearance of a fully developed turbulent pipe flow.

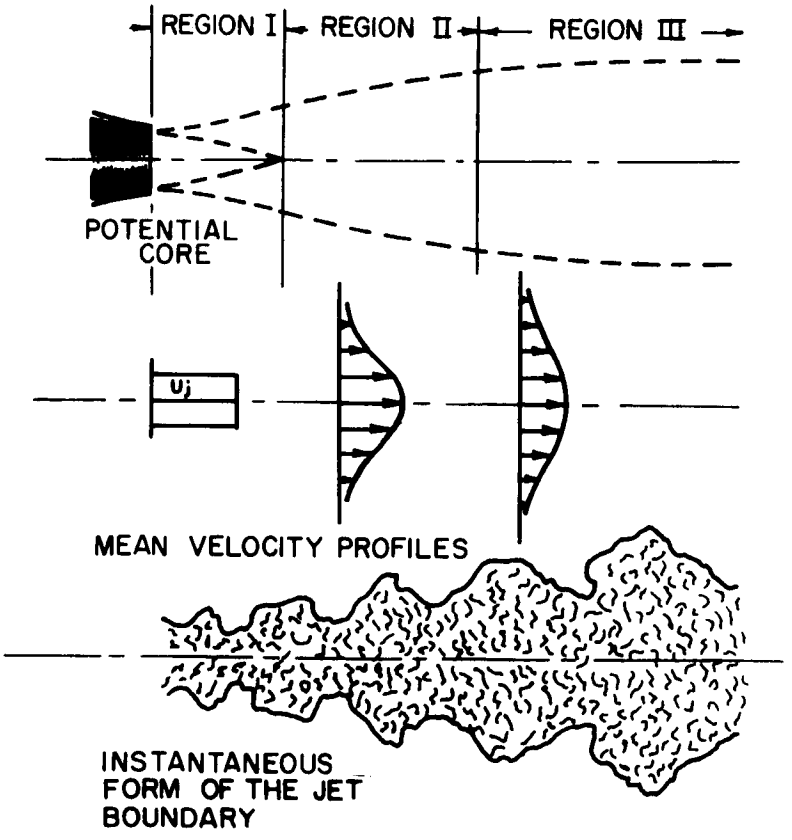

FIGURE 10. AXISYMMETRIC TURBULENT JET

the mixing layer reaches the axis. The growth of the mixing layer is observed to be approximately linear and the velocity profiles, as a function of a radial difference normalized with respect to the width of the mixing layer, exhibit similarity.[9(a)] At some point downstream from the end of Region I, the flow becomes developed in the sense that the radial profiles of axial velocity exhibit similarity (Region III). That is, the radial distribution of velocity, normalized with respect to the velocity at the centerline of the jet becomes a function of $r/r_{\frac{1}{2}}$ only. The radius $r_{\frac{1}{2}}$ is the radius at which the velocity is half that at the axis of the jet. In Region III, $r_{\frac{1}{2}}$ increases linearly with distance in the downstream direction. The velocity at the centerline decreases as $1/Z$ where Z is the streamwise coordinate along the jet. Region II, between Regions I and III, termed the transition region, has been found to exhibit non-similar velocity profiles. The decay of the centerline velocity begins in the transition region. For most purposes, the transition region may be considered to be rather short, on the order of 2 nozzle diameters in length.

The boundary of the jet flow, introduced in Sec. III, was defined to enclose the region containing significant time-averaged vorticity. The instantaneous position of a jet surface has the appearance shown in Fig. 10. The jet surface separates regions of irrotational fluid from those of turbulent, rotational fluid. The above definition of the jet boundary, then, would be a surface enclosing the extreme positions of the instantaneous surface of the jet flow.

The mass rate of flow, associated with the jet flow, increases in the downstream direction. Thus, the boundary of the jet flow is not

a streamtube since fluid from the environment crosses the boundary to become entrained in the jet flow. In the developed flow region of an axisymmetric jet, the rate of increase of the mass flow rate per unit length along the jet becomes constant. This rate of increase in the mass rate of flow in the jet per unit length of the jet is termed the mass entrainment rate, E_m. The mass entrainment rate is simply related to the normal component of velocity at points on the boundary of the jet. For an axisymmetric jet, the mass entrainment rate may be expressed as

$$E_m = 2\pi\, r_o\, U_n\, \rho$$

where r_o is the radius of the boundary and U_n is the component of velocity normal to the boundary and directed inward toward the jet axis. Recalling that the boundary conditions required for determining the aerodynamic field by means of the scalar potential (Sec. IIIA) involved specification of the normal component of velocity on the boundary of the jet flow, it is apparent that those boundary conditions are equivalent to specification of the E_m.

Now, as noted in Sec. IIIA, E_m is known for jet flows only with a rather high degree of uncertainty. That is true from both analytical and experimental viewpoints. For example, Ricou and Spalding[10] examined the available data and analytical relations finding that if the entrainment were expressed as

$$E_m = K_1 \sqrt{M\rho} \tag{35}$$

where M is the momentum flux and ρ the mass density of the jet fluid, then values for K_1 were found to range from 0.22 to 0.404. Experiments

by Ricou and Spalding[10] to obtain the value of the entrainment rate yielded a value of 0.282 for the mixing of an air jet with air. On the other hand Wygnanski[11] has found the higher value for K_1, corresponding to the Schlichting profile, of 0.404 yielded agreement with data he obtained. Other studies appear to show similar uncertainties in the entrainment rate.[8] Such uncertainties might be expected because of the sensitivity of the entrainment to regions of the jet near its edge, where measurements are difficult to obtain with accuracy and where theoretical relations there may not be expected to be accurate, that is, at least in the boundary layer approximation.

From the foregoing remarks, it is apparent that however accurately the geometry of the problem of computing the aerodynamic field may be treated, the boundary conditions are known only with a high degree of uncertainty for methods based on the use of the scalar potential alone. The following discussion, then, is concerned with similar computations based on the use of the Stokes potentials. The use of the Stokes potentials for the computation involves data for the jet flow known with higher accuracy. Thus, its use might be expected to yield more accurate results under some conditions.

A. Formulation of the Problem

Consider an axisymmetric, incompressible, turbulent jet exhausting normally through an infinite plane baffle plate into a quiescent atmosphere. $\vec{U}$ is uniquely defined in the semi-infinite, simply connected region τ by specifying the curl of $\vec{U}$ throughout τ and the normal component of $\vec{U}$ on the surface S bounding the region τ. Since the time-averaged flow is assumed to be axisymmetric and without swirling action,

the vorticity has only one component ω_θ (cylindrical coordinates), as shown in Sec. IID. The vorticity is solely peripheral. This implies that the aerodynamic field is also axisymmetric with only r and z components. The entire domain of vorticity will be assumed to be that of the mixing region around the potential core and of the fully developed region of the jet flow. The transition region of the jet flow is not considered separately in this formulation. That is, the fully developed part of the jet flow is simply presumed to start at the end of the potential core.

As discussed in Sec. II the aerodynamic velocity field may be separated into the sum of two fields $\vec{U}_{S\tau}$ and $\vec{E}_p$. The boundary conditions to be satisfied for the domain are that the normal velocity component on the plane baffle plate be zero; it will be presumed that the normal velocity component at points of the plane within the circumference of the jet orifice is uniform and equal to U_j, the jet velocity. The velocity at distant points approaching infinity must, of course, approach zero. The simplest means for satisfying those boundary conditions for this problem is to use the method of images. An image of the jet flow is placed along the negative Z axis. Contributions to the normal component of velocity at the baffle plane due to $\vec{U}_{S\tau}$ for the sum of the jet flow and its image thus vanish. The normal boundary condition remains to be satisfied by the $\vec{E}_p$ field*.

---

*Strictly speaking, to be consistent with the discussion of Sec. III, one should regard $\vec{E}_p$ as the sum of the contributions of the image of the region of vorticity plus the $\vec{E}_p$ field actually considered, for the semi-infinite domain. There is no fundamental difference involved, however, so there should be no confusion in the matter.

The normal component of $\vec{L}_p$ is zero at points in the baffle plane outside the circumference of the jet orifice, and U_j at points in the plane within the circumference of the jet orifice.

The aerodynamic velocity field $\vec{U}$ for the axisymmetric jet has two components (r and z) in cylindrical coordinates. Recalling Equations (12) and (15) the contributions to the r and z components of $\vec{U}$ due to the vorticity in the jet flow $\vec{U}_{S\tau}$ may be expressed as

$$U_{S\tau r} = \frac{1}{4\pi} \int_{\tau} \cos\theta_1 \, \Omega_{\theta 1} \, \frac{(z-z_1)}{R^3} \, r_1 \, dr_1 \, dz_1 \, d\theta_1 \tag{36}$$

$$U_{S\tau z} = -\frac{1}{4\pi} \int_{\tau} \Omega_{\theta 1} \, \frac{(r_1 - r\cos\theta_1)}{R^3} \, r_1 \, dr_1 \, dz_1 \, d\theta_1 \tag{37}$$

where the notation corresponds with that for cylindrical coordinates discussed in Sec. IID. The nonsubscripted variables refer to the field point $\vec{X}$, and the subscript 1 denotes values evaluated at the source point $\vec{X}_1$. The geometry associated with the Equations (36) and (37) is illustrated in Fig. 11. A small segment of the jet is shown in Fig. 11 as a truncated cone. The integrals of Equations (36) and (37) are taken over the points within the jet flow and its image. The value R in Equations (36) and (37) indicates the magnitude of $\vec{R} = \vec{X} - \vec{X}_1$, as shown in Fig. 11.

The irrotational and solenoidal part of $\vec{U}$, denoted by $\vec{E}_p$, satisfies the boundary conditions for the semi-infinite domain and is represented by Equation (14). For the present application, the equations may be written in component form as follows.

$$E_{pr} = \frac{U_j}{2\pi} \int_{S} \frac{(r - r_1\cos\theta_1)}{R^3} \, r_1 \, dr_1 \, d\theta_1 \tag{38}$$

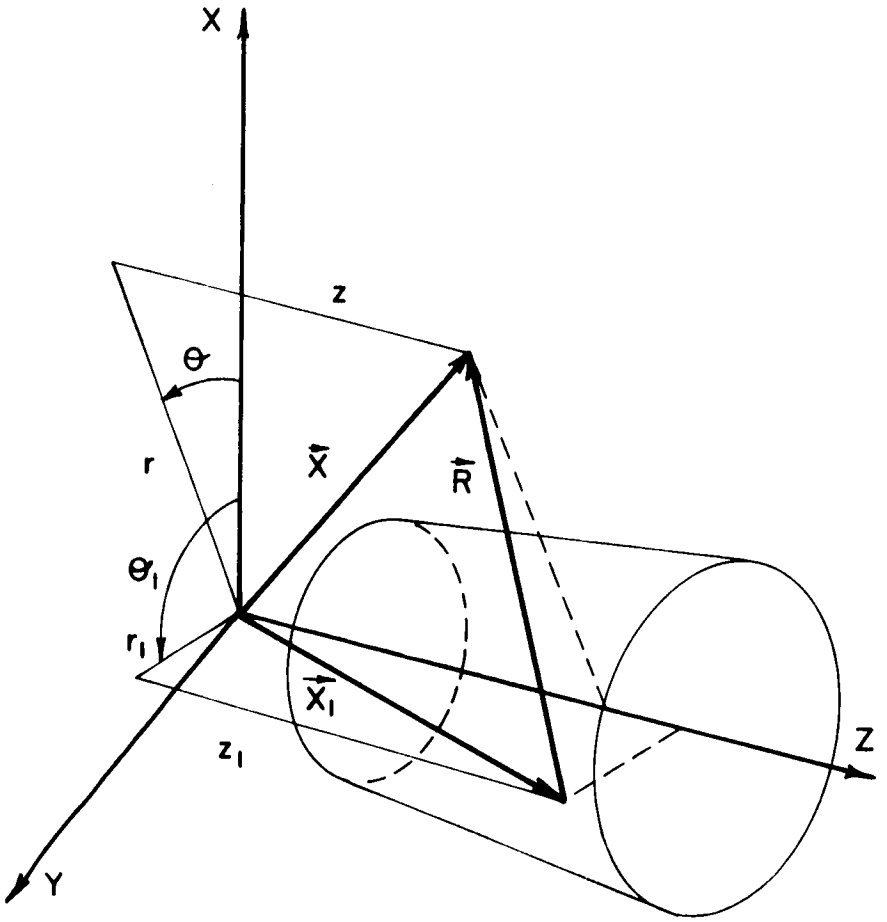

FIGURE 11. GEOMETRY ASSOCIATED WITH THE VOLUME INTEGRALS FOR $\bar{U}_{s\tau}$

$$E_{pz} = \frac{U_j}{2} \int_S \frac{(z-z_1)}{R^3} r_1 \, dr_1 \, d\theta_1 \tag{39}$$

where the notation corresponds to that previously discussed. The geometry for Equations (38) and (39) is shown in Fig. 12. The surface S surrounding the domain consists of an infinite plane at z = 0 and the remaining surrounding surface at infinity. The normal component of velocity along the boundary is zero except at the orifice. At points in the plane within the orifice circumference the normal component of velocity is presumed to be uniform with the magnitude U_j, the exit velocity of the jet. Thus, the only surface contributing to the surface integral is a flat disk of radius r_j, the exit radius of the jet orifice.

Integrating over the θ_1 direction and recalling that $\Omega_{\theta 1}$ is independent of θ_1, the above equations can be written as follows.

$$U_{S\tau r} = \frac{1}{2\pi r} \int_S \frac{\Omega_{\theta 1} (z-z_1)}{\sqrt{(r + r_1)^2 + (z-z_1)^2}} \left[\frac{r^2 + r_1^2 + (z-z_1)^2}{(r-r_1)^2 + (z-z_1)^2} \right.$$

$$\left. E(k) - K(k) \right] dr_1 \, dz_1 \tag{40}$$

$$U_{S\tau z} = -\frac{1}{2\pi} \int_S \frac{\Omega_{\theta 1}}{\sqrt{(r+r_1)^2+(z-z_1)^2}} \left[\frac{r^2-r_1^2 + (z-z_1)^2}{(r-r_1)^2+(z-z_1)^2} E(k) - K(k) \right] dr_1 \, dz_1 \tag{41}$$

$$E_{pr} = \frac{U_j}{\pi} \int_r \frac{r_1}{\sqrt{(r+r_1)^2 + z^2}} \left[\frac{r^2-r_1^2-z^2}{(r-r_1)^2 + z^2} E(k) + K(k) \right] dr_1 \tag{42}$$

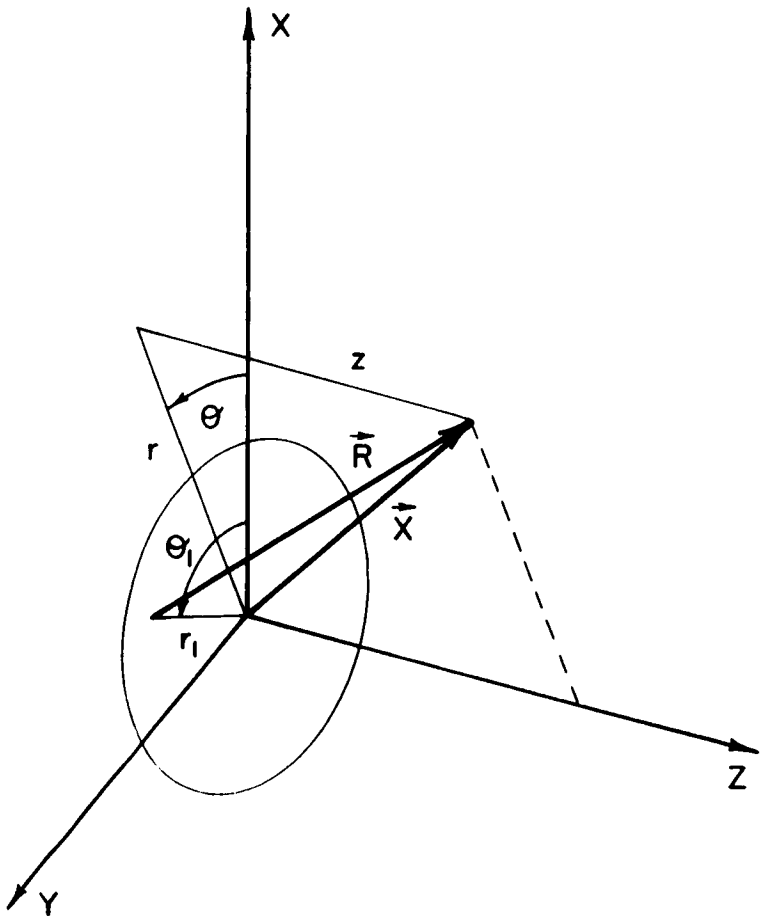

FIGURE 12. GEOMETRY ASSOCIATED WITH THE SURFACE INTEGRAL FOR $\vec{E}_p$

$$E_{pz} = \frac{2\,U_j\,z}{\pi} \int_r \frac{r_1}{\sqrt{(r + r_1)^2 + z^2}} \frac{E\,(k)}{[(r-r_1)^2 + z^2]} dr_1 \qquad (43)$$

where K (k) is a complete elliptic integral of the first kind and E (k) is a complete elliptic integral of the second kind. Derivations of Equations (40), (41), (42), and (43) are presented in Appendix B. Note that the integrals in Equations (40) through (43) involve integration only over the r_1 and z_1 coordinates in the jet flow.

B. Numerical Method

The integrals in Equations (40) through (43) may be evaluated numerically. For the purpose of numerical integration, it is convenient to transform the variables of integration in such a way that the domains of integration become rectangular. This may be accomplished in the following manner. Denote the inner radius of the mixing layer in the potential core region by r_I and the outer radius of the jet by r_o. The geometry for the jet flow is shown in Fig. 13a.

Introduce the transformation for the coordinates (r_1, z_1) in the mixing layer of the potential core region to the transformed variables (x_1, y_1).

$$\left.\begin{aligned} x_1 &= (r_1 - r_{I1})/(r_{o1} - r_{I1}) \\ y_1 &= z_1/r_j \end{aligned}\right\} \qquad (44)$$

where $r_{I1} = r_I\,(z_1)$,

$r_{o1} = r_o\,(z_1)$, and

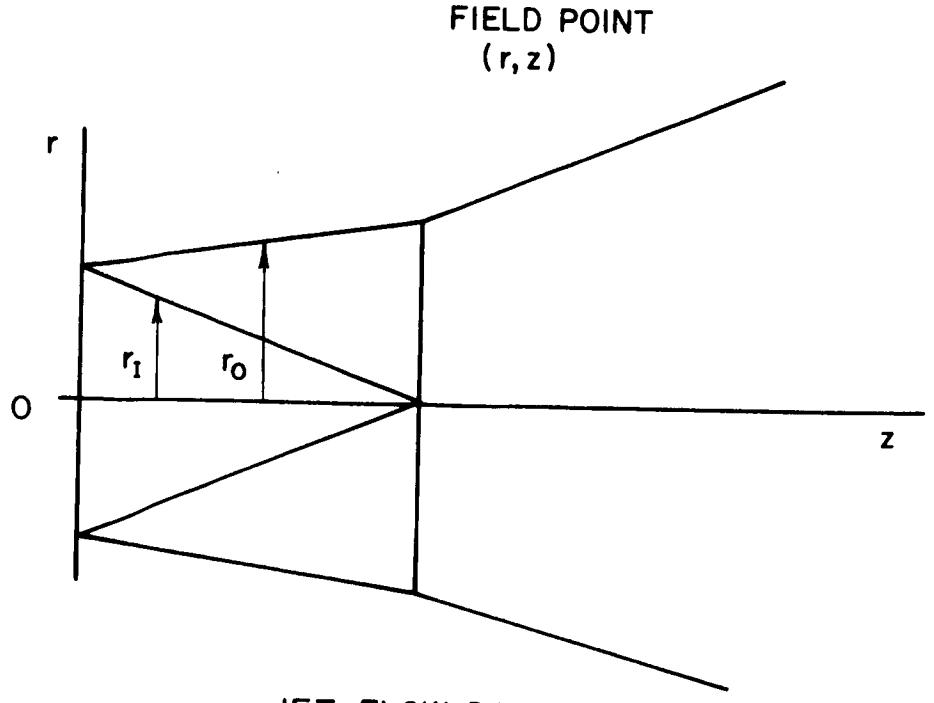

a. JET FLOW DOMAIN

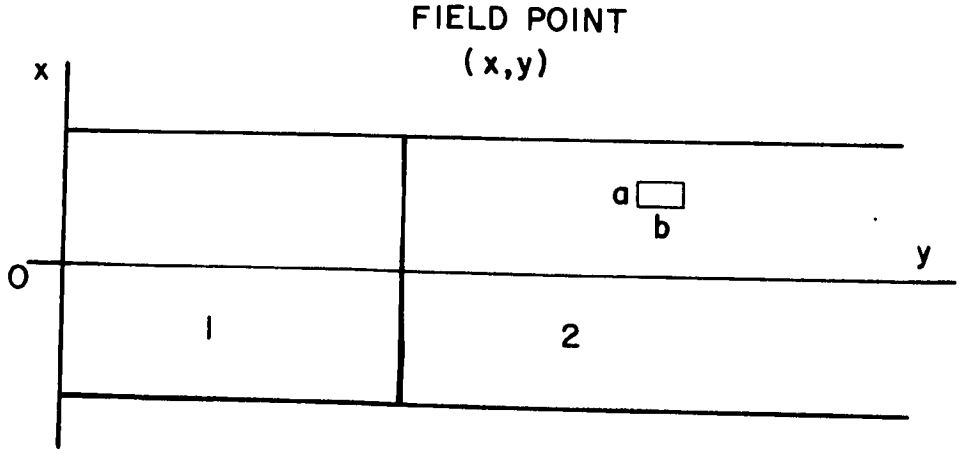

b. TRANSFORMED JET FLOW DOMAIN

FIGURE 13. GEOMETRY OF THE JET FLOW DOMAIN AND TRANSFORMED JET FLOW DOMAIN

r_j = the radius of the jet orifice

For the developed region of the jet, the transformation from (r_1, z_1) to (x_1, y_1) employed is as follows.

$$\left.\begin{aligned} x_1 &= r_1/r_{o1} \\ y_1 &= z_1/r_j \end{aligned}\right\} \quad (45)$$

The notation corresponds to that described above. The coordinates for the surface integration over the orifice area in the plane $z_1 = 0$, let

$$\left.\begin{aligned} x_1 &= r_1/r_j \\ y_1 &= z_1 = 0 \end{aligned}\right\} \quad (46)$$

Finally, for the field point coordinates, introduce the transformation from (r, z) to (x, y) as follows.

$$\left.\begin{aligned} x &= r/r_o\ (z) \\ y &= z/r_j \end{aligned}\right\} \quad (47)$$

The transformations (44), (45), (46), and (47) transform the original domain in the (r, z) plane to the rectangular domain in the (x, y) plane as shown in Fig. 13. Region 1 is the mixing region surrounding the core. The fully developed jet flow is represented by region 2. It should be noted that the region of integration in the x_1 direction extends only from 0 to $+\infty$. The region of integration in the y_1 direction contains, in addition to the interval $(0, +\infty)$, the region of integration over the image from 0 to $-\infty$.

It is convenient, in addition, to normalize the velocity components with respect to U_j, and the vorticity component with respect to U_j/r_j. Thus, the appropriate relations are

$$\left.\begin{aligned} U_x &= U_{S_\tau r}/U_j & E_x &= E_{pr}/U_j \\ U_y &= U_{S_\tau z}/U_j & E_y &= E_{pz}/U_j \\ \Omega &= \Omega_\theta r_j/U_j & 1 &= U_j/U_j \end{aligned}\right\} \quad (48)$$

Substituting the relations (44) to (48) into Equations (40) through (43) yields the following equations.

$$U_x = -\frac{r_j}{2\pi r_o x}\int_{-\infty}^{\infty}\int_0^1 \frac{(r_{o1}-r_{I1})\,\Omega\,(y_1-y)}{\sqrt{\left\{r_o x + [(r_{o1}-r_{I1})\,x_1 + r_{I1}]\right\}^2 + r_j^2\,(y-y_1)}}$$

$$\left[\frac{r_o^2\,x^2 + [(r_{o1}-r_{I1})\,x_1 + r_{I1}]^2 + r_j^2\,(y-y_1)^2}{\left\{r_o x - [(r_{o1}-r_{I1})\,x_1 + r_{I1}]\right\}^2 + r_j^2\,(y-y_1)^2}\,E(k_1) - K(k_1)\right]\,dx_1\,dy_1$$

$$-\frac{r_j}{2\,r_o x}\int_{-\infty}^{\infty}\int_0^1 \frac{r_{o1}\,\Omega\,(y_1-y)}{\sqrt{(r_o x + r_{o1}\,x_1)^2 + r_j^2\,(y-y_1)^2}}$$

$$\left[\frac{r_o^2\,x^2 + r_o^2 x_1^2 + r_j^2\,(y-y_1)^2}{(r_o x - r_{o1}\,x_1)^2 + r_j^2\,(y-y_1)^2}\,E(k_2) - K(k_2)\right]\,dx_1\,dy_1 \quad (49)*$$

---

*The integration is to be performed over the jet flow (0 to ∞) and its image (0 to $-\infty$). It should be noted that y_1 is replaced by $-y_1$ and Ω is replaced by $-\Omega$ for the image integration.

$$U_y = -\frac{1}{2\pi}\int_{-\infty}^{\infty}\int_0^1 \frac{(r_{o1}-r_I)\,\Omega}{\sqrt{\left\{r_o x + [(r_{o1}-r_{II})+r_{II}]\right\}^2 + r_j^2\,(y-y_1)^2}}$$

$$\left[\frac{r_o^2x^2 - [(r_{o1}-r_{II})\,x_1 + r_{II}]^2 + r_j^2\,(y-y_1)^2}{\left\{r_o x - [(r_{o1}-r_{II})\,x_1 + r_{II}]\right\}^2 + r_j^2\,(y-y_1)^2}\,E(k_1) - K(k_1)\right] dx_1\,dy_1$$

$$-\frac{1}{2\pi}\int_{-\infty}^{\infty}\int_0^1 \frac{r_{o1}\;\Omega}{\sqrt{(r_o x + r_{o1}x_1)^2 + r_j^2\,(y-y_1)^2}}$$

$$\left[\frac{r_o^2x^2 - r_{o1}^2x_1^2 + r_j^2\,(y-y_1)^2}{(r_o x - r_{o1}x_1)^2 + r_j^2\,(y-y_1)^2}\,E(k_2) - K(k_2)\right] dx_1\,dy_1 \qquad (50)^*$$

$$E_x = \frac{r_j^2}{\pi r_o x}\int_0^1 \frac{x_1}{\sqrt{r_o x + r_j x_1)^2 + r_j^2\,y^2}}\left[\frac{r_o^2x^2 - r_j^2x_1^2 - r_j^2\,y^2}{(r_o x - r_j x_1)^2 + r_j^2\,y^2}\right.$$

$$\left.E(k_3) + K(k_3)\right] dx_1 \qquad (51)$$

$$E_y = \frac{r_j^3}{\pi}\int_0^1 \frac{2\,x_1 y}{\sqrt{(r_o x + r_j x_1)^2 + r_j^2\,y^2}}\,\frac{E(k_3)}{[(r_o x - r_j x_1)^2 + r_j^2\,y^2]}\,dx_1 \qquad (52)$$

where for Equations (49) and (50) the first integrals on the right side are taken over the core region and the second integrals are taken over

---

*The integration is to be performed over the jet flow (0 to ∞) and its image (0 to $-\infty$). It should be noted that y_1 is replaced by $-y_1$ and Ω is replaced by $-\Omega$ for the image integration.

the developed region. The moduli k_1, k_2 and k_3 for the complete elliptic integral functions are

$$k_1^2 = \frac{4\, r_o x\, [(r_{o1}-r_{I1})\, x_1 + r_{I1}]}{\left\{r_o x + [(r_{o1}-r_{I1})\, x_1 + r_{I1}]\right\}^2 + r_j^2\, (y-y_1)^2} \tag{53}$$

$$k_2^2 = \frac{4\, r_o x\, r_{o1}\, x_1}{(r_o x + r_{o1} x_1)^2 + r_j^2\, (y-y_1)^2} \tag{54}$$

$$k_3^2 = \frac{4\, r_o x\, r_j\, x_1}{(r_o x + r_j\, x_1)^2 + r_j^2\, y^2} \tag{55}$$

It should be noted that the transformations employed do not strictly lead to the integrals in Equations (49) and (50) because the transformed coordinates are not orthogonal. Nonetheless, the error involved in the approximation of the differential surface element can be shown to be of negligible order because of the small spreading angles of the jet. Numerical integration of the equations by this method and by a different method not involving a transformation of the domain yielded identical results to four significant figures.

For the purposes of numerical computation, the numerical algorithms for evaluating the complete elliptic integrals were taken from references 12, 13, and 14. Those algorithms were found to be compact and of demonstrated accuracy to six significant figures. The algorithms are listed in Appendix C.

The integrals in Equations (49) and (50) are of the form

$$A = \int_S f(x_1, y_1)\, dx_1\, dy_1 \tag{56}$$

where the variables (x, y) not entering the integration process are suppressed for convenience of notation. The method of integration adopted for the numerical evaluation of the integrals employed the trapezoidal rule for double integrals[15]. The algorithm may be obtained as follows. Let $f(x_1, y_1)$ be locally approximated by the relation

$$f(x_1, y_1) = \alpha + \beta\, y_1 + \gamma\, x_1 + \delta\, x_1\, y_1 \tag{57}$$

in a rectangular element of the domain of dimensions a and b (Refer to Fig. 13). Assume for the purpose of discussion that the origin of coordinates is at the lower left corner of the element and define the functions f_0, f_1, f_2, and f_3 as follows.

$$\left.\begin{aligned} f_0 &= f(0, 0) & f_2 &= f(0, b) \\ f_1 &= f(a, 0) & f_3 &= f(a, b) \end{aligned}\right\} \tag{58}$$

The coefficients in Equation (57) may then be expressed in terms of these values.

$$\alpha = f_0 \qquad \gamma = (f_1 - f_0)/a$$
$$\beta = (f_2 - f_0)/b \qquad \delta = (f_3 - f_2 - f_1 + f_0)/ab$$

Evaluation of the integral in Equation (56) then results in the algorithm

$$I = \frac{ab}{4}(f_0 + f_1 + f_2 + f_3)$$

where I denotes the numerical approximation for A over the small elemental surface considered.

The integrals in Equations (51) and (52) involve integration with respect to a single variable. The trapezoidal rule was adopted for the numerical integration of those integrals. For an integral of the form

$$A' = \int g\ (x_1)\ dx_1$$

the numerical algorithm for a small increment of length a may be written

$$I' = \frac{a}{2}\ (g_0 + g_1)$$

where $g_0 = g\ (0)$ and $g_1 = g\ (a)$, taking the origin arbitrarily at 0 for the purpose of discussion as before.

The integration method employing the trapezoidal rule, either for single or double integrals, is of second order, the error decreasing as h^2 where h is a characteristic size of the element of the domain[15]. More precisely,

$$A - I = \varepsilon = c_1\ a^2 + c_2\ b^2$$

for the double integrals, and

$$A' - I' = \varepsilon' = c_0\ a^2$$

for the single integrals. This second order behavior of the method has been found to hold in the computations made in this study, as evidenced by the changes in the solution occurring when the grid size was successively halved.

The division of the different regions into a network of elemental areas was as follows. For the mixing layer of the potential core region (first integrals in Equations (49) and (50), a square grid was chosen in the x_1, y_1 plane. For the fully developed region (second integrals

in Equations (49) and (50), a rectangular grid with aspect ratio of 10 was chosen, with the longer dimension in the streamwise direction. Computations for the fully developed region employing aspect ratios of 5 and 2.5 were also made and compared with the aspect ratio of 10. These comparisons showed identical results to three significant figures.

C. Computations for Selected Vorticity Distributions

Several theoretical jet velocity profiles were selected for the purpose of comparing the aerodynamic fields computed according to the foregoing method. For the mixing layer around the potential core, the relations suggested by Squire and Trouncer[16] (cosine distribution) and that of Abramovich[9(a)] were employed. For the developed region of the jet, the velocity profiles selected were those of (a) Squire and Trouncer[16], (b) Schlichting[17(a)], and (c) the Gaussian distribution[18]. The vorticity distributions employed were determined by differentiation of radial distributions of the axial velocity. Contributions to the vorticity due to the radial velocity component can be shown to be negligible.* Computations were made to determine the radial and axial velocity components and values for the pressure coefficient, C_p, at points along the plane baffle plate and at a series of points in the aerodynamic field away from the baffle plate for each of the representative velocity profiles.

---

*For example, the contribution to the vorticity from the radial velocity component of the Schlichting profile is less than 1 percent at $r_1/r_{\frac{1}{2}} \leq 1.2$. The contribution increases to 4 percent for $2.8 < r_1/r_{\frac{1}{2}} \leq 3.2$ and decreases to less than 2 percent at $r_1/r_{\frac{1}{2}} = 4.0$.

In addition to the above computations, computations were made for the Squire and Trouncer profiles (both that for the potential core and that for the fully developed region) to evaluate the sensitivity of the aerodynamic field to contributions from various regions of the jet flow. For example, the contributions of different axial elements of the vorticity in the jet flow were separately evaluated to determine the range of integration in the axial direction necessary to obtain accurate values for the velocity components at the field points. A separate tabulation of the contributions from different regions in the jet flow was made to indicate those regions making the largest contributions.

The contributions to $\vec{U}$ due to the irrotational and solenoidal part of the field, $\vec{E}_p$, were the same for all the jet velocity profiles evaluated. A uniform velocity distribution over the area of the jet nozzle was employed in determining the $\vec{E}_p$ field. To evaluate the influence of nonuniformities in the velocity profile at the nozzle exit plane, several nonuniform profiles chosen to yield the same mass rate of flow were examined.

1. Vorticity Distributions Corresponding to the Selected Velocity Profiles

a. Mixing Layer of the Potential Core Region. The two velocity profiles considered for the mixing layer around the potential core were

$$U_{z1} = \frac{U_j}{2}[1 - \cos \pi \eta] \qquad \text{[Squire and Trouncer]} \qquad (59)$$

$$U_{z1} = U_j [1 - (1 - \eta^{3/2})^2] \qquad \text{[Abramovich]} \qquad (60)$$

where $\eta = (r_o - r_1)/(r_o - r_I)$ and $r_I \leq r_1 \leq r_o$. Evaluating the vorticity distributions corresponding to Equations (59) and (60), neglecting the contribution to the peripheral component of vorticity due to the term $\partial u_{r1}/\partial z_1$, yields

$$\Omega_{\theta 1} = - \frac{\pi U_j}{2 (r_o - r_I)} \sin \pi \eta \quad \text{[Squire and Trouncer]} \qquad (61)$$

and

$$\Omega_{\theta 1} = - \frac{3 U_j (1 - \eta^{3/2}) \eta^{1/2}}{(r_o - r_I)} \quad \text{[Abramovich]} \qquad (62)$$

For the geometry of the core region, a core length of 12 r_j was used as suggested in Ref. 19. For this core length and assuming r_I is a straight line, an angle of spread of 4.8^o for r_I was obtained. Applying the relation for the conservation of linear momentum to the jet between the exit of the nozzle and the end of the core region yields

$$U_j^2 \pi r_j^2 = 2 \pi \int_o^{r_o} U_{z1}^2 r_1 \, dr_1$$

Substituting the value of U_{z1} from Equation (59) into the above relation results in an angle of spread for r_o of 6.7^o.

The results of computations for the radial and axial velocity components at a series of points in the aerodynamic field are presented in Tables 1 and 2. The values shown in Tables 1 and 2 were determined for the vorticity distributions of Equations (61) and (62) respectively. The values in Tables 1 and 2 for $U^C_{S\tau r}/U_j$ and $U^C_{S\tau z}/U_j$ are for convenience denoted by U^C_x and U^C_y respectively. They represent only the parts of the total velocity components (normalized by U_j) of

TABLE 1. FIELD POINT VELOCITIES - CONTRIBUTIONS FROM THE MIXING LAYER OF THE POTENTIAL CORE [SQUIRE AND TROUNCER (COSINE) VELOCITY DISTRIBUTION]*

y = 0		r_o/r_j = 1
x	U_x^C	U_y^C
1.1	-7532.0	0
2	-1477.0	0
4	-356.6	0
12	-30.11	0
20	-6.427	0

y = 12		r_o/r_j = 2.42
x	U_x^C	U_y^C
1.1	658.8	-96.08
2	146.3	-47.46
4	20.27	-19.70
12	-0.5179	-1.152
20	-0.1675	-0.1475

y = 24		r_o/r_j = 4.62
x	U_x^C	U_y^C
1.1	6.235	10.57
2	6.359	4.780
4	0.2415	-0.2443
12	-0.02591	-0.09729
20	-0.01222	-0.01218

y = 36		r_o/r_j = 6.83
x	U_x^C	U_y^C
1.1	0.8499	1.724
2	1.007	.9480
4	0.4950	0.01292
12	-0.00455	-0.02083
20	-0.002530	-0.002620

*$y = Z/r_j$ $x = r/r_o$ $U_x^C = (U_{S\tau\, r}/U_j)$ $U_y^C = (U_{S\tau\, z}/U_j$

All tabular velocity ratios have been multiplied by a factor of 10^4.

TABLE 2. FIELD POINT VELOCITIES - CONTRIBUTIONS FROM THE MIXING LAYER OF THE POTENTIAL CORE REGION (ABRAMOVICH VELOCITY DISTRIBUTION)*

y = 0		r_o/r_j = 1
x	U_x^C	U_y^C
1.1	-7595	0
2	-1514	0
4	-378.1	0
12	-33.55	0
20	-7.242	0

y = 12		r_o/r_j = 2.42
x	U_x^C	U_y^C
1.1	797.7	-127.1
2	168.1	-58.01
4	22.64	-22.74
12	.5898	-1.304
20	-.1900	-.1671

y = 24		r_o/r_j = 4.62
x	U_x^C	U_y^C
1.1	7.128	12.05
2	7.256	5.432
4	2.742	-.28539
12	-.02946	-.1103
20	-.01386	-.01382

y = 36		r_o/r_j = 6.83
x	U_x^C	U_y^C
1.1	.9659	1.960
2	1.147	1.073
4	.5591	.01210
12	-.00521	-.02344
20	-.00285	-.00294

*$y = Z/r_j$ $x = r/r_o$ $U_x^C = U_{S\tau r}/U_j$ $U_y^C = U_{S\tau z}/U_j$

All tabular velocity ratios have been multiplied by a factor of 10^4.

the aerodynamic field due to the integration over the vorticity distribution in the mixing layer of the potential core region. In other words, they represent the first of the two integrals in Equations (49) and (50). It can be observed that the magnitude of the radial velocity ratio decreases in the radial direction. Similarly, at field positions $z = 12\ r_j$ and greater the magnitude of the axial velocity ratio decreases in the radial direction. The change in the direction of the velocity in some cases for $r/r_o \geq 4$ may be noted. Comparing the computed results for the vorticity distribution of Equation (62) [Abramovich] with those of Equation (61) [Squire and Trouncer], it can be observed that the magnitudes of U_x^C and U_y^C were generally higher, some field points 11 percent higher, for the vorticity distribution based upon Equation (62) [Abramovich].

b. The Developed Region. The three velocity profiles considered for the developed region were

$$U_{z_1} = \frac{U_c}{2} \left(1 + \cos \pi \frac{r_1}{r_o}\right) \qquad \text{[Squire and Trouncer]} \qquad (63)$$

$$U_{z_1} = U_c \ \text{EXP} \left[- r_1^2/(2\ C_2^2\ z_1^2)\right] \qquad \text{[Gaussian]} \qquad (64)$$

where $C_2 = .081$

$$U_{z_1} = U_c/(1 + 0.125\ \xi^2)^2 \qquad \text{[Schlichting]} \qquad (65)$$

where $\xi = 18.5\ r_1/z_1$

In the above equations, U_c is the centerline velocity of the jet. Based upon a virtual origin of

$$e = 1.2\ r_j$$

where e is measured from the face of the nozzle exit along the negative z_1 axis, the centerline velocity may be expressed by[19]

$$U_c = (U_j\ 13.2\ r_j)/(z_1 + e) \qquad (66)$$

Evaluating the vorticity distributions corresponding to these velocity distributions, again neglecting the contribution to the peripheral component of vorticity due to the term $\partial U_{r1}/\partial z_1$; yields

$$\Omega_{\theta 1} = -\frac{U_c\ \pi}{2\ r_o} \sin \pi \frac{r_1}{r_o} \qquad \text{[Squire and Trouncer]} \qquad (67)$$

$$\Omega_{\theta 1} = -\frac{r_1\ U_c}{C_2^2\ z_1^2} \exp\ (-\ r_1^2/2\ C_2^2\ z_1^2) \qquad \text{[Gaussian]} \qquad (68)$$

$$\Omega_{\theta 1} = -\frac{171\ U_c\ r_1}{z_1^2\ (1 + 0.125\ \xi^2)^3} \qquad \text{[Schlichting]} \qquad (69)$$

The velocity distributions corresponding to Equations (63) to (65) and the vorticity distributions corresponding to Equations (67) to (69) are shown in Fig. 14. The geometry for the region of vorticity (lateral spreading of the jet) for the Squire and Trouncer distribution was based upon the selected virtual origin ($e = 1.2\ r_j$) and conservation of linear momentum for the jet. The angle of spread determined for r_o in the developed region (boundary of the jet flow) was 10.4^o. However, it should be noted that the vorticity distributions for the Schlichting and Gaussian profiles approach zero asymptotically in the

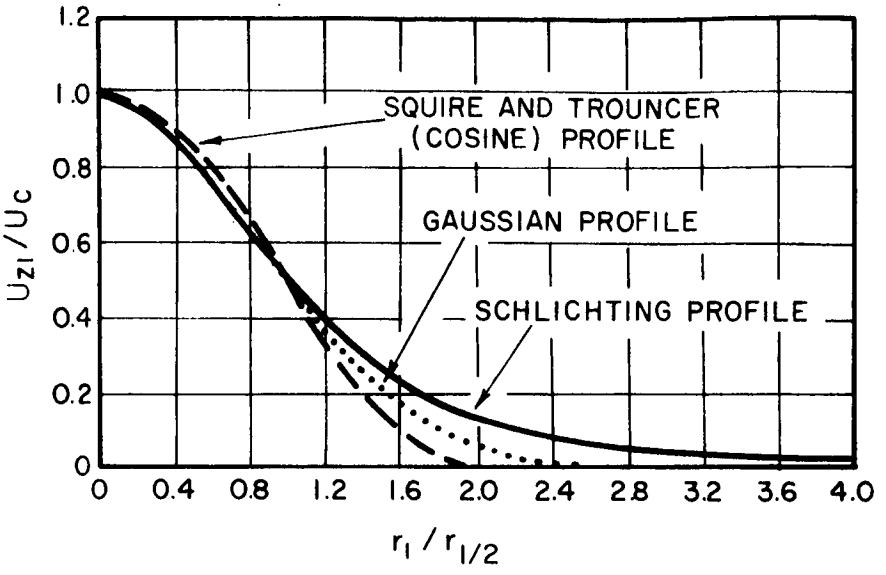

a. VELOCITY DISTRIBUTION

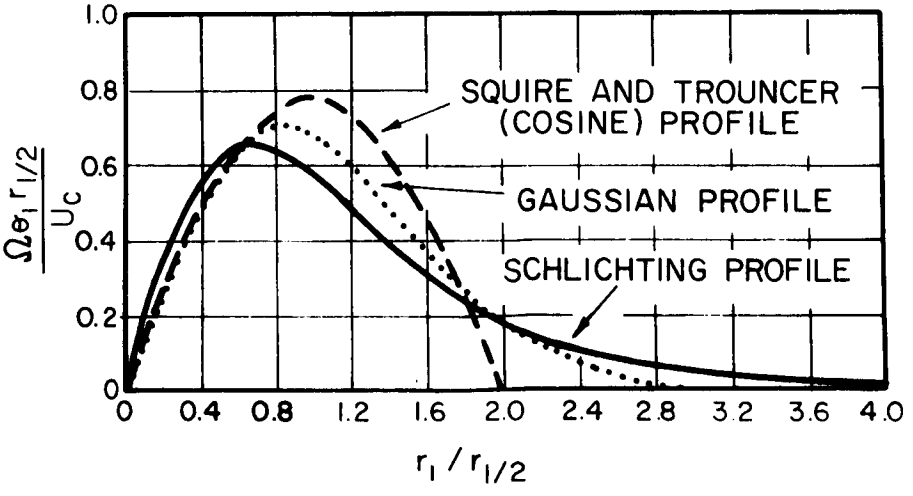

b. VORTICITY DISTRIBUTION

FIGURE 14. VELOCITY AND VORTICITY DISTRIBUTION IN THE DEVELOPED REGION

radial direction. Thus, a large angle of spread, 20^{o}, was selected for the jet boundaries of both the Schlichting and Gaussian profiles. For this angle of spread, the value of vorticity on the jet boundary for the Schlichting profile was less than 5% of the maximum vorticity and for the Gaussian profile it was less than 0.1% of the maximum vorticity. Although the jet boundaries differed, the locus of the radii ($r_{\frac{1}{2}}$) of the half velocity points was essentially the same for all three distributions over the range of integration.

The results of computations, using the Squire and Trouncer, Gaussian, and Schlichting distributions are presented in Tables 3, 4, and 5 respectively. The values U_x^D and U_y^D represent only those components of the total velocity ratio due to the vorticity distribution in the developed region. The values tabulated were determined for the vorticity distributions of Equations (67), (68) and (69). The values represent the second of the two integrals in each of Equations (49) and (50).

It should be noted that the value of r_o employed to normalize the radial field position r was based on the lateral spreading of the Squire and Trouncer vorticity region. For this selection of r_o, the radial field positions r = 1.1 and 2.0 fell within and on the nominal jet boundaries for the cases of the Schlichting or Gaussian profiles in the developed region. Thus, calculations for these field positions were not made for the Schlichting and Gaussian profiles except along the baffle plate. The results in Tables 3 to 5 show that the smallest contributions to field point velocities are those associated with the Squire and Trouncer distribution. The largest contributions come from the developed region based on the Schlichting profile. It may

TABLE 3. FIELD POINT VELOCITIES - CONTRIBUTIONS FROM THE DEVELOPED REGION [SQUIRE AND TROUNCER (COSINE) VELOCITY DISTRIBUTION]*

$y = 0$		$r_o/r_j = 1$
x	U_x^D	U_y^D
1.1	-7.630	0
2	-13.51	0
4	-24.57	0
12	-36.40	0
20	-28.92	0

$y = 12$		$r_o/r_j = 2.42$
x	U_x^D	U_y^D
1.1	-839.2	129.9
2	-261.2	50.06
4	-84.57	15.23
12	-22.27	.3172
20	-12.92	-.2799

$y = 24$		$r_o/r_j = 4.62$
x	U_x^D	U_y^D
1.1	-133.9	-11.15
2	-76.31	-5.82
4	-37.49	-1.115
12	-11.09	-.6497
20	-5.884	-.5461

$y = 36$		$r_o/r_j = 6.83$
x	U_x^D	U_y^D
1.1	-87.51	-3.129
2	-48.55	-2.380
4	-24.06	-1.381
12	-6.857	-.8861
20	-3.214	-.5906

* $y = Z/r_j$ $\quad x = r/r_o$ $\quad U_x^D = U_{S\tau r}^D/U_j$ $\quad U_y^D = U_{S\tau z}/U_j$

All tabular velocity ratios have been multiplied by a factor of 10^4.

TABLE 4. FIELD POINT VELOCITIES - CONTRIBUTIONS FROM THE DEVELOPED REGION (GAUSSIAN VELOCITY DISTRIBUTIONS)*

$y = 0$	$r_o/r_j = 0$	
x	U_x^D	U_y^D
1.1	-8.672	0
2	-15.38	0
4	-28.08	0
12	-42.65	0
20	-34.64	0

$y = 12$	$r_o/r_j = 2.42$	
x	U_x^D	U_y^D
4	-99.19	21.21
12	-27.30	0.8492
20	-16.11	-0.2097

$y = 24$	$r_o/r_j = 4.62$	
x	U_x^D	U_y^D
4	-46.86	0.1710
12	-13.98	-0.6453
20	-7.487	-0.6502

$y = 36$	$r_o/r_j = 6.83$	
x	U_x^D	U_y^D
4	-30.63	-1.005
12	-8.741	-1.043
20	-4.126	-0.7379

* $y = z/r_j$ $\quad x = r/r_o$ $\quad U_x^D = U_{S\tau r}^D/U_j$ $\quad U_y^D = U_{S\tau z}/U_j$

All tabular velocity ratios have been multiplied by a factor of 10^4.

TABLE 5. FIELD POINT VELOCITIES - CONTRIBUTIONS FROM THE DEVELOPED REGION (SCHLICHTING VELOCITY DISTRIBUTION)*

$y = 0$		$r_o/r_j = 1$
x	U_x^D	U_y^D
1.1	-11.46	0
2	-20.37	0
4	-37.31	0
12	-57.34	0
20	-46.53	0

$y = 12$		$r_o/r_j = 2.42$
x	U_x^D	U_y^D
4	-135.3	27.55
12	- 36.46	0.9814
20	- 21.43	-0.3151

$y = 24$		$r_o/r_j = 4.62$
x	U_x^D	U_y^D
4	-62.26	-0.3407
12	-18.57	-0.8891
20	- 9.950	-0.8568

$y = 36$		$r_o/r_j = 6.83$
x	U_x^D	U_y^D
4	- 40.50	-1.554
12	- 11.60	-1.375
20	- 5.499	-0.9707

*$y = z/r_j$ $x = r/r_o$ $U_x^D = U_{S\tau r}^D/U_j$ $U_y^D = U_{S\tau z}/U_j$

All tabular velocity ratios have been multiplied by a factor of 10^4.

be also observed that both U_x^D and U_y^D are negative for all profiles at the axial position y = 36.

2. Regional Contributions to the Aerodynamic Field

a. Relative Contributions of Different Regions of Vorticity along the Length of the Jet. In contrast with Equations (49) and (50) which have limits in the axial integrations of 0 to ∞, the numerical computations for Equations (49) and (50) were limited to a finite region of vorticity. To show the effect of not including more distant regions in the integrations, the velocity ratios U_x^D along the baffle plate (y = 0) were computed for a sequence of finite regions of vorticity, successively extending the region of integration farther downstream. Table 6 presents the resulting velocity ratios as the region of integration was extended in the axial direction (y_1) and in the image direction ($-y_1$). The results shown in Table 6 indicate that for points on the order of 10 diameters away from the jet in the plane of the baffle plate, the integration should extend in the neighborhood of 100 jet diameters downstream for acceptable numerical accuracy. The requirement to extend the integration in the downstream direction diminishes for points closer to the jet, and presumably increases for more distant points.

b. Contributions from Radial Elements of the Distribution of Vorticity. An investigation was conducted to determine which radial elements (Δx_1) of the vorticity distribution made the largest contribution to the velocity U_x at different field positions along the baffle plate. The results of this investigation are shown in Table 7.

TABLE 6. FIELD POINT VELOCITIES - EFFECT OF EXTENDING THE REGION OF INTEGRATION [SQUIRE AND TROUNCER (COSINE) VELOCITY DISTRIBUTION]*

$y = 0$	Developed Region			$r_o/r_j = 1$
x	U_x^D (y_1=26)	U_x^D (y_1=65)	U_x^D (y_1=130)	U_x^D (y_1=260)
1.1	-6.88	-7.44	-7.60	-7.64
2	-12.22	-13.22	-13.45	-13.52
6	-28.20	-31.09	-31.77	-31.98
10	-30.99	-35.52	-36.64	-36.98
16	-24.48	-30.77	-32.48	-33.02
20	-19.26	-26.22	-28.29	-29.16

* $y = z/r_j$ $x = r/r_o$ $y_1 = z_1/r_j$ $U_x^C = U^C_{S\tau r}/U_j$ $U_x^D = U^D_{S\tau r}/U_j$

All tabular velocity ratios have been multiplied by a factor of 10^4.

TABLE 7. FIELD POINT VELOCITIES - CONTRIBUTIONS FROM RADIAL ELEMENTS OF THE JET*

y = 0	Core Region			r_o/r_j = 1	
Δx_1	$\Delta U_x^C(x=1.1)$	$\Delta U_x^C(x=2)$	$\Delta U_x^C(x=4)$	$\Delta U_x^C(x=12)$	$\Delta U_x^C(x=20)$
0-.1	- 164.6	- 26.35	- 4.57	-0.19	-0.03
.1-.2	- 489.2	- 81.29	-15.07	-0.73	-0.13
.2-.3	- 781.6	-135.8	-27.12	-1.56	-0.30
.3-.4	-1010.	-183.7	-39.43	-2.64	-0.53
.4-.5	-1147.	-218.3	-50.19	-3.81	-0.79
.5-.6	-1175.	-233.6	-57.30	-4.85	-1.03
.6-.7	-1084.	-225.1	-58.63	-5.44	-1.18
.7-.8	- 879.9	-190.4	-52.42	-5.26	-1.16
.8-.9	- 576.9	-122.9	-37.61	-4.03	-0.90
.9-1.0	- 202.4	- 47.07	-14.19	-1.60	-0.36
TOTAL = U_x^C =	-7510.6	-1472	-356.5	-30.11	-6.41

y = 0	Developed Region			r_o/r_j = 1	
Δx_1	$\Delta U_x^D(x=1.1)$	$\Delta U_x^D(x=2)$	$\Delta U_x^D(x=4)$	$\Delta U_x^D(x=12)$	$\Delta U_x^D(x=20)$
0-.1	-0.00472	-00.01	-00.01	-00.02	-00.01
.1-.2	-0.05112	-00.09	-00.16	-00.23	-00.18
.2-.3	-0.1954	-00.34	-00.62	-00.90	-00.71
.3-.4	-0.4628	-00.82	-01.48	-02.15	-01.69
.4-.5	-0.8287	-01.47	-02.66	-03.89	-03.05
.5-.6	-1.216	-02.15	-03.91	-05.74	-04.51
.6-.7	-1.506	-02.67	-04.85	-07.16	-05.64
.7-.8	-1.562	-02.77	-05.05	-07.48	-05.90
.8-.9	-1.259	-02.44	-04.08	-06.08	-04.81
.9-1.0	-0.5160	-00.92	-01.67	-02.51	-01.99
TOTAL = U_x^D =	7.602	-13.48	-24.49	-36.16	-28.49

* $y = z/r_j$ $\quad \Delta x_1 = \Delta r_1/r_o$ $\quad x = r/r_o$ $\quad \Delta U_x^C = \Delta U_{S\tau r}^C/U_j$ $\quad \Delta U_x^D = \Delta U_{S\tau r}^D/U_j$

All tabular velocity ratios have been multiplied by a factor of 10^4.

The values ΔU_x^C for the core region and ΔU_x^D for the developed region represent only that part of the aerodynamic field due to the individual radial elements Δx_1 in the respective regions. That is, ΔU_x^C and ΔU_x^D are the results obtained by employing Equations (49) and (50) to integrate over the individual radial elements in the respective regions. The total velocity ratios U_x^C and U_x^D are also presented in Table 7. It may be observed that the radial element (Δx_1) of vorticity making the largest contribution to the field point velocity shifts within a range of (.5 - .6) to (.6 - .7) for the core regions. For the developed region it may be observed that the radial element making the largest contribution is (ΔX_1) = (.7 - .8). In addition, it may be noted that the contribution to the total field point velocity ratios from radial element (ΔX_1) = (.9 - 1.0) varies from 3 to 7% of the total contribution.

3. The Potential Field

The irrotational and solenoidal part of the velocity field $\vec{U}_1$ denoted by $\vec{E}_p$, satisfies the boundary conditions for $\vec{U}$ as discussed in Section III A. The results of computations for the radial and axial velocity ratios of $\vec{E}_p$, E_x and E_y respectively, are presented in Table 8. The values E_x and E_y shown in the table were determined for a uniform velocity distribution over the area of the jet nozzle and represent the results of integration of Equations (51) and (52). It may be noted that the contribution from the potential field to E_x is significantly lower at y = 12 in comparison with y = 0 and the contributions continue to decrease as y increases.

TABLE 8. FIELD POINT VELOCITIES - CONTRIBUTIONS FROM THE POTENTIAL FIELD*

$y = 0$		$r_o/r_j = 1$
x	E_x	E_y
1.1	7396	0
2	1390	0
4	320.1	0
12	34.81	0
20	12.51	0

$y = 12$		$r_o/r_j = 2.42$
x	E_x	E_y
1.1	7.092	16.09
2	11.08	13.82
4	13.17	8.199
12	4.691	.9712
20	1.957	.2430

$y = 24$		$r_o/r_j = 4.62$
x	E_x	E_y
1.1	1.716	4.059
2	2.711	3.525
4	3.322	2.159
12	1.257	.2723
20	.5312	.06901

$y = 36$		$r_o/r_j = 6.83$
x	E_x	E_y
1.1	.7537	1.809
2	1.194	1.577
4	1.480	.9763
12	.5724	.1259
20	.2428	.03204

* $y = z/r_o$ $x = r/r_o$ $E_x = E_{pr}/U_j$ $E_y = E_{pz}/U_j$

All tabular velocity ratios have been multiplied by a factor of 10^4.

To investigate the effect of a non-uniform velocity distribution over the area of the jet nozzle, several non-uniform velocity distributions were employed. An equation representing velocity distributions for turbulent flow in a pipe was selected from reference 17(b) for this purpose.

$$U_{z1} = U_m \left(\frac{r_j - r_1}{r_j}\right)^m$$

where U_m is the peak centerline velocity. Employing the constraint that the mass flow rate be the same as for the uniform velocity profile U_j, yields

$$U_m = \frac{U_j}{2} (m^2 + 3m + 2)$$

The profiles selected for comparison were based on the following values of m and U_m.

m = .025	$U_m = 1.04\ U_j$
m = .05	$U_m = 1.08\ U_j$
m = .25	$U_m = 1.4\ U_j$

Evaluating Equations (51) and (52) with the selected non-uniform profiles, the results obtained were as follows. In comparison with the uniform velocity profile, the largest change in field point velocities E_{pr} and E_{pz} resulted from the profile with the largest peak centerline velocity of 1.4 U_j representing the largest deviation from the uniform profile considered. Even though the field position $r/r_j = 1.1$, $z/r_j = 0$ showed a 10.4 percent decrease in E_{pr}, at the field position $r/r_j = 2.0$,

$z/r_j = 0$ the percent decrease in Γ_{pr} was only 2.6 percent. At axial positions ($z/r_j = 12$) the change in field point velocities only affected the third significant figure. For the other profiles considered, the deviations from uniformity were considerably less, and the differences in computed $\vec{E}_p$ values as compared with those for the uniform profile were insignificant.

4. Summary of Results for the Selected Velocity Profiles

The combined results for the field point velocity ratios due to the mixing layer of the potential core region $\vec{U}^C_{S\tau}/U_j$, the developed region $\vec{U}^D_{S\tau}/U_j$, and the potential flow $\vec{E}_p/U_j$ are presented in Tables 9 to 11. The field point velocity ratios resulting from a mixing layer based upon the relation (Equation (59)), suggested by Squire and Trouncer are the same for all combined results. Likewise, a uniform velocity distribution over the area of the jet nozzle was employed for all results. Thus, $\vec{U}^C_{S\tau}/U_j$ and $\vec{E}_p/U_j$ were the same for all combined results. Variations in the combined results may be attributed to differences in the vorticity distributions employed for the developed region.

The combined results employing the Squire and Trouncer distribution, Equation (66), for the developed region are shown in Table 9, where

$$U_r = U_x + E_x$$

$$U_z = U_y + E_y$$

The values U_x and U_y represent those parts of the total velocity ratios U_r and U_z due to the vorticity distribution in both the core and developed

TABLE 9. TOTAL FIELD POINT VELOCITIES [SQUIRE AND TROUNCER (COSINE) VELOCITY DISTRIBUTION]*

y = 0							r_o/r_j = 1	
x	U_x	E_x	U_r	U_y	E_y	U_z	C_p	U_z/U_r
1.1	-7539.	7396.	-143.	0	0	0	2.04	0
2	-1487.	1390	-97.33	0	0	0	.948	0
4	-381.1	320.1	-61.07	0	0	0	.373	0
12	-66.52	34.81	-31.71	0	0	0	.101	0
20	-35.34	12.51	-22.83	0	0	0	.0521	0

y = 12							r_o/r_j = 2.42	
x	U_x	E_x	U_r	U_y	E_y	U_z	C_p	U_z/U_r
1.1	-180.3	7.092	-173.2	33.98	16.08	49.96	3.25	-2883
2	-114.8	11.07	-103.7	2.600	13.82	16.42	1.10	-1583
4	-64.30	13.16	-51.14	-4.47	8.199	3.728	.263	-729
12	-22.79	4.690	-18.10	-0.8349	0.9712	0.1363	.0328	-75.3
20	-13.09	1.956	-11.13	-0.4279	0.243	-0.1845	.0124	166

*All tabular velocity ratios have been multiplied by a factor of 10^4 (including C_p and U_z/U_r).

TABLE 9. (cont.)*

y = 24						r_o/r_j = 4.62		
x	U_x	E_x	U_r	U_y	E_y	U_z	C_p	U_z/U_r
1.1	-127.6	1.716	-125.9	-0.584	4.059	3.475	1.59	-2760
2	-69.95	2.711	-67.24	-1.046	3.525	2.479	.453	-3686
4	-35.07	3.322	-31.75	-2.959	2.159	.7997	.101	-252
12	-11.12	1.258	-9.862	-0.7469	0.2723	-0.4746	.00975	481
20	-5.896	0.5312	-5.365	-0.5583	0.06901	-0.4892	.00290	912

y = 36						r_o/r_j = 6.83		
x	U_x	E_x	U_r	U_y	E_y	U_z	C_p	U_z/U_r
1.1	-86.65	0.7536	-85.90	-1.404	1.809	.405	.738	-47.12
2	-47.54	1.194	-46.35	-1.431	1.576	.145	.215	-31.19
4	-23.56	1.479	-22.08	-1.367	0.9763	-0.3917	.0488	177
12	-6.862	0.572	-6.289	-0.9070	0.1259	-.7811	.00402	1242
20	-3.217	0.243	-2.974	-0.5932	0.03204	-.5612	.00092	1887

*All tabular velocity ratios have been multiplied by a factor of 10^4 (including C_p and U_z/U_r).

region of the jet. That is, they represent the sum of the integrals in Equations (49) and (50). The value C_p represents the coefficient of pressure

$$C_p = \frac{p - p_\infty}{1/2\ \rho\ U_j^2} = (U_r^2 + U_z^2)$$

As previously stated, U_r and U_z are the total velocity ratios due to both the vorticity distribution and the potential field. The combined results employing the Gaussian Profile, Equation (68), for the developed region are shown in Table 10. The values tabulated for Table 11 correspond to the Schlichting distribution, Equation (69), for the developed region. It may be noted that the largest C_p values are obtained for the Schlichting velocity profile. In addition, it may be observed that the potential field contribution and the vorticity field contribution are of the same magnitude and opposite signs at radial field positions 1.1 and 2.0 along the baffle plate. For example, examining Table 9, it may be observed that along the baffle plate, $y = 0$, the ratio of $\vec{E}_p/\vec{U}_{S\tau}$ varies from .98 at $x = 1.1$ to .35 at $x = 20$. At $y = 12$ the ratio varies from a minimum .095 at $x = 1.1$ to a maximum of .24 at $x = 4$ and then decreases to a value of .12 at $x = 20$. For the field positions at $y = 24$ and $y = 36$, the maximum ratios .10 and .085 occur respectively at $x = 12$.

D. Approximate Computational Models

In the interest of making computations of the type discussed in the foregoing sections less elaborate for engineering purposes, several approximate models of the vorticity distribution in the jet were

TABLE 10. TOTAL FIELD POINT VELOCITIES (GAUSSIAN VELOCITY DISTRIBUTION)*

y = 0							r_o/r_j = 1	
x	U_x	E_x	U_r	U_y	E_y	U_z	C_p	U_z/U_r
1.1	-7541	7396	-145	0	0	0	2.10	0
2	-1492	1390	-102	0	0	0	1.04	0
4	-384.6	320.1	-64.5	0	0	0	.417	0
12	-72.76	34.81	-37.95	0	0	0	.0815	0
20	-41.06	12.51	-28.55	0	0	0	.0815	0

y = 12							r_o/r_j = 2.42	
x	U_x	E_x	U_r	U_y	E_y	U_z	C_p	U_z/U_r
4	-78.91	13.16	-65.75	1.50	8.199	9.699	0.4417	-1475
12	-27.81	4.690	-23.12	-0.303	0.9712	0.668	0.0535	-288.9
20	-16.27	1.956	-15.21	-0.357	0.243	-0.114	0.0231	74.95

*All tabular velocity ratios have been multiplied by a factor of 10^4 (including C_p and U_z/U_r).

TABLE 10. (cont.)*

y = 24						r_o/r_j = 4.62		
x	U_x	E_x	U_r	U_y	E_y	U_z	C_p	U_z/U_r
4	-46.62	3.321	-43.31	-0.0734	2.159	2.086	.188	-482
12	-14.01	1.258	-12.75	-0.743	0.2723	-0.471	.0163	369
20	-7.499	0.5312	-6.968	-0.6624	0.06901	-0.593	.00489	851

y = 36						r_o/r_j = 6.83		
x	U_x	E_x	U_r	U_y	E_y	U_z	C_p	U_z/U_r
4	-30.13	1.479	-28.65	-0.9926	0.9763	-0.0163	.0821	5.93
12	-8.746	0.572	-8.174	-1.064	0.1259	-0.9381	.00667	1147
20	-4.128	0.243	-3.885	-0.740	0.03204	-.708	.00151	1822

*All tabular velocity ratios have been multiplied by a factor of 10^4 (including C_p and U_z/U_r).

TABLE 11. TOTAL FIELD POINT VELOCITIES
(SCHLICHTING VELOCITY DISTRIBUTION)*

y = 0							r_o/r_j = 1	
x	U_x	E_x	U_r	U_y	E_y	U_z	C_p	U_z/U_r
1.1	-7543	7396	-147	0	0	0	2.16	0
2	-1497	1390	-107	0	0	0	1.14	0
4	-393.9	320.1	-73.8	0	0	0	.546	0
12	-87.45	34.81	-52.64	0	0	0	.277	0
20	-52.95	12.51	-40.44	0	0	0	.163	0

y = 12							r_o/r_j = 2.42	
x	U_x	E_x	U_r	U_y	E_y	U_z	C_p	U_z/U_r
4	-115.0	13.16	-101.8	7.851	8.199	16.05	10.52	1576
12	-36.98	4.690	-32.29	-0.1705	0.9712	0.8007	0.1043	248
20	-21.59	1.956	-19.64	-0.4626	0.243	-0.2196	.0386	112

*All tabular velocity ratios have been multiplied by a factor of 10^4 (including C_p and U_z/U_r).

TABLE 11. (cont.)

y = 24							r_o/r_j = 4.62	
x	U_x	E_x	U_r	U_y	E_y	U_z	C_p	U_z/U_r
4	-62.02	3.321	-58.7	-0.5849	2.159	1.574	.345	-268
12	-18.59	1.258	-17.33	-0.986	0.2723	-0.714	.030	412
20	-9.962	0.5312	-9.431	-0.869	0.06901	-0.800	.0089	848

y = 36							r_o/r_j = 6.83	
x	U_x	E_x	U_r	U_y	E_y	U_z	C_p	U_z/U_r
4	-40.0	1.479	-38.52	-1.541	0.9763	-0.565	.1484	146
12	-11.61	0.572	-11.04	-1.396	0.1259	-1.274	.0123	1150
20	-5.501	0.243	-5.258	-0.973	.03204	-.941	.00285	1789

*All tabular velocity ratios have been multiplied by a factor of 10^4 (including C_p and U_z/U_r).

examined. For comparison purposes, the models were based on the Squire and Trouncer profiles, assumed for the purposes of numerical comparisons to be exact. The radial distributions of vorticity selected were (a) a triangular function, (b) a uniform step-function and (c) a delta function. The latter corresponded to replacing the distributed vorticity in the jet by a vortex sheet.

The motivation for examining the approximate models was to acquire some insight into the applicability and use of approximate models which can reduce the mathematical complexity of Equations (49) and (50). It should be noted that the ease of computation increases as one proceeds from the approximate model (a) to the approximate model (c). The circulation strength per unit length, Γ', based upon the centerline velocity, was chosen to be the same for all approximate models. The triangular vorticity profile required integration of a point by point distribution of vorticity, which was also required for the Squire and Trouncer Model. The second approximate model, the uniform vorticity profile, employed an average vorticity per unit length as opposed to a point by point distribution employed in the previous model. In the third model examined, the vorticity was confined to a vortex sheet. Thus, the region of integration, for Equations (49) and (50) employing the vortex sheet model was a surface as opposed to a volume.

1. Triangular Vorticity Profile

For this model, the sinusoidal distributions of Equations (61) and (67) were replaced with the following triangular distributions.

$$\left.\begin{aligned} \Omega_{\theta_1} &= -\Omega_m\,(r_1-r_I)/(r_m-r_I) \text{ for } r_I \le r_1 \le r_m \\ \Omega_{\theta_1} &= -\Omega_m\,(r_o-r_1)/(r_o-r_m) \text{ for } r_m < r_1 \le r_o \end{aligned}\right\} \quad \text{core region} \qquad (70)$$

$$\left.\begin{aligned} \Omega_{\theta_1} &= -\Omega_m\, r_1/r_m \text{ for } r_1 \le r_m \\ \Omega_{\theta_1} &= -\Omega_m\,(r_o-r_1)/(r_o-r_m) \text{ for } r_m < r_1 \le r_o \end{aligned}\right\} \quad \text{developed region} \qquad (71)$$

In Equations (70) and (71), r_m is the value of r_1 when $\Omega_{\theta_1} = \Omega_m$ (the maximum value of vorticity at an axial position). To determine the value of Ω_m Equation (34) was employed for both the core and developed regions.

$$\int_S \vec{\Omega}_1 \cdot dS_1 = \int_C \vec{U}_1 \cdot d\vec{L}_1 = \Gamma \qquad (34)$$

where S here refers to a meridional section of the jet from the axis outward and of unit length along the jet, and C is a curve bounding that section. Assuming that only the centerline velocity contributes significantly to the line integral of Equation (34) and substituting the values of vorticity from Equations (70) and (71) yields, after integration over r_1

$$\Omega_m = \frac{2\,U_j}{r_o-r_I} \qquad \left[\begin{matrix}\text{core}\\ \text{region}\end{matrix}\right] \qquad (72)$$

and

$$\Omega_m = \frac{2\,U_C}{r_o} \qquad \left[\begin{matrix}\text{developed}\\ \text{region}\end{matrix}\right] \qquad (73)$$

2. Uniform Vorticity Profile

Employing Equation (34), the average vorticity in the core region and the developed region may be expressed as

$$\langle \Omega_{\theta_1} \rangle = - \frac{U_j}{r_o - r_I} \qquad \begin{bmatrix} \text{core} \\ \text{region} \end{bmatrix} \tag{74}$$

$$\langle \Omega_{\theta_1} \rangle = - \frac{U_C}{r_o} \qquad \begin{bmatrix} \text{developed} \\ \text{region} \end{bmatrix} \tag{75}$$

where, as in the case of the triangular model, all contributions to the circulation with exception of the centerline velocity are treated as negligible. The average vorticity for the core region Equation (74) extends to the edges of the mixing layer. The average vorticity in the developed region Equation (75) extends to the edge of the jet.

3. Vortex Sheet Model

Employing Equations (74) and (75), letting $(r_o - r_I)$ approach zero but maintaining a constant product of $\Omega_{\theta_1} (r_o - r_I)$ yields for the core region and developed region

$$\Omega_{\theta_1} (r_o - r_I) = - U_j \, \delta (r_m) \qquad \text{[core region]} \tag{76}$$

$$\Omega_{\theta_1} (r_o - r_I) = - U_C \, \delta (r_m) \qquad \text{[developed region]} \tag{77}$$

The strength of the vortex sheet per unit length in the z_1 direction, denoted by γ, is then given by U_j or U_C, respectively. This conical sheet of vorticity was placed along the half-velocity line of the jet. For the core region, the angle of the half-velocity line was taken to

be zero. The half-velocity line for the fully developed region was chosen to diverge from the virtual origin of the jet at a half angle of 5^{o}. These choices correspond approximately with those observed in turbulent jets.[20] The vorticity distributions for the core region Equations (70), (74), and (76), and for the developed region Equations (71), (75), and (77) are shown in Fig. 15. The distributions, Equations (61) and (67), obtained from the Squire and Trouncer (cosine) velocity distribution are also shown. The ordinate $\Omega_{\theta_1} (r_o-r_I)/U_j$ and the abscissa $(r_o-r_1)/(r_o-r_I)$ are for the core region. It should be noted that the vorticity of the vortex sheet (delta function) is infinite. It may be observed that the triangular profile represents the best approximation in comparison with the uniform profile and the vortex sheet.

4. Result of Computations Based on the Approximate Models

The results of computations, using the triangular profile, the uniform profile, the vortex sheet model and the Squire and Trouncer (cosine) reference profile are presented in Table 12. The values tabulated were determined for the vorticity distributions of Equations (70), (71), (74), (75), (76), (77), (61) and (67). The values U_x and U_y represent both integrals in Equations (49) and (50) respectively. It may be determined from Table 12 that the ratios of the contribution of the individual approximate models to that of the Squire and Trouncer (cosine) velocity profile have the following trend. For y = 0 the ratio U_x^I/U_x^{ref} varies from .98 at the point x = 1.1 to .92 at x = 20. In contrast, the ratio U_x^{II}/U_x^{ref} varies from 1.004 at x = 1.1 to 1.55

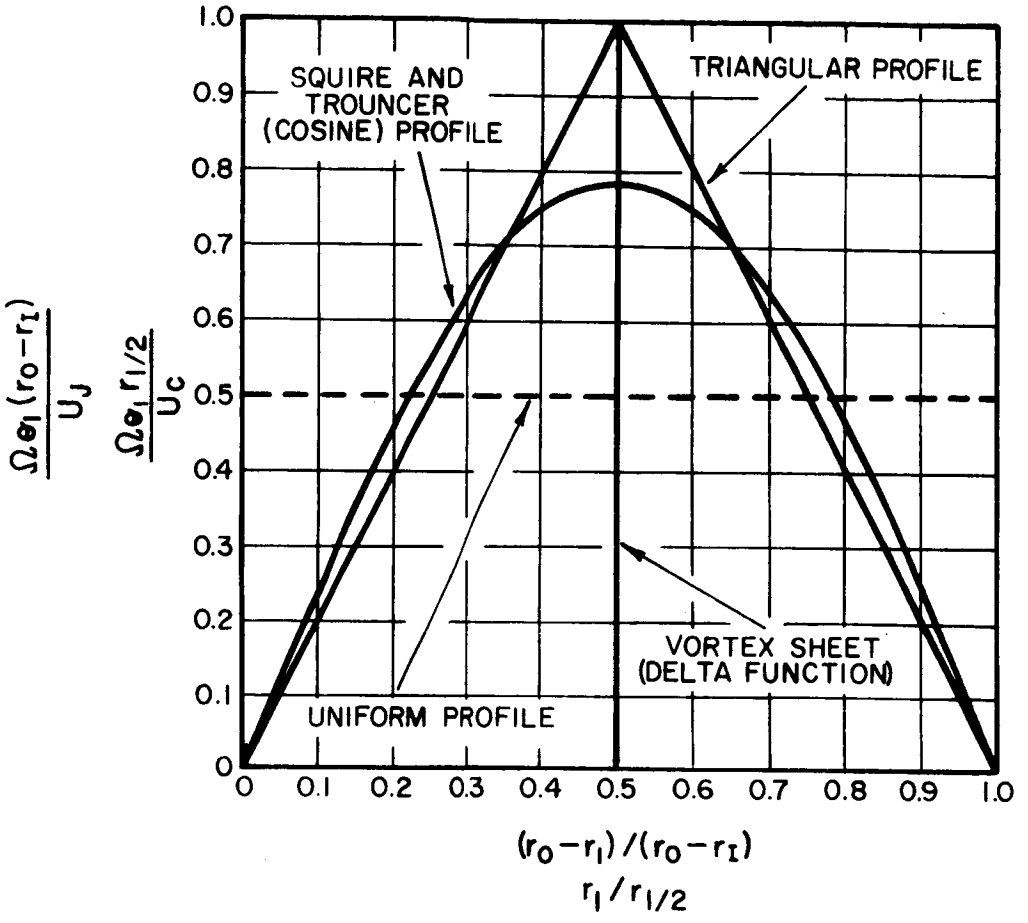

FIGURE 15. APPROXIMATE MODELS FOR THE VORTICITY DISTRIBUTION

at x = 20. Comparing the vortex sheet model at y = 0, the ratio U_x^{III}/U_x^{ref} varies from .97 at x = 1.1 to .66 at x = 20.

TABLE 12. FIELD POINT VELOCITIES - CONTRIBUTIONS FROM THE COMBINED MIXING AND DEVELOPED REGION*

y = 0								r_o/r_j = 1
x	U_x^I	U_x^{II}	U_x^{III}	$U_x^{ref.}$	U_y^I	U_y^{II}	U_y^{III}	$U_y^{ref.}$
1.1	-7412	-7573	-7381	-7539	0	0	0	0
2	-1456	-1525	-1393	-1487	0	0	0	0
4	-365.1	-414.9	-326.3	-381.1	0	0	0	0
12	-61.43	-93.53	-46.71	-66.52	0	0	0	0
20	-32.67	-54.81	-23.33	-35.34	0	0	0	0

y = 12								r_o/r_j = 2.42
x	U_x^I	U_x^{II}	U_x^{III}	$U_x^{ref.}$	U_y^I	U_y^{II}	U_y^{III}	$U_y^{ref.}$
1.1	-160.2	-520.3	-94.26	-180.3	41.51	-19.3	55.63	33.98
2	-102.4	-265.2	-62.37	-114.8	6.65	23.33	14.25	2.6
4	-58.72	-116.78	-40.48	-64.30	-2.95	1.99	-0.36	-4.47
12	-21.26	-37.10	-16.06	-22.79	-0.6307	-1.009	-0.2105	-0.8349
20	-12.29	-21.06	-9.454	-13.09	-0.3603	-.8537	-0.1940	-0.4279

*I = The triangular profile, II = The uniform profile, III = The vortex sheet model, ref. = The Squire and Trouncer (cosine) profile. All velocity ratios have been multiplied by a factor of 10^4.

TABLE 12. (cont.)*

y = 24								r_o/r_j = 4.62
x	U_x^I	U_x^{II}	U_x^{III}	$U_x^{ref.}$	U_y^I	U_y^{II}	U_y^{III}	$U_y^{ref.}$
1.1	-121.9	-210.4	-96.55	-127.6	.763	-9.64	3.881	-0.584
2	-66.40	-119.07	-51.92	-69.95	-.001	-4.217	2.335	-1.046
4	-33.05	-59.10	-25.46	-35.07	-.9178	-2.527	-.6743	-2.959
12	-10.48	-17.79	-8.137	-11.12	-.6564	-1.621	-.4110	-0.7469
20	-5.676	-8.945	-4.366	-5.896	-.5178	-1.188	-.3856	-0.5583

y = 36								r_o/r_j = 6.83
x	U_x^I	U_x^{II}	U_x^{III}	$U_x^{ref.}$	U_y^I	U_y^{II}	U_y^{III}	$U_y^{ref.}$
1.1	-82.63	-144.2	-66.30	-86.65	-0.935	-3.933	0.4525	-1.404
2	-45.25	-79.34	-36.03	-47.54	-1.002	-3.588	0.1270	-1.431
4	-22.33	-38.98	-17.56	-23.56	-1.091	-3.062	-0.4048	-1.367
12	-6.492	-10.52	-5.092	-6.862	-0.8382	-1.979	-0.6179	-0.9070
20	-3.048	-4.464	-2.396	-2.217	-0.5581	-1.128	-0.4340	-0.5932

*I = the triangular profile, II = The uniform profile, III = The vortex sheet model, ref. = The Squire and Trouncer (cosine) profile. All velocity ratios have been multiplied by a factor of 10^4.

V. DISCUSSION

The results of the computations for the axisymmetric jet serve to illustrate the character of the method of computation employing the Stokes potentials. For example, the relative contribution of the potential part of the field $\vec{E}_p$ as compared with the part $\vec{U}_{S\tau}$ due to vorticity is of some interest. In principle, at least, the potential part may be determined with considerable accuracy, for example, for more general jet flows, whereas the vorticity contributions are likely to be less accurately known. Comparisons of the computed results with the available experimental data and with other theories illustrate the strengths and weaknesses of the method of computation and of the existing theoretical velocity profiles for the jet flow.

A. Contribution of $\vec{E}_p$ Relative to $\vec{U}_{S\tau}$

The results presented in the previous section, Sec. IV, (Tables 9 to 11), show that $\vec{E}_p$ is opposite in sign to $\vec{U}_{S\tau}$ along the baffle plate for the example considered. The field point velocity $\vec{U}$ along the plate is determined by the difference between the magnitudes of $\vec{E}_p$ and $\vec{U}_{S\tau}$. If these values, $\vec{E}_p$ and $\vec{U}_{S\tau}$, are of approximately the same magnitude, errors in $\vec{E}_p$ or $\vec{U}_{S\tau}$ are magnified in the computed resultant $\vec{U}$. Errors of this type are most significant near the source, and they become insignificant sufficiently far from the source. It may be observed from Table 9, for example, that errors of

this type are likely to be important at X = 1.1 on the baffle plate. At this position, a 2 per cent increase in the magnitude of U_x ($U_x = U_{s\tau_r}/U_j$) increases the magnitude of U_r (U_r = radial component of $\vec{U}$) from 143 to 294, other terms involved being considered constant. In contrast to this magnification of error, at field points away from the source (Table 9) the relative contribution of $\vec{E}_p$ to the total field point velocity rapidly decreases. That is, neglecting the contribution from $\vec{E}_p$ entirely at y = 36 results in a maximum error of about 1 per cent in the field point velocity ratio $\vec{U}/U_j$.

B. Comparison of Computed Results with Experimental Data and Other Theories

1. Comparison with Experimental Data

Experimentally determined pressure coefficients on a baffle plate in the plane of the nozzle may be compared with the theoretical predictions of the coefficient of pressure for the selected vorticity distributions. The available experimental data include results obtained by Wygnanski[11] and by Gentry and Margason[21]. The corresponding experimental and theoretical values of C_p are shown in Table 13. A comparison of the experimental data, C_p^2 and C_p^3, with the theoretical values for C_p^8 are shown in Fig. 16.

Comparing the experimentally determined pressure coefficients, the values determined by Wygnanski, C_p^1 and C_p^2, are lower than those obtained by Gentry and Margason, C_p^3 and C_p^4, by more than a factor of 2 at the points close to the source. This disagreement between the different experimental data could have been a consequence of differing

Table 13. EXPERIMENTAL AND THEORETICAL VALUES OF $-C_p \times 10^4$*

y = 0	EXPERIMENTAL RESULTS					COMPUTED RESULTS $r_o/r_j = 1$				
X	C_p^1	C_p^2	C_p^3	C_p^4		C_p^5	C_p^6	C_p^7	C_p^8	
1			16.3	9.6						
1.1						2.04	2.10	2.16	4.43	
2	2.9	2.5	6.1	4.4		.948	1.04	1.14	2.09	
4	1.2	.8	2.0	1.4		.373	.417	.546	.908	
8			1.0	.7						
12						.101	.144	.277	.302	

*1 Wygnanski's data for Reynold's no. of 53,800

2 Wygnanski's data for Reynold's no. of 51,500

3 Gentry's and Margason's data for a plenum-chamber to ambient pressure ratio of 1.32

4 Gentry's and Margason's data for a plenum-chamber to ambient pressure ratio of 2.04

5 Squire and Trouncer velocity profile (Table 9)

6 Gaussian velocity profile (Table 10)

7 Schlichting velocity profile (Table 11)

8 Schlichting velocity profile for developed region and Abramovich velocity profile for core region (Tables 5 and 2)

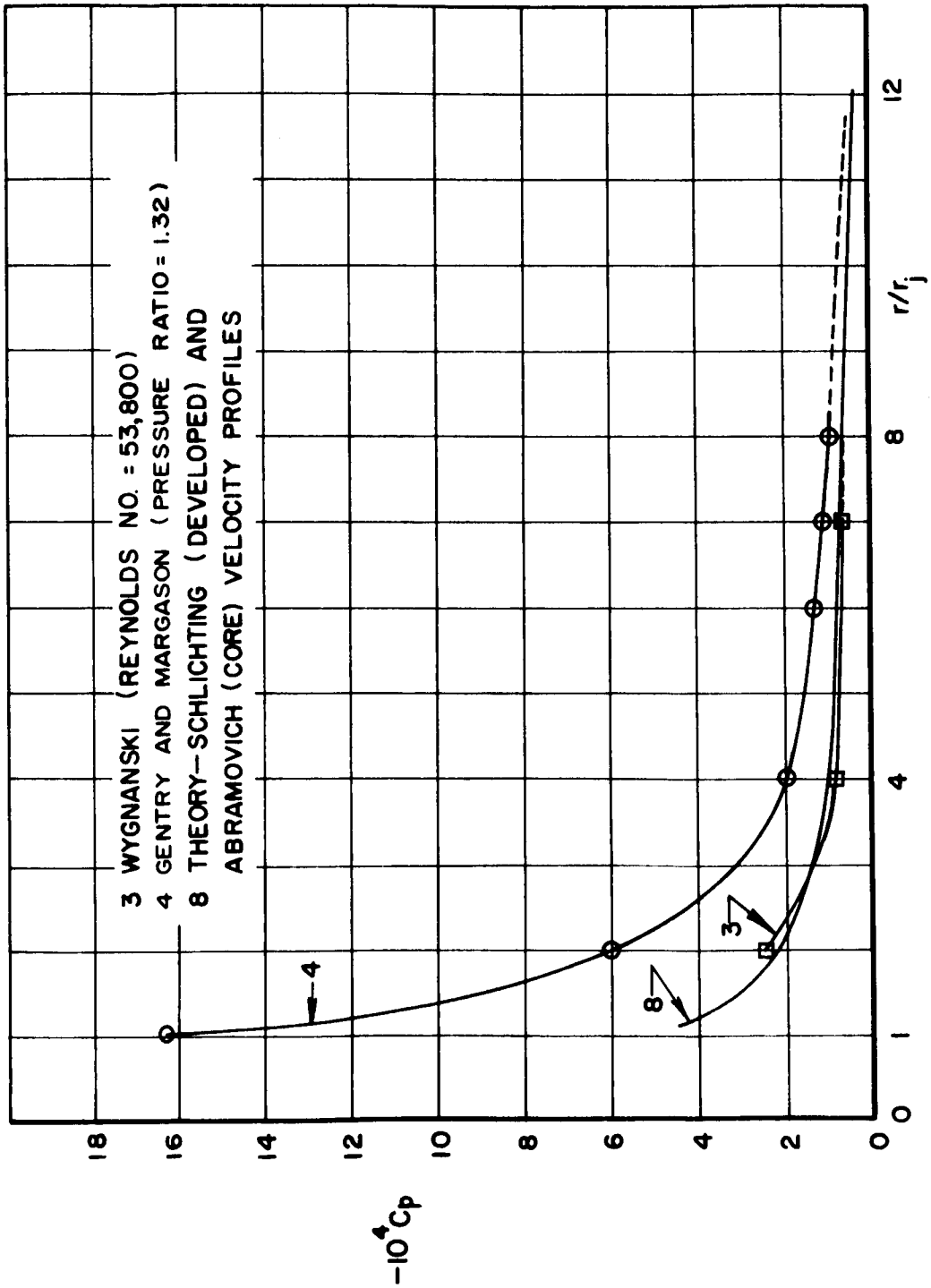

FIGURE 16. COMPARISON OF EXPERIMENTAL DATA WITH THEORETICAL VALUES

velocity profiles at the exit orifice. For example, for the data of Table 9, a 2 per cent reduction of E_x would yield a C_p^5 value of 9.6 as opposed to 2.04 at X = 1.1 and a value of 1.56 as opposed to .948 at X = 2.0. From the results of Section IV 3, showing the sensitivity of Ep_r to non-uniformities in the velocity profile at the nozzle exit, it is apparent that such a change could easily be accounted for. Changes in theoretical E_x values become less significant as x increases beyond about 2. The different experimental data also tend to show better agreement at the more distant field points. It may be observed in Table 13 and Fig. 16 that the theoretical magnitudes of C_p are generally lower than the experimental values.

The pressure coefficient C_p^8 shows reasonably close agreement with Wygnanski's data, as might be anticipated because Wygnanski's data had been found to compare well with other results computed using the Schlichting profile (Equation (65)) for the developed region of the jet. The use of the Abramovich relation (Equation (60)) for the velocity profile in the mixing layer in the determining of C_p^8 should be expected to yield more accurate results as compared with the cosine profile of Squire and Trouncer (Equation (59)). Experimental data for the velocity profile in the mixing layer have been found to agree quite closely with the Abramovich relation[9]. It may be noted that the computed C_p magnitudes close to the nozzle are significantly smaller for the cosine profile as compared with that of Abramovich, accounting for part of the difference between the magnitudes of C_p^{5-7} and the experimental data, C_p^{1-4}.

On the basis of the above comparison, it may be recommended that computations according to the theory making use of the Stokes potentials are likely to be reasonably accurate, if

(1) the velocity profile of the jet at the nozzle exit plane is accurately known,

(2) the Abramovich relation, Equation (60), is employed for the mixing layer of the potential core region, and

(3) the Schlichting profile, Equation (69), is employed for the fully developed region of the jet, with computations involving integration only within a 20° half-angle cone.

These recommendations apply, of course, only to the example considered, that of an axisymmetric jet exhausting normally through a plane baffle plate. Nonetheless, the sensitivity to those parameters observed for this case seem likely to be applicable to more general jet flows.

2. Comparison With Other Theoretical Models

Wygnanski[11], employing a distribution of sinks along the axis of symmetry to satisfy approximately the boundary conditions on the boundary separating the jet flow from the aerodynamic field, obtained the following equation for the pressure coefficient along the baffle plate.

$$C_p^9 = -\frac{1}{4\pi^2 x^2}\left[0.715 - \frac{0.514}{[1 + (x/12)^2]^{1/2}}\right]^2 \qquad (78)$$

where $x = r/r_j$

In developing the model, Wygnanski chose the value of 0.404 for the numerical constant K_1, in the developed region Equation (35), corresponding to the Schlichting velocity profile. Values for this constant have been found to range from 0.220 to 0.404 as noted in Sec. IV.

Stewart[22], also examined the irrotational flow field external to a jet. From similarity considerations, Stewart expressed the mean flow near the axisymmetric jet boundary as $U_\phi = C/\rho$, where ϕ, ρ are the colatitude angle and the radius in a spherical coordinate system (Fig. 3) with the virtual origin of the jet located at the origin of the coordinates and with the flow along the Z axis. For a jet emerging normally through an infinite plane baffle plate, it was found that the velocity potential ϕ could be expressed by

$$\phi = C \tan \phi_0 \ln (\rho \sin \phi) \tag{79}$$

where ϕ_0 = the half cone angle containing all of the turbulent region of the jet (about 12.5°)

Employing Equation (79) and Equation (35) with $K_1 = 0.404$, the corresponding pressure coefficient along the baffle plate ($\phi = \pi/2$) may be expressed as

$$C_p^{10} = (-0.252/x)^2 \tag{80}$$

where $x = r/r_j$

A comparison of Wygnanski's results, the results according to Stewart's theory Equation (80), and the results of computations employing Stokes potentials with Schlichting's velocity profile for the developed region is presented in Table 14.

Table 14. COMPARISON WITH OTHER THEORETICAL MODELS - $C_p X 10^4$*

y = 0				r_o/r_j = 1
x	C_p^7	C_p^8	C_p^9	C_p^{10}
1.1	2.16	4.43	8.58	11.1
2	1.14	2.09	2.77	3.34
4	0.546	0.908	0.755	0.836
12	0.277	0.302	0.219	0.093
20	0.163	0.171	0.129	0.033

*7 Schlichting velocity profile for developed region and Squire and Trouncer velocity profile for the core region (Table 11)

8 Schlichting velocity profile for developed region and Abramovich velocity profile for core region (Tables 5 and 2)

9 Wygnanski, Equation (78)

10 Stewart, Equation (80)

As mentioned in Sec. VB2, the best agreement with the experimental data may be expected for C_p^8 as compared with C_p^7. Wygnanski's relation Equation (78) for C_p^9, yields values which had been shown to fit rather well his experimental data[11], also corresponds well with C_p^8 as might be expected. The results obtained from Equation (80), C_p^{10}, agree fairly well with C_p^9 at small values of x but decrease in magnitude more rapidly as x increases to larger values. This difference in C_p^9 and C_p^{10} is most likely inherent in the different modeling of the jet. Wygnanski employed a line of sinks and Stewart's representation corresponded to application of the boundary conditions on the surface of the jet. The core region was not represented by Stewart's model at all. Rather, the developed region was presumed to originate at the point source. On the other hand, Wygnanski's analysis does not strictly represent the actual geometry, as does the present theory or Stewart's theory. Therefore, the values of C_p^8 and C_p^9 as might be expected show differences at small values of x.

C. Comparison of Computations for the Approximate Models with the Computations for the Reference Model (Squire and Trouncer Profile)

The three approximate models for the radial distribution of vorticity in the jet (triangular, uniform, and vortex sheet), Section IV D, were chosen to have identical values for the circulation per unit length. The common value of Γ' corresponded to that for the Squire and Trouncer velocity profiles for both the potential core and developed regions of the jet. The computed values for C_p along the baffle plate, Table 12, compared quite well with the reference values

except for the uniform and vortex sheet models at points distant from the axis. As could be anticipated, the results for the triangular profile agreed more closely with those for the reference computation even at the distant points. The agreement of all of the results at points nearer the axis could be expected because

(a) the C_p values close to the axis depend strongly on the form of the mixing layer in the potential core region,

and

(b) the circulation per unit length and the moments of the vorticity distributions for the approximate models of the potential core layer closely corresponded to that for the reference profile

On the other hand, for computations downstream and at points far from the axis, where contributions from the developed region of the jet become significant, the agreement between results for the approximate models and for the reference profile was significantly poorer, except for those of the triangular profile. The disagreement may be attributed to the difference between the moments of the vorticity distributions for the uniform and vortex sheet models, as compared with that of the reference profile. Those differences were greatest for the developed region with the geometry chosen for the computations. With the discussion of Sec. III C in mind, the proper choice for the radial position of the vortex sheet, for example, would be such that the moment of vorticity distribution is maintained in agreement with that for the reference profile. The radial position of the vortex sheet was simply chosen to coincide with the half-velocity points in

the jet which also corresponded with the points of peak vorticity (Fig. 15). For more accurate results, then, the divergence angle of the cone joined by the vortex sheet should have been larger.

Even though the approximate models yield somewhat different results as compared with those for the reference profile, the agreement could be acceptable for some computational purposes for all of the approximate models. The triangular profile best represents the data for the reference profile as could be expected. The vortex sheet model, even with the poor choice for its geometry, did yield the reference values to a reasonable approximation. Because the computations for the vortex sheet model are by far the simplest, the latter comparison suggests the use of such a model for most computational purposes.

D. Evaluation of the Integral Moment of Vorticity

The vorticity magnitude at a field point has been shown to be directly proportional to the magnitude of the integral moment of vorticity

$$I_m = \int \vec{X}_1 \times \vec{\Omega}_1 \, d\tau_1 \tag{81}$$

Recalling Equation (32), one has

$$\vec{U}_{S\tau} = \frac{1}{8\pi} \nabla \left((\nabla \frac{1}{X}) \cdot \int \vec{X}_1 \times \vec{\Omega}_1 \, d\tau_1 \right) \tag{32}$$

Now, for the examples considered in the previous sections, involving an axisymmetric jet, the vorticity is entirely peripheral. I_m may then be determined as a summation of integrals of the form in Equation (81) for small slices of the jet as discussed in Section III C. This enables

the evaluation of the significance of local contributions of the vorticity along the jet to the field point velocity.

Considering a small section of the jet flow (refer to Fig. 8) for the axisymmetric jet, the magnitudes of an integral moment of vorticity per unit length along the jet may be expressed as

$$I_m' = 2\pi \int r_1^2 \, \Omega_{\theta 1} \, dr_1 \tag{82}$$

The small section is considered to be a plane slice of the axisymmetric jet flow field of infinitesimal thickness.

Introducing the following transformations into Equation (82)

$$\left.\begin{aligned} \Lambda &= \Omega_{\theta 1} \, (r_o - r_I)/U_j \\ \mu &= (r_o - r_1)/(r_o - r_I) \end{aligned}\right\} \text{[core region]}$$

$$\left.\begin{aligned} \Lambda &= \Omega_{\theta 1} \, r_o/U_j \\ \mu &= r_1/r_o \end{aligned}\right\} \text{[developed region]}$$

yields for the core region

$$\frac{I_m'}{2\pi \, U_j r_o^2} = -\int \left[1 - \frac{2\,(r_o - r_I)}{r_o^2}\,\mu + \frac{(r_o - r_I)^2 \mu^2}{r_o^2}\right] \Lambda \, d\mu \tag{83}$$

and for the developed region

$$\frac{I_m'}{2\pi U_j r_o^2} = \int \mu^2 \, \Lambda \, d\mu \tag{84}$$

The values of the integral, Equation (83), were calculated for the mixing layer of the potential core region based on the Squire and Trouncer profile, Equation (61), and on the approximate models, Equations (70), (74), and (76). The values of the integral, Equation (84), were calculated for the developed region based on the Squire and Trouncer profile Equation (67), the approximate models Equations (71), (75), and (77), the Gaussian profile Equation (68), and the Schlichting profile Equation (69). The results of these calculations for the mixing region were as follows.

$$\frac{I_m'}{2\pi U_j r_o^2} = -1 + \frac{r_o - r_I}{r_o} - \frac{(r_o - r_I)^2}{r_o^2}\gamma \tag{85}$$

where

γ = .297 [Squire and Trouncer profile]

.290 [Triangular Vorticity profile]

.333 [Uniform Vorticity profile]

.250 [Vortex Sheet]

For the developed region, the results of these calculations were

$$\frac{I_m'}{2\pi U_j r_o^2} = \gamma \tag{86}$$

where

γ = -.297 [Squire and Trouncer profile]

-.290 [Triangular Vorticity profile]

-.333 [Uniform Vorticity profile]

-.250 [Vortex Sheet]

-.390 [Gaussian profile]

-.500 [Schlichting profile]

It may be observed for the core region that the magnitude of the integral moment of vorticity Equation (85) is approximately the same for all four profiles. Note that the third term on the right side of Equation (85), differing slightly for the different profiles, makes the smallest contribution to I_m'. This provides confirmation of the statement in the previous subsection C concerning the close correspondence of the I_m's for the different profiles in the core region.

In contrast to the above results for the core region, the integral moment of vorticity Equation (86) differs significantly for the six profiles considered. This substantiates the explanation presented in subsection C for the disagreement among the computations for the different profiles, where contributions from the developed region of the jet become significant.

Based upon the proportionality $\vec{U}_{S_T} \alpha I_m$, as previously discussed, the ratio of the integral moments and the field point velocities for the developed region for different profiles should be approximately proportional. Selecting the values of U_x and U_y for the Gaussian profile Table 10 and the Squire and Trouncer profile Table 9 at y = 36, x = 20 yields a ratio of 1.28 for $\vec{U}_{S_T}$'s. The ratio of I_m's for the profiles is 1.31. Thus, the proportionality is fairly close. Selecting other profiles similar results are obtained.

Recall that the computed values of C_p as shown in Tables 10 and 11 were based upon a half-angle spread of 20° in the developed region

of the jet for both the Gaussian and Schlichting profiles. It should be noted that a more acceptable half-angle of spread would have been 10 to 15^{o}[9(b)]. Most experimental observations, for example, indicate the maximum spreading of the jet boundary to lie within that range of half-angles[23].

In order to evaluate the effect of reducing the half-angle to correspond more closely with the observations, the half-angle of 10^{o}, used for the Squire and Trouncer profile, was also employed for the Gaussian and Schlichting profiles. The spreading angle of the half-velocity line was left unchanged for the profiles. Reducing the half-angle of the spreading of the jet boundary, then, had the effect of neglecting the vorticity associated with the Schlichting and Gaussian at points outside the boundary. The results of the computations for both the Gaussian and Schlichting profiles yielded lower C_p values than those shown in Table 9 for the Squire and Trouncer profile.

It appears that all three of the profiles considered are not truly representative of the observed vorticity distribution in the developed region of the jet. The Squire and Trouncer profile with a reasonable half-angle of spread of 10^{o} yields values of C_p which are too low in comparison with experimental data (Table 13). The Gaussian profile, even for a spreading half-angle of 20^{o}, yielded results below the experimental data. The best agreement with the experimental data employing the Schlichting profile was found for a half-angle of spread for the jet of 20^{o}. In comparison with typical observed spreading angles, a half-angle spread of 20^{o} is not reasonable. However, as previously mentioned, even at this large angle of spread the value of

vorticity at the boundary of the jet flow for the Schlichting profile is still about 5 per cent of the maximum. A more reasonable profile with the same general shape for the developed region would be characterized by a vorticity distribution such that the half-angle of spread is about 10 to 15^{o}. In addition, it would be expected that the moment of vorticity should be larger, either due to a larger peak vorticity or a redistribution of the vorticity profile.

VI. CONCLUSIONS

The following conclusions may be drawn regarding the computation of the aerodynamic field of a jet according to the method of Stokes potentials (scalar and vector potentials). The conclusions, for the most part, are supported by the application of the method to the axisymmetric jet exhausting through a plane baffle plate.

(1) The most significant information required for the computations are the velocity profile at the exit plane of the nozzle, and the integral moment of vorticity along the jet.

It was found that the potential part of the velocity in the aerodynamic field $\vec{E}_p$ was significant for most of the points computed. This was especially true for points near the origin of the jet. The need for the integral moment of vorticity I_m was anticipated from consideration of the asymptotic behavior of the theory in Sec. III C. This is strictly true for jets for which the only vorticity present is peripheral as in the case of the axisymmetric jet. For jets of a more complex nature, there would also likely be a requirement for knowledge of the integral moment of streamwise vorticity in the jet. For the axisymmetric jet, reasonable values for the integral moment of vorticity could be obtained from values for the velocity on the axis and the radius of the half-velocity point as functions of distance along the jet, without further knowledge of the jet velocity profile.

(2) At field points on the baffle plate within approximately one diameter from the edge of the jet, the contribution $\vec{U}^{D}_{S\tau}$ due to the developed region of the jet was negligible; at all other field points considered, to approximately 20 jet radii from the region of the jet in either the streamwise or lateral direction, all three components $\vec{E}_p$, $\vec{U}^{C}_{S\tau}$ and $\vec{U}^{D}_{S\tau}$ were of comparable magnitudes. At more distant field points, the developed region tends to dominate, as might be expected.

Since both $\vec{E}_p$ and $\vec{U}^{C}_{S\tau}$ remained relatively large, but of opposite sign, at distances to approximately 6 jet radii from the edge of the jet, both must be known with relatively high accuracy for field points on the baffle plate within that range. This significance of the velocity profile of the jet at the nozzle exit has been observed experimentally[21]. Theoretical considerations have been heretofore limited to speculations as to the influence of the jet velocity profile on the mixing layer and consequent changes in the entrainment rate.

(3) The computations tended generally to underestimate the C_p magnitudes observed experimentally, except for the case where the Schlichting profile was employed, together with an overall spreading half-angle of 20° for the jet flow, which compared well only with Wygnanski's data.

The comparison with experimental data indicates a need for improvement, both in the experimental data and in the analytical characterization of the jet flow. The experimental data available were not consistent, differing by more than a factor of 2 (perhaps 4, considering the

Ricou and Spalding results). Moreover, the Schlichting profile, yielding the most favorable comparison, is not compatible with experimental observations of the spreading angle of the jet boundary. The analytical results were found to be comparable with both the experimental data and the other theories, within the limit of the state of the art.

Theories relying on the scalar potential yield acceptable and simpler relations for the axisymmetric jet. The method of Stokes potentials however, offers the added benefit of explicitly accounting for nonuniformities in the initial velocity profile of the jet, simpler computations for more complex jet flows, the prospect for developing simpler vortex sheet models, and less reliance on data that are difficult to obtain for the more complex flows (for example, reasonable results may be obtained from measured values for U_c and $r_{\frac{1}{2}}$, as opposed to determinations of entrainment required for the method employing the scalar potential alone).

(4) The approximate vortex sheet model was found to yield results comparable to those obtained with the complete vorticity profiles, and thus may be recommended for computational purposes.

The vortex sheet model might be expected to be useful because (a) it should yield precise results asymptotically if I_m is properly chosen, and (b) for regions of the jet close to the nozzle, I_m is known with some accuracy because the mixing layer is relatively narrow there and grows only gradually. The computations for the axisymmetric jet supported this view. There appears to be little justification, considering the state of the art, to employ more complex models.

LIST OF REFERENCES

LIST OF REFERENCES

1. Lass, H., Vector and Tensor Analysis, McGraw-Hill, New York, 1950, p. 119.

2. Borisenko, A. I., and Tarapov, I. E., Vector and Tensor Analysis With Applications, Prentice Hall, 1968, pp. 223-225.

3. Truesdell, G., and Toupin, R. A., Encyclopedia of Physics, Edited by S. Flugge, Vol. III/1 Principles of Classical Mechanics and Field Theory, Springer-Verlag, 1960, p. 828.

4. Morse, P. M., and Feshback, H., Methods of Theoretical Physics, McGraw-Hill, New York, 1953, pt. I, (a) pp. 52-54, (b) pp. 791-895.

5. Kellogg, O. D., Foundations of Potential Theory, Dover Publications, Inc., New York, 1953, pp. 246-247.

6. Batchelor, G. K., An Introduction to Fluid Dynamics, Cambridge University Press, New York, 1967, (a) pp. 84-87, (b) p. 120.

7. Townsend, A. A., The Structure of Turbulent Shear Flow, Cambridge University Press, New York, 1956.

8. Skifstad, J. G., "Aerodynamics of Jets Pertinent to VTOL Aircraft," T. R. AFAPL-TR-69-28, Air Force Aero Propulsion Laboratory, Wright-Patterson AFB, Ohio, March 1969, p. 72.

9. Abromovich, G. N., The Theory of Turbulent Jets, M.I.T. Press, Cambridge, Massachusetts, 1963, (a) pp. 176-177, (b) p. 509.

10. Ricou, F. P., and Spalding, D. B., "Measurements of Entrainment by Axisymmetrical Turbulent Jets," J. Fluid Mech., Vol. 11, 1961, pp. 21-32.

11. Wygnanski, I., "The Flow Induced by Two-Dimensional and Axisymmetric Turbulent Jets Issuing Normally From an Infinite Plane Surface," Aeron. Quart., Vol. XV, Nov. 1964, pp. 373-380.

12. Herndon, J. R., "Algorithm 55, Complete Elliptic Integral of the First Kind," CACM*, 4, 1961, p. 180.

---

*CACM = Communications of the Association for Computing Machinery.

APPENDICES

13. Herndon, J. R., "Algorithm 56, Complete Elliptic Integral of the Second Kind," CACM, 4, 1961, p. 180.

14. Thacher, H. C. Jr., "Certification of Algorithm 55, Complete Elliptic Integral of the First Kind," CACM, 6, 1963, p. 166.

15. Salvador, M. G., and Baron, M. L., Numerical Methods in Engineering, Prentice Hall, N. J., 1961, pp. 198-200.

16. Squire, H. B., and Trouncer, J., "Round Jets in a General Strem," Tech. Report No. 1974, Jan. 1944, Brit. Aeron. Res. Council.

17. Schlichting, H., Boundary Layer Theory, 6th Ed., McGraw-Hill, New York, 1968, (a) pp. 699-700, (b) p. 563.

18. Albertson, M. L., Dai, Y. B., Jensen, R. A., and Rouse, H., "Diffusion of Submerged Jets," Transactions, A.S.C.E., Vol. 115, 1950, pp. 647-657.

19. Hinze, J. O., Turbulence, McGraw-Hill, New York, 1959, pp. 421-427.

20. Kuchemann, D., and Weber, J., Aerodynamics of Propulsion, McGraw-Hill, New York, 1953, pp. 235-236.

21. Gentry, G. L., and Margason, R. J., "Jet-Induced Lift Losses on VTOL Configurations Hovering in and out of Ground Effect," NASA TN D-3166, February, 1966.

22. Stewart, R. W., "Irrotational Motion Associated with Free Turbulent Flows," J. Fluid Mech., Vol. 1, 1956, pp. 593-606.

23. Tuve, G. L., and Priester, G. B., "The Control of Air Streams in Large Spaces," Trans. ASHVE, Vol. 50, 1944, p. 153.

24. Byrd, P. F., and Friedman, M. D., Handbook of Elliptic Integrals for Engineers and Physicists, Springer-Verlag, 1954.

25. Halleen, R. M., "A Literature Review on Subsonic Free Turbulent Shear Flow," A.F.O.S.R. TN 5444, 1964 (U.S.A.F); Report MO-11 (Thermosciences Division, Mech. Engr. Dept., Stanford Univ., Stanford, Calif.); AD 606 758.

APPENDIX A

Annotated Bibliography on Axisymmetric Jets

Experimental and theoretical investigations of axisymmetric turbulent jets have been far too numerous to attempt a complete review here. Rather, a synopsis of some of the studies is presented in the form of an annotated bibliography. More complete discussions may be found in Abramovich[9], Hinze[19], Townsend[7], and in review papers (e.g., Halleen[25], Skifstad[8]).

1. Taylor, G. I., "Eddy Motion in the Atmosphere", Phil. Trans. Roy. Soc. London, Series A, Vol. 215, 1915, pp. 1 - 26.

Taylor developed a purely phenomenological theory concerning vortex motions. He assumed that the vorticity could be considered as a transferable quantity. That is, the vorticity would be conserved along the path of a lump of fluid over a certain distance. Based upon this assumption, he obtained the relationship

$$\varepsilon_\Omega = \frac{\ell_\Omega^2}{2} \left| \frac{d\bar{U}_1}{dx_2} \right|$$

where ε_Ω is the coefficient of eddy diffusion for vorticity, ℓ_Ω is Taylor's mixing length for vorticity, and $d\bar{U}_1/dx_2$ is the time mean value of vorticity for two-dimensional flow uniform in the x_1 direction. Taylor extended this theory to three-dimensional flow. This three-dimensional theory is known as the modified vorticity-transport theory.

2. Zimm, W., "Uber die Stromungsvorgange im freien Luft strahl," Forschungsarbeiten aus dem Gebiete des Ingenieurwesens, No. 234, 1921

Zimm conducted an experimental investigation of an axisymmetric jet issuing into a quiescent atmosphere. In the Zimm experiments the jet exit velocity was non-uniform, that is

$$U_m/U_{cp} = 1.1$$

where U_m is the peak exit velocity and U_{cp} is the exit velocity close to the boundary of the jet. The experimental data for the decay of the centerline velocity in the developed region of the jet could be approximated by the expression

$$U_c/U_J = 0.96/(az/r_J)$$

where U_c is the centerline velocity, U_J is the average jet exit velocity, z is the axial distance downstream from the jet exit, r_J is exit radius of the jet, and a is a numerical constant with a value of 0.070.

3. Prandtl, L., "Uber die ausgebildete Turbulenz," ZAMM, Vol. 5, 1925, pp. 135-139 (also Proc. Ind. Intern. Cong. Appl. Mech., Zurich, 1926, pp. 62-75.)

Prandtl introduced a phenomenological theory concerning momentum. He assumed that the momentum could be considered as a transferable quantity. That is, the momentum is conserved along the path of a lump of fluid over a certain distance. Based upon this assumption he obtained the two-dimensional relationship

$$\varepsilon_m = \ell_m^2 \left| \frac{d\bar{U}_1}{dx_2} \right|$$

where ϵ_m is the coefficient of eddy diffusion for momentum, ℓ_m is Prandtl's mixing length for momentum, and $d\bar{U}_1/dx_2$ is the difference in mean velocity, between the end of the path and the start of the path from where the lump originated, divided by the path length.

4. Tollmein, W., "Berechnung Turlenter Ausbreitungsvorgange," ZAMM, Vol. 6, 1926, pp. 468-478 (also NACA TM 1085 [1945])

Tollmein published an analytical investigation of the axially symmetric jet. His results were obtained by employing the "mixing length" concept as introduced by Prandtl. His results showed for the fully developed jet that

$$U_c \alpha 1/(Z + e)$$

where U_c is the centerline velocity, Z is the main flow direction, and e is the position of the virtual origin measured from the face of the nozzle exit along the negative z axis. The above results were based on assuming the pressure in the jet was constant. To improve his analysis, he considered pressure differences and concluded that the pressure differences were so small that no modifications of the velocities were necessary. In addition, Tollmein obtained an analytical representation of the velocity profile for both the transverse and longitudinal component of velocity. The use of one empirical constant enabled his analytical results to be brought into very good agreement with results of experimental investigations.

5. Townend, H. C. H., "Flow Induced by a Jet of Air," Rept. No. ARC 1934, June, 1934, British Aeronautical Research Council.

Townend experimentally examined the flow induced by a jet of air. He interpreted his results as consisting of a jet with bounding eddies

constituting discrete vortex rings. In addition, it appeared as if the jet was alternately accelerated and decelerated as each successive vortex ring passed downstream. The overall effect was a kind of pumping action.

6. Kuethe, A. M., "Investigations of the Turbulent Mixing Regions Formed by Jets," J. Appl. Mech., Vol. 11, No. 3, 1935, pp. A87-A95.

Kuethe considered the turbulent mixing surrounding the jet and obtained a solution for the region surrounding the potential core of the jet. He assumed no pressure difference between the jet and the surrounding air. He used as a first approximation to the longitudinal velocity profile in the mixing layer

$$U_z = (1 - n'^{3/2})$$

where $n' = (r - r_I)/(r_o - r_I)$ and r is the radial distance $(r_I \leq r \leq r_o)$, r_I is the radius of the potential core, and r_o is the jet radius.

7. Abramovich, G. N., The Theory of Turbulent Jets, M.I.T. Press, Cambridge, Mass., 1963, pp. 177-208.

Abramovich presented formulas for the core region and developed region of the jet. He employed for the velocity profile in the mixing layer surrounding the core the empirical relation

$$U_z = U_J [1 - (1- n^{3/2})^2]$$

where $n = (r_o - r)/(r_o - r_I)$ and r is the radial distance $(r_I \leq r \leq r_o)$, r_I is the radius of the potential core, and r_o is the jet radius. This relation agreed quite closely with experimental data. Abramovich showed that the velocity profiles in the fully developed region were affine,

the increase in the thickness or width of the submerged jet ($r_o - r_I$) was equal to the axial distance (z) times a constant, and the centerline velocity of the jet in the fully developed region was inversely proportional to z. In addition, for the transition he concluded that one may assume that the equal velocity lines in the transition region were extensions of the equal velocity lines of the potential core region of the jet.

8. Howarth, L., "Concerning the Velocity and Temperature Distributions in Plane and Axially Symmetrical Jets," Proc. Cambridge Phil. Soc., London, Vol. 34, Pt. 2, 1938, pp. 185-203.

Howarth made calculations of the velocity profile for the developed region of an axisymmetric jet. He employed Taylor's mixing length for his calculations. Assuming the eddy velocities of the jet were isotropic he obtained results equivalent to employing Prandtl's mixing length. Assuming Taylor's mixing length was homogeneous, he obtained results equivalent to employing Taylor's modified vorticity transfer theory. Pressure gradients, radial components of velocity, and derivatives of radial components of velocity with respect to the axial direction, were considered negligible for all calculations.

9. McElroy, G. E., "Air Flow at Discharge of Fan-Pipe Lines in Mines-Part II-Effect of Size and Shape of Pipe and of Adjacent Walls on Velocity and Entrainment Ratios," Rept. of Invest. No. 3730, Nov. 1943, Bureau of Mines, U.S. Dept. of Int.

McElroy conducted an experimental investigation and suggested the following simple approximate formula for entrainment in the developed region of the jet

$$E_m' = C\ Z/D$$

where $E_m' = (Q - Q_o)/Q_o$ is the ratio of the quantity of entrained air in the air stream at any cross section, $Q - Q_o$, to the quantity discharged Q_o and is called the entrainment ratio, Z is the distance from the orifice, D is the diameter of the round jet orifice, and C is a constant (about .35). He stated among a number of conclusions:

(1) The velocity at any point in the air stream and the amount of entrained air in the stream at any section vary directly with the discharge velocity.

(2) Conditions that increase centerline velocity ratios generally decrease entrainment ratios and vice versa.

(3) Centerline velocity ratios vary with region. In the potential core region they are essentially constant. In the transition region, they decrease as the square root of the distance; in the developed region, they decrease directly with distance.

(4) The angle of expansion of the developed jet appears to be almost 24^o.

(5) Velocity distributions vary with regions. In the mixing layer of the core region, the relation of the mean velocity to maximum velocity changes rapidly with distance. In the transition and developed regions, mean velocities probably approximate 40 percent of the maximum velocities.

(6) Entrainment ratios vary with regions. Analyses of the experimental data show continuously increasing entrainment ratios with increasing axial distance.

10. Tuve, G. L. and Priester, G. B., "The Control of Air Streams in Large Spaces," Trans. ASHVE, Vol. 50, 1944, p. 153.

Tuve and Priester conducted an experimental investigation. They concluded that the maximum air velocity at any cross section of the air stream beyond 25 diameters downstream varies approximately as follows:

(1) directly proportional to the exit velocity,

(2) directly proportional to the diameter of the outlet, and

(3) inversely proportional to the distance from the outlet.

On the basis of an effective outlet area, they obtained an equation for entrainment ratio

$$E = \frac{0.785\ K}{R\ Z\ \sqrt{Ae}}\left(\sqrt{\frac{Ae}{0.785}} + 2\ Z\ \mathrm{Tan}\ \frac{\theta}{2}\right)^2 - 1.0$$

where

K = constants of proportionality (tabulated)

R = ratio of maximum velocity to average velocity at any cross section (range 2.4 to 3.0)

θ = average spreading angle of the jet (22.5^{o} to 25.4^{o})

Z = axial distance from outlet

Ae = effective outlet area

11. Squire, H. B., and Trouncer, J., "Round Jets in a General Stream," Tech. Rept. No. 1974, Jan. 1944, British Aeron. Research Council

Squire and Trouncer conducted a mathematical analysis of an axi-symmetric jet with a secondary stream. However, within this analysis they included the case for a secondary stream of zero velocity. They examined the flow in the potential core region and the developed region separately and then fitted the solutions together. They determined

the inflow induced by the jet based upon employing cosine distributions for the longitudinal velocity profiles. For the mixing layer and the developed region, the respective relations were

$$U_Z = (U_j/2)(1 - \cos \pi \eta) \qquad \text{[mixing layer]}$$

$$U_Z = (U_C/2)[1 + \cos (\pi r/r_o)] \qquad \text{[developed region]}$$

where U_Z is the longitudinal velocity, U_j is the exit velocity of the jet, U_C is the centerline velocity in the developed region, $\eta = (r_o - r)/(r_o - r_I)$ and r is the radial position ($r_I \leq r \leq r_o$), r_I is the inside radius of the mixing layer, and r_o is the outside radius of the jet. In addition, they made a determination of inflow velocity by assuming a system of sinks along the jet axis.

12. Cleeves, U. and Boelter, L.M.K., "Isothermal and Non-Isothermal Air Jet Investigations," Chem. Engr. Progr., Vol. 43, 1947, pp. 123-134.

Cleeves and Boelter conducted an experimental investigation. They concluded that the transverse distribution of the axial component of velocity (U_Z) in the developed region can be approximately correlated by using a dimensionless group. This group was obtained from the transfer of momentum in the jet, that is U_Z/U_C versus $r/r_{\frac{1}{2}}$, where $r_{\frac{1}{2}}$ is the radial position r at $U_Z/U_C = 0.5$ and U_C is the centerline velocity at the radial position.

13. Ribner, H. S., "Field of Flow about a Jet and Effect of Jets on Stability of Jet Propelled Airplanes," NACA Wartime Report L-213, (ARC L6C13, 1946).

Ribner conducted a mathematical analysis of an axially symmetric jet with a secondary flow. He investigated the induced flow effects on stability and trim of an aircraft as the jet passes near the tail surfaces. His analysis was only applicable to the developed jet and

he ignored velocity components induced parallel to the jet axis. For the spreading of the jet near the origin, he obtained a linear relationship with the axial distance Z. Far from the origin, he obtained an expression for jet spreading as the one-third power of the axial distance. In addition, he concluded that the jet-induced flow inclination varies nearly inversely as the radial distance from the jet axis within the region between the jet boundary and twice the radius of the jet boundary at distances greater than 8 orifice diameters downstream of the jet exit.

14. Liepmann, H. W. and Laufer, J., "Investigations on Free Turbulent Mixing," NACA TN 1257, Aug. 1947.

Liepmann and Laufer conducted an analytical investigation of two-dimensional free turbulent mixing. They concluded that the mixing length theories had lost much of their value in that the main results of these theories could be obtained by dimensional reasoning.

15. Hinze, J. O. and Van Der Hegge Zijnen, B. G., "Transfer of Heat and Matter in the Turbulent Mixing Zone of an Axially Symmetrical Jet," Appl. Sci. Res., Vol. A1, 1948.

Hinze and Van Der Hegge Zijnen made measurements of the radial distribution of the mean values of the axial component of velocity, the temperature, and gas concentration. They compared these results with previous investigators and found that theories based on a constant coefficient of shearing stress across the jet flow gave the best agreement with measured radial velocity distribution in a central zone of the jet.

16. Albertson, M. L., Dai, Y. B., Jensen, R. A., and Rouse, H., "Diffusion of Submerged Jets," Proc. of Amer. Soc. of Civil Engr., Dec. 1948.

Albertson, et al., derived the approximate characteristics of the mean flow pattern for flow from slots and orifices. Experimental data were used to justify the analytical results and provide the empirical constants. In agreement with other investigators they found it unnecessary to make any assumption as to the distribution of turbulence to obtain an approximate mean velocity distribution.

17. Corrsin, S., and Uberoi, M. S., "Further Experiments on the Flow and Heat Transfer in a Heated Turbulent Air Jet," NACA TN 1865, 1949.

Corrsin and Uberoi conducted an experiment on a heated jet issuing in still ambient fluid. They suggested that useful results in shear flow problems are obtainable with less difficulty by use of integrated equations of motion and reasonable guesses for the velocity profile. One conclusion they made was up to a local maximum density ratio, ρ_∞/ρ min of about 1.3, simple geometrical similarity still exists in the developed region, within the accuracy of measurements. The minimum density at a section of the jet was denoted by ρ min and ρ_∞ was the density of the receiving medium. In addition, they concluded that the pressure and temperature profile functions are basically the same as in the constant density jet up to ρ_∞ / ρmin = 1.3.

18. Corrsin, S., and Kistler, A. L., "Free Stream Boundaries of Turbulent Flows," NACA Rept. 1244, 1955.

Corrsin and Kistler completed an experimental and theoretical study of the free stream boundary separating the turbulent fluid from non-turbulent fluid. Their suggested theoretical model gave constant mean vorticity at the boundary, local vorticity production, and a uniform suction (induced) velocity. Experimentally they determined for the

round jet that the mean velocity at the boundary is chiefly radially inward. The angle of spread for the half-cone of the developed region was determined to be 10.8^{o} (no-wall).

19. Phillips, O. M., "The Irrotational Motion Outside a Free Turbulent Boundary," Proc. Cambridge Phil. Soc., Vol. 51, 1955, pp. 220-229.

Phillips analytically considered the irrotational motion of an infinite fluid when the normal velocity across a plane is a stationary random function of position. He postulated conditions which corresponded closely to the motion outside a free turbulent boundary.

20. Stewart, R. W., "Irrotational Motion Associated with Free Turbulent Flows," J. Fluid Mech., Vol. 1, 1956, pp. 593-606.

Stewart conducted a theoretical examination of the irrotational motion external to a self preserving turbulent wake and jet. He found a mean flow towards the center of the jet and pointed out that it is possible for the vorticity free fluid between bulges of turbulent fluid to obtain the mean velocity of the turbulent fluid. However, he concluded that this was a very short range effect and the motion in the external region can be considered irrotational. From similarity considerations, Stewart expressed the mean flow near the axisymmetric jet boundary as $U_{\phi} = C\rho^{-1}$, where ϕ, ρ are the colatitude angle and the radius in a spherical coordinate system with the jet exit located at the origin and directed along the z axis. For a jet emerging normally through an infinite plane baffle plate, he found that the velocity potential ϕ can be expressed by

$$\phi = C \tan \phi_0 \, \ell n \, (\rho \sin \phi)$$

where ϕ_o = the half cone angle containing all of the turbulent region of the jet (about 12.5°).

21. Miller, D. R. and Comings, E. W., "Static Pressure Distribution in the Free Turbulent Jet," J. Fluid Mech., Vol. 3, 1957, pp. 1-16.

Miller and Comings made measurements of mean velocity, turbulent stress, and static pressure in the mixing layer of a jet of air issuing from a slot (2-D) into still air. Appreciable deviations from constant pressure conditions were found. They obtained negative static pressure readings everywhere in the mixing layer except in the potential core wedge.

22. Ricou, F. P. and Spalding, D. B., "Measurements of Entrainment by Axisymmetrical Turbulent Jets," J. Fluid Mech., Vol. 11, 1961, pp. 21-32.

Ricou and Spalding made measurements of entrainment by means of a porous-walled, cylindrical chamber. The flow rate through the porous wall was adjusted until no axial pressure gradients could be detected. The entrained fluid as a result of the radial inflow was then presumed to be equal to that of a free jet. For the fully developed jet they obtained a relationship for the mass entrainment as a function of axial position. As in previous work by other investigators, they had to determine a numerical constant (K_1 of Equation (35)). Their experimental value was 0.282 which was within the range of values 0.22 to 0.404, determined by earlier investigators.

23. Wygnanski, I., "The flow Induced by Two-Dimensional and Axisymmetric Turbulent Jets Issuing Normally from an Infinite Plane Surface," Aeron. Quart., Vol. XV, 1964, pp. 373-380.

Wygnanski made an analytical investigation of turbulent jets. The pressure distribution on the surface from which the jet was issuing

was determined. In his analysis, he replaced the jet with a line of sinks with variable strength. His results agreed with the experimental data he presented.

24. Gentry, C. L. and Margason, R. J., "Jet-Induced Lift Losses on VTOL Configurations Hovering In and Out of Ground Effect," NASA TN D-3166, Feb. 1966.

Gentry and Margason conducted an experimental investigation of pressure distribution on a plate from which a jet flow was exhausting. The case where the plate was flush with a large wall and the case where the plate was exposed to the atmosphere on both sides were studied. Pressure coefficients on the plate were measured in both cases. In comparing their results for the large wall with those of Wygnanski, they show that Wygnanski's data is about 25 percent less.

In general, many mathematical analysis and experimental studies of jets issuing from nozzles with diameters ranging from 0.102 to 20 inches and with velocities ranging from 13 to 1000 ft/sec have been made. For the developed region, using the concept of similarity, theories for mean velocity distributions give about the same picture. However, they yield a velocity distribution which is too sharp an apex on the jet axis in comparison with experimental results. As is to be expected, near the jet boundary comparison of the analytical velocity profile with the experimentally determined distribution show a deviation from the measured distribution.

APPENDIX B

Derivation of the Equations for the Aerodynamic Field of an Axisymmetric Jet

This Appendix contains derivations of the equations for determining the aerodynamic velocity field for an axisymmetric jet according to the method which make use of the Stokes potentials. The derivations are for a semi-infinite domain where Green's function is given by 2/R. Starting from Equation (15)

$$\vec{U} = \vec{U}_{S\tau} + \vec{E}_p \qquad (15)$$

where

$$\vec{U}_{S\tau} = \frac{1}{4\pi}\int_{\tau} (\nabla_1 \times \vec{U}_1) \times \frac{\vec{R}}{R^3}\, d\tau_1$$

and

$$\vec{E}_p = -\frac{1}{4\pi}\int_{S} \nabla\left(\frac{2}{R}\right) \vec{U}_1 \cdot d\vec{S}_1$$

Since the flow is axisymmetric ($\nabla_1 \times \vec{U}_1 = \Omega_{\theta 1}\, i_{\theta 1}$), the equation for $\vec{U}_{S\tau}$ can be written as

$$\vec{U}_{S\tau} = \frac{1}{4\pi}\int_{\tau} \frac{\Omega_{\theta 1}\, i_{\theta 1} \times R}{R^3}\, d\tau_1$$

For the geometry of Fig. 11, noting that θ may be put equal to zero without loss of generality, $\vec{R}$ can be written as

$$\vec{R} = (r \cos \theta_1 - r_1)\, \vec{i}_{r1} - r \sin \theta_1\, \vec{i}_{\theta 1} + (z - z_1)\, \vec{i}_{z1}$$

The source point coordinate system is the appropriate system for the volume integration. Substituting this result into the equation for $\vec{U}_{S\tau}$ yields

$$\vec{U}_{S\tau} = \frac{1}{4\pi} \int_{\tau} \frac{\Omega_{\theta 1}\,(z - z_1)\, \vec{i}_{r1} - \Omega_{\theta 1}\,(r \cos \theta_1 - r_1)\, \vec{i}_{z1}}{R^3}\, d\tau_1$$

which can be separated into r and z components in the field point coordinate system.

$$U_{S\tau r} = \frac{1}{4\pi} \int_0^{2\pi} \int_{-\infty}^{\infty} \int_0^{r_1} \frac{\cos \theta_1\, \Omega_{\theta 1}\,(z - z_1)\, r_1\, dr_1\, dz_1\, d\theta_1}{R^3}$$

$$U_{S\tau z} = -\frac{1}{4\pi} \int_0^{2\pi} \int_{-\infty}^{\infty} \int_0^{r_1} \frac{\Omega_{\theta 1}\,(r_1 - r \cos \theta_1)}{R^3}\, r_1\, dr_1\, dz_1\, d\theta_1$$

Making use of the identity that

$$\nabla \frac{1}{R} = -\frac{\vec{R}}{R^3}$$

the equation for $\vec{E}_p$ may be written as

$$\vec{E}_p = \frac{1}{2\pi} \int_S \left(\frac{\vec{R}}{R^3}\right) \vec{U}_1 \cdot d\vec{S}_1$$

Using the geometry of Fig. 12, noting that θ may again be put equal to zero, $\vec{R}$ can be written as

$$\vec{R} = (r \cos \theta_1 - r_1)\, \vec{i}_{r1} - r \sin \theta_1\, \vec{i}_{\theta 1} + z\, \vec{i}_{z1}$$

Substituting this result into equation for $\vec{E}_p$ along with U_j for $\vec{U}_1 \cdot \vec{n}$ yields

$$\vec{E}_p = \frac{U_j}{2\pi} \int_S \frac{(r \cos \theta_1 - r_1)\, \vec{i}_{r1} - r \sin \theta_1\, \vec{i}_{\theta 1} + z\, \vec{i}_{z1}}{R^3}\, dS_1$$

Separating the above relation into r and z components yields

$$E_{pr} = \frac{U_j}{2\pi} \int_0^{2\pi} \int_0^{r_1} \frac{(r - r_1 \cos \theta_1)}{R^3}\, r_1\, dr_1\, d\theta_1$$

$$E_{pz} = \frac{U_j z}{2\pi} \int_0^{2\pi} \int_0^{r_1} \frac{r_1}{R^3}\, dr_1\, d\theta_1$$

Consider next the integral over θ_1 for $U_{S\tau r}$

$$\int_0^{2\pi} \frac{\cos \theta_1\, d\theta_1}{(a - b \cos \theta_1)^{3/2}}$$

where $a = r^2 + r_1^2 + (z - z_1)^2$ and $b = 2rr_1$

Let

$$I_1 = 2 \int_0^{\pi} \frac{d\theta_1}{(a - b \cos \theta_1)^{3/2}}$$

and

$$I_2 = 2 \int_0^{\pi} \frac{\cos \theta_1 \, d\theta_1}{(a-b \cos \theta_1)^{3/2}}$$

then

$$a\, I_1 - b\, I_2 = 2 \int_0^{\pi} \frac{d\theta_1}{(a-b \cos \theta_1)^{1/2}}$$

Solving this relation for I_2, the integral over θ_1 for $U_{S\tau r}$, yields

$$I_2 = \frac{2a}{b} \int_0^{\pi} \frac{d\theta_1}{(a-b \cos \theta_1)^{3/2}} - \frac{2}{b} \int_0^{\pi} \frac{d\theta_1}{(a-b \cos \theta_1)^{1/2}}$$

These integrals may be evaluated in terms of complete elliptic integral functions.[24] Thus,

$$\int_0^{\pi} \frac{d\theta_1}{(a-b \cos \theta_1)^{3/2}} = \frac{g}{a-b} \; E\,(A,k)$$

where

$$g = 2/\sqrt{a+b}, \quad k^2 = 2b/(a+b)$$

and

$$A = \sin^{-1} \sqrt{b\,(1-\cos \theta_1)/k^2(a-b \cos \theta_1)}$$

Substituting the value for θ_1 in the relation for A yields $A = \sin^{-1} 1 = \pi/2$. Thus, $E\,(A,k) = E\,(\pi/2, k) = E\,(k)$ a complete elliptic integral of the second kind. Now, substituting for g, one obtains

$$\frac{2a}{b} \int_0^{\pi} \frac{d\theta_1}{(a-b \cos \theta_1)^{3/2}} = \frac{4a}{b\,(a-b)} \frac{E\,(k)}{\sqrt{a+b}}$$

Similarly,

$$-\frac{2}{b}\int_0^{\pi}\frac{d\theta_1}{(a-b\cos\theta_1)^{1/2}} = -\frac{4K(k)}{b\sqrt{a+b}}$$

where K (k) is a complete elliptic integral of the first kind. Substituting these results for the right side of the equation for I_2 yields

$$I_2 = \frac{4}{b\sqrt{a+b}}\left[\frac{a}{a-b}E(k) - K(k)\right]$$

Likewise integrating over θ_1 for $U_{S\tau z}$ with

$$I_2 = 2\int_0^{\pi}\frac{d\theta_1}{(a-b\cos\theta_1)^{3/2}} - 2\int_0^{\pi}\frac{\cos\theta_1\, d\theta_1}{(a-b\cos\theta_1)^{3/2}}$$

yields

$$I_2 = \frac{4}{\sqrt{a+b}\,(a-b)}E(k) - \frac{4}{b\sqrt{a+b}}\left[\frac{a}{a-b}E(k) - K(k)\right]$$

Substituting the respective results into the integrand of the equations for $U_{S\tau r}$ and $U_{S\tau z}$, yields

$$U_{S\tau r} = \frac{1}{2\pi r}\int_S \frac{\Omega_{\theta_1}(z-z_1)}{\sqrt{(r+r_1)^2+(z-z_1)^2}}\left[\frac{r^2+r_1^2+(z-z_1)^2}{(r-r_1)^2+(z-z_1)^2}E(k) - K(k)\right] dr_1\, dz_1 \qquad (40)$$

$$U_{S\tau z} = -\frac{1}{2\pi}\int_S \frac{\Omega_{\theta_1}}{\sqrt{(r+r_1)^2+(z-z_1)^2}}\left[\frac{r^2-r_1^2+(z-z_1)^2}{(r-r_1)^2+(z-z_1)^2}\right.$$

$$E(k) - K(k) \Big] \; dr_1 \, dz_1 \tag{41}$$

In order to obtain Equations (42) and (43), the equations for E_{pr} and E_{pz} are rewritten as

$$E_{pr} = \frac{U_j r}{2\pi} \int_0^{2\pi} \int_0^{r_1} \frac{r_1 \, dr_1 \, d\theta_1}{(a - b \cos\theta_1)^{3/2}} - \frac{U_j}{2\pi} \int_0^{2\pi} \int_0^{r_1} \frac{r_1^2 \cos\theta_1}{(a - b\cos\theta_1)^{3/2}} \cdot dr_1 \, d\theta_1$$

$$E_{pz} = \frac{U_j z}{2\pi} \int_0^{2\pi} \int_0^{r_1} \frac{r_1 \, dr_1 \, d\theta_1}{(a - b\cos\theta_1)^{3/2}}$$

Integrating over θ_1, yields

$$E_{pr} = \frac{U_j}{\pi} \int_r \frac{r_1}{\sqrt{(r + r_1)^2 + z^2}} \left[\frac{r^2 - r_1^2 - z^2}{(r - r_1)^2 + z^2} E(k) + K(k) \right] dr_1 \tag{42}$$

$$E_{pz} = \frac{2 U_j z}{\pi} \int_r \frac{r_1}{\sqrt{(r + r_1)^2 + z^2}} \frac{E(k)}{[(r - r_1)^2 + z^2]} \, dr_1 \tag{43}$$

APPENDIX C

Algorithms for Complete Elliptic Functions

The following algorithm computes the complete elliptic integral of the first kind with modulus k'[12].

$$K(k) = \{[(0.032024666t + 0.054544409)t + 0.097932891]_{\wedge}^{t} + 1.3862944\} - \{[(0.010944912t + 0.060118519)t + 0.12475074]t + 0.5\} \ln(t)$$

where $t = 1 - k^2$

The following algorithm computes the complete elliptic integral of the second kind with modulus k'[13].

$$E(k) = \{[(0.040905094t + 0.085099193)t + 0.44479204]t + 1.0\} - \{[(0.01382999t + 0.08150224)t + 0.24969795]t\} \ln(t)$$

where $t = 1 - k^2$